KU Leuven
Biomedical Sciences Group
Faculty of Medicine
Department of Neurosciences

Amyloid load in the brain of cognitively intact older adults

Katarzyna ADAMCZUK

Jury

Promoter:	Prof. dr. Rik Vandenberghe	
Chair:	Prof. dr. Bénédicte Dubois	Dissertation presented
Jury members:	Prof. dr. William Klunk	in partial fulfilment
	Prof. dr. Eric Salmon	of the requirements
	Prof. dr. Jos Tournoy	for the degree of Doctor
	Prof. dr. Wim Van Paesschen	in Biomedical Sciences

September 2015

Financial support by the Research Foundation - Flanders (FWO) (PhD fellowship, G.0660.09), SAO-FRMA (09013, 11020, 13007), KU Leuven (OT/08/056, OT/12/097), IWT VIND, IWT TGO BioAdapt AD, Belspo IAP (P7/11) and GE Healthcare Ltd. is gratefully acknowledged.

"Only those who will risk going too far
can possibly find out how far one can go."
T.S. Eliot

Contents

Abbreviations **5**

1 Introduction **7**

1.1 Pathological hallmarks of Alzheimer's disease 7

1.2 Why is Aβ pathology particularly interesting? 8

1.2.1 Long accumulation phase of Aβ peptides 8

1.2.2 Amyloid−positive cognitively normal elderly 9

1.2.3 Preclinical Alzheimer's disease 10

1.3 Biomarkers of brain Aβ amyloidosis 11

1.3.1 Amyloid positron emission tomography 12

1.3.2 Cerebrospinal fluid Aβ42 12

1.4 Genetic effects on amyloid load 14

1.4.1 Polymorphism of apolipoprotein E 15

1.4.2 Other genetic factors 15

1.5 Functional brain activity and amyloid load 16

1.5.1 Language and associative-semantic system 16

1.5.2 Memory domain 17

1.6 Aims of the thesis 18

2 Experimental techniques **21**

2.1 Positron emission tomography 21

2.1.1 Principles, acquisition, and reconstruction 21

2.1.2 Preprocessing 22

2.1.3 Signal quantification 23

2.1.4 Statistical analysis 24
2.2 Magnetic resonance imaging 24
2.2.1 Basic principles 24
2.2.2 Functional MRI principles and acquisition 25
2.2.3 Preprocessing 26
2.2.4 Signal modelling and statistical analysis 26
2.3 Neuropsychological tests 27
2.3.1 Conventional tests 27
2.3.2 Experimental language tests 28

3 Polymorphism of brain derived neurotrophic factor influences β amyloid load in cognitively intact apolipoprotein E ε4 carriers 29
3.1 Abstract 29
3.2 Introduction 30
3.3 Subjects and methods 31
3.3.1 Subjects 31
3.3.2 Image acquisition 31
3.3.3 Image analysis 32
3.3.4 Relationship to episodic memory test scores 34
3.4 Results 35
3.4.1 Effect of APOE and BDNF polymorphisms on SUVR . 35
3.5 Discussion 40

4 Functional changes in the language network in response to increased amyloid deposition in cognitively intact older adults 45
4.1 Abstract 45
4.2 Introduction 46
4.3 Materials and methods 47
4.3.1 Participants 47
4.3.2 Experimental language tests 48
4.3.3 Functional MRI 50
4.3.4 Flutemetamol PET 52
4.3.5 Statistical analysis 54
4.4 Results 56

4.4.1 Analysis of behavioral scores during fMRI 56
4.4.2 Whole-brain voxelwise analysis 57
4.4.3 Genotype effect on fMRI response and relationship between fMRI response and SUVR 62
4.4.4 Relationship with offline language measures 63
4.5 Discussion 63

5 Amyloid imaging in cognitively normal older adults: Comparison between ^{18}F-flutemetamol and ^{11}C-Pittsburgh Compound B 69
5.1 Abstract 69
5.2 Introduction 70
5.3 Materials and methods 71
5.3.1 Participants 71
5.3.2 Amyloid PET 72
5.3.3 Statistical analysis 75
5.4 Results 75
5.5 Discussion 81
5.5.1 Conclusion 83

6 Diagnostic value of cerebrospinal fluid Aβ ratios in preclinical Alzheimer's disease 85
6.1 Abstract 85
6.2 Introduction 86
6.3 Methods 86
6.3.1 Participants 86
6.3.2 Amyloid PET 87
6.3.3 Lumbar puncture and CSF analysis 89
6.3.4 Statistical analysis 89
6.4 Results 90
6.5 Discussion 92
6.5.1 Added value of Aβ isoforms Aβ38 and Aβ40 94
6.5.2 Ratio of Aβ42 over total tau 94
6.5.3 Potential study limitations 95
6.5.4 Conclusion 95

7 General discussion **97**

7.1 Preclinical AD in practice 97

7.2 Neuronal response to amyloid injury 101

7.3 Clinical applicability 104

Summary **107**

Samenvatting **109**

Bibliography **111**

Acknowledgements **141**

Curriculum vitae **145**

Abbreviations

Aβ	amyloid β
AD	Alzheimer's disease
ANOVA	analysis of varience
APOE	apolipoprotein E
AUC	area under the ROC curve
BOLD	blood oxygenation level dependent
CDR	clinical dementia rating
Comp	composite cortical VOI
CSF	cerebrospinal fluid
CT	computed tomography
ELISA	enzyme-linked immunosorbent assay
fMRI	functional magnetic resonance imaging
FWE	family-wise error
FWHM	full width at half maximum
GM	grey matter
GWAS	genome-wide association study
HC	healthy controls
MCI	mild cognitive impairment
MMSE	Mini-Mental State Examination
MNI	Montreal Neurological Institute
MR(I)	magnetic resonance (imaging)
MTG	middle temporal gyrus
PET	positron emission tomography
PIB	Pittsburgh compound B
PVE	partial volume effect
RF	radiofrequency
ROC	receiver operating characteristic
RT	reaction time
SD	standard deviation
SOT	standard-of-truth
STS	superior temporal sulcus
SUVR	standardized uptake value ratio

TE	echo time
TR	repetition time
Ttau	total tau
VOI	volume of interest
WM	white matter

1 Introduction

Parts of this chapter have been published as:

1. Rik Vandenberghe, Katarzyna Adamczuk, Patrick Dupont, Koen Van Laere, Gaël Chételat. Amyloid PET in clinical practice: Its place in the multidimensional space of Alzheimer's disease. 2013 *Neuroimage Clin* 26:497-511.
2. Rik Vandenberghe, Katarzyna Adamczuk, Koen Van Laere. The interest of amyloid PET imaging in the diagnosis of Alzheimer's disease. 2013 *Curr Opin Neurol* 26:646-655.

1.1 Pathological hallmarks of Alzheimer's disease

Cognitive and behavioral decline due to neurodegenerative disease is highly prevalent across the world. Apart from the pervasive personal and familial impact, the public health burden may become unsurmountable for healthcare systems over the next decades [1, 2] unless more efficacious interventions to prevent, halt or slow down Alzheimer's disease (AD) [3] are discovered. The ability to characterize directly in humans the underlying pathophysiological processes is fundamental to progress in AD research and therapy. The initial abnormalities in AD probably occur at the functional level, involving synaptic and neuronal dysfunction, possibly initiated by abnormalities in soluble amyloid β42 (Aβ42). The exact temporal relationship between the diverse structural alterations that follow is still a matter of active neuropathological and in vivo research.

The principal structural changes are:

- Aβ amyloid aggregates, which may take different forms [4]: According

to some authors, diffuse plaques should not be considered as pathological since they are not associated with synapse loss or neuronal loss, key features of Alzheimer's disease [5]. Others have suggested that diffuse amyloid plaques are related to the presymptomatic stage of AD [6]. In contrast to diffuse plaques, neuritic plaques stain with thioflavine S or Bielschowsky, indicative for the presence of tau pathology invading or surrounding the plaque. A time sequence analogous to that described for neurofibrillary tangles (NFTs) has been developed to describe the propagation of amyloid, starting in neocortical areas (phase 1) and then spreading to allocortical regions including, among other regions, entorhinal cortex, cornus ammonis 1 (CA1), anterior and posterior cingulate (phase 2), basal forebrain nuclei, diencephalic nuclei and striatum (phase 3), brain stem nuclei (phase 4) and further into the molecular layer of the cerebellum (phase 5) [7]. At a certain stage the increase in β amyloid aggregates may level off, also referred to as a 'growth arrest' of the amyloid plaques [8, 9].

- Neurofibrillary tangles (NFT) and neuropil threads [4]. Initially, neurofibrillary tangles are mainly present in entorhinal and perirhinal cortex spreading to the hippocampus (stage I/II). They subsequently spread to inferior temporal and lateral temporal cortex (stage III/IV) and then become widely distributed over neocortical association zones (stages V/VI) [10, 4, 11]. These NFT stages correlate relatively well with neuronal loss and with the severity of clinical symptoms [12, 13, 14, 15, 16, 17, 18].

- Loss of synaptic density [19, 20, 21, 22], starting in the dentate gyrus and correlated to episodic memory scores [21].

- Neuronal loss, starting in entorhinal cortex [23], and correlated to cognitive scores [15].

1.2 Why is Aβ pathology particularly interesting?

1.2.1 Long accumulation phase of Aβ peptides

There is a general consensus that Aβ amyloid aggregation is a fundamental feature of AD [24]. The interesting characteristic of this process is that it begins years before clinical symptoms. Studies in Alzheimer's disease mutation carriers showed that increased amyloid load can be detected by amyloid positron emission tomography (PET) tracers 15 years before expected symptom onset [25, 26] and by cerebrospinal fluid (CSF) Aβ42 levels 25 years before the symptoms [26] (Figure 1.1). These fundamental findings showed that Aβ accumulation could be used as an early biomarker for AD-related changes. This is in agreement with one of the most influential current AD models [27, 28],

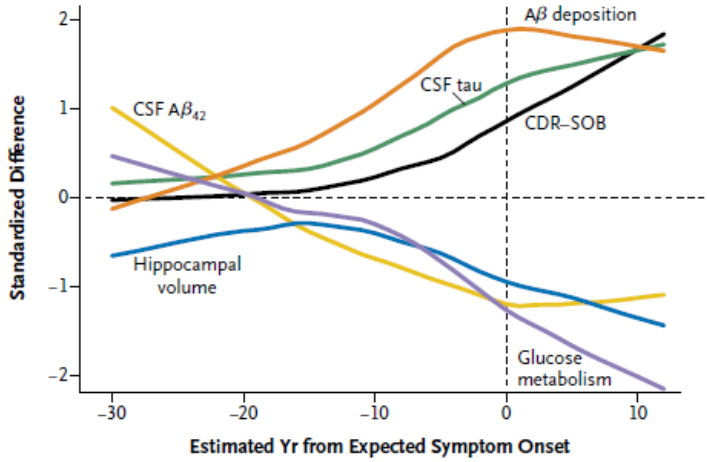

Figure 1.1: Biomarkers' changes as a function of years from expected Alzheimer's disease symptom onset. Standardized differences between mutation carriers and non-carriers indicated that decreasing CSF Aβ42 and increasing PET Aβ are the earliest detectable changes, followed by increasing CSF tau, hippocampal atrophy and hypometabolizm, and cognitive decline (CDR-SOB: Clinical Dementia Rating - Sum of Boxes). Adapted from [26].

which assumes that CSF alterations in Aβ42, amyloid aggregation, volume loss on structural magnetic resonance image (MRI) and cognitive decline follow an orderly temporal sequence, initiated by changes in amyloid and culminating in the clinical expression of cognitive symptoms. On the contrary, alternative models emphasize the partial independence of the different in vivo measures of Alzheimer's disease [29, 30, 31, 32]. Therefore, the definite role of Aβ accumulation in AD-related neurodegeneration needs further clarification. So far, we can conclude that (1) change in Aβ level occurs early in the disease, making it a useful early AD biomarker, and (2) together with other factors it contributes to the disease progression.

1.2.2 Amyloid−positive cognitively normal elderly

Neuropathological studies show that a substantial portion of healthy older subjects has increased levels of amyloid β in their brains without cognitive deficits [33, 34, 35, 36]. Concordantly, PET scans with amyloid tracers show that a proportion of healthy older subjects has a positive amyloid scan, which can be indistinguishable from what is seen in clinically probable AD (see for review [37]). The proportions of subjects with increased Aβ in their brain are variable in different studies and strongly dependent on the age of the subjects. The

prevalence of a positive amyloid scan below the age of 60 years in the absence of clinical symptoms is observed in around 13% of subjects [38], so that a positive scan is more likely to be related to the clinical symptoms compared with the older age group. At the other end of the age spectrum, a third of cognitively intact subjects above the age of 78 [39, 40] has a positive amyloid scan, and 50% above the age of 82 [41]. As a consequence, the specificity in terms of a clinical disease diagnosis necessarily will be relatively lower in this age group. Nonetheless, an amyloid-positive finding has an important prognostic implication. Cognitively intact amyloid-positive subjects show more cognitve decline during up to 10 years preceding the scan than amyloid-negative subjects, even when matched for Apolipoprotein E $\varepsilon 4$ status [42]. Increased Aβ load is associated with a higher chance to convert to mild cognitive impairment (MCI) or AD [43] and a greater rate of grey matter atrophy [44]. Similarly, cerebrospinal fluid Aβ42 levels are also abnormal (lower) in a considerable proportion of the cognitively intact elderly [45, 46, 47, 48, 49]. Asymptomatic mutation carriers, in one of three genes - amyloid precursor protein (APP), presenilin 1 (PSEN1), and presenilin 2 (PSEN2) - have lower CSF Aβ42 10 to 20 years before their estimated age of symptom onset and before the detection of cognitive decline [50]. In cognitively intact older adults reduced CSF Aβ42 is associated with faster global and hippocampal grey matter atrophy [51] and worse cognitive performance [52, 53]. Longitudinally, these subjects have faster and larger cognitive decline [52, 54] and are at increased risk for future pathological Aβ accumulation [49]. APOE $\varepsilon 4$ status also plays a role in decreased CSF Aβ42 levels and in higher cortical Aβ deposition [48].

1.2.3 Preclinical Alzheimer's disease

Preclinical AD, also termed asymptomatic AD, refers to the presence of AD-related pathophysiological processes, such as amyloid aggregation, in individuals who currently do not manifest cognitive deficits [55, 56] (Figure 1.2). According to National Institute on Aging and Alzheimer's Association (NIA-AA) criteria, subjects in preclinical stage 1 have a positive amyloid biomarker, such as amyloid PET scan or CSF Aβ42. In stage 2 they additionally have one or more positive biomarkers for neurodegeneration, such as (a) hypometabolism in an AD-like pattern on ^{18}F-fluorodeoxyglucose-PET, or (b) elevated CSF tau or phospho-tau levels, or (c) cortical thinning in typical AD areas or hippocampal atrophy on structural MRI. In stage 3 individuals additionally have evidence of subtle cognitive decline [55]. When these three stages of preclinical AD were evaluated in a population-based sample of 450 cognitively normal subjects an additional category was found to be necessary [39]. A SNAP category - suspected non-AD pathophysiology, which denotes subjects with normal amyloid biomarker but abnormal biomarker for neurodegeneration. In this sample 43% of individuals were classified as stage 0 (normal AD biomarkers and no evidence of subtle cognitive impairment), 16% as stage 1, 12% as stage 2, 3% as stage 3, and 23% as SNAP. Longitudinal follow-up studies of individuals in different

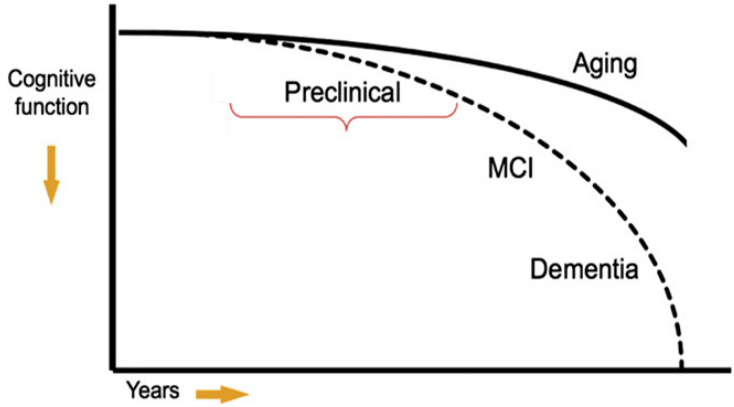

Figure 1.2: The clinical course of Alzheimer's disease. Preclinical Alzheimers's disease stage encompasses presympromatic autosomal dominant mutation carriers and asymptomatic biomarker positive individuals. Note that some individuals in the preclinical stage will not progress to clinical dementia. Adapted from [55].

stages showed that in preclinical stages 1-3 subjects had greater risk for progression to MCI or dementia [57] and future cognitive decline and mortality [58] than those in stage 0. Interestingly, the SNAP group had similar conversion rate to MCI as the amyloid-positive group [57]. Subjects in stages 2 and 3 had higher rates of medial temporal neurodegeneration compared with the other stages [59]. Such preclinical AD stages offer a window of opportunity for early preventive action. According to a commonly held view, disease-modifying therapies (e.g. anti-amyloid) may be most efficient in the earliest disease stages.

1.3 Biomarkers of brain Aβ amyloidosis

Modern techniques such as amyloid PET or CSF Aβ42 measurement allow one to detect brain amyloidosis directly in vivo. These biomarkers have been extensively studied in patients with AD and MCI, and have been widely accepted as biomarkers for the diagnosis of AD. Recommendations for the use of these biomarkers were included in the diagnostic guidelines for AD and MCI, from the NIA-AA [60, 61] and International Working Group (IWG) [62, 56, 63]. At present time they should be used to increase the certainty of AD dementia diagnosis as underlying cause of AD or MCI, but not yet for routine diagnostic purposes.

1.3.1 Amyloid positron emission tomography

The amyloid PET tracers developed to date belong to various chemical classes. According to a postmortem study of homogenized brain tissue in AD and controls, thioflavin T derivatives (such as ^{11}C-Pittsburgh compound B (PIB) and its derivative ^{18}F-flutemetamol), stilbenes (^{18}F-florbetapir and ^{18}F-florbetaben, among others), and benzofuranes (^{18}F-NAV4694) share a common high-affinity binding site that explains most of the signal in AD [64]. At the time of writing three ^{18}F-labeled tracers were approved by the Food and Drugs Administration (FDA) and European Medicines Agency (EMA) for estimation of amyloid plaques in patients evaluated for cognitive decline: ^{18}F-flutemetamol [65, 66] (Figure 1.3), ^{18}F-florbetaben [67], and ^{18}F-florbetapir [68]. The majority of the currently available ^{18}F-ligands has been compared in vivo with ^{11}C-PIB [31, 69]: Neocortical values for retention of ^{18}F-amyloid ligands correlate well with neocortical values of retention of ^{11}C-PIB. For ^{18}F-florbetapir [70, 71], the regression slope is less steep than for other ligands, suggesting a smaller dynamic range [31, 69]. For the ^{18}F-ligands in general, correlation in subcortical white matter is much lower, and only ^{18}F-AZD4694 has a high correlation value with ^{11}C-PIB also in white matter [72]. Test-retest values (% difference between two time points divided by the average obtained at the two time points) of standardized uptake value ratios (SUVRs) for a composite cortical volume of interest with cerebellum as reference have been reported for ^{18}F-flutemetamol (1.5%, S.D. 0.7) [73], ^{18}F-florbetapir (2.4%, S.D. 1.41) [74], ^{18}F-florbetaben (6.2%, range 0.6-12.2) [75] and ^{18}F-NAV4694 (7.5%, S.D. 6.5) [76]. Fleiss' κ has been reported for ^{18}F-flutemetamol (0.86-0.96) [73, 77], ^{11}C-PIB (0.90) [78], ^{18}F-florbetapir (0.58-0.76) [74, 79] and ^{18}F-florbetaben (0.60 [80]; 0.89-0.94 [81]). Cohen's effect sizes to discriminate AD from healthy controls vary from study to study, even for the same compounds, ranging between 1.3 and 3.8 [78, 80, 75, 82, 72, 81]. So far no published studies are available that have directly compared performance between ^{18}F-amyloid ligands within the same subjects in vivo which would be highly informative for the clinician.

1.3.2 Cerebrospinal fluid Aβ42

CSF assay is commonly used in clinical workup to measure markers of AD pathology: Aβ42, total tau protein (t-tau), and tau phosphorylated at threonine 181 (p-tau). CSF Aβ42 reflects fibrillar brain Aβ deposits as was shown by postmortem samples [83] and cortical biopsies [84]. Lower levels of Aβ42 in CSF are observed in clinically probable AD [85, 86, 87, 58] and MCI patients [88] compared with controls (Figure 1.4), and they predict progression to clinically probable AD in MCI and older controls with high accuracy up to 10 years before the onset of severe cognitive symptoms qualifying for dementia due to Alzheimer's [89, 46, 90, 58]. Amyloid peptide in the CSF can be detected by means of different methods. In one of the common procedures, after collection of the CSF (with or without a priori fasting), the sample is

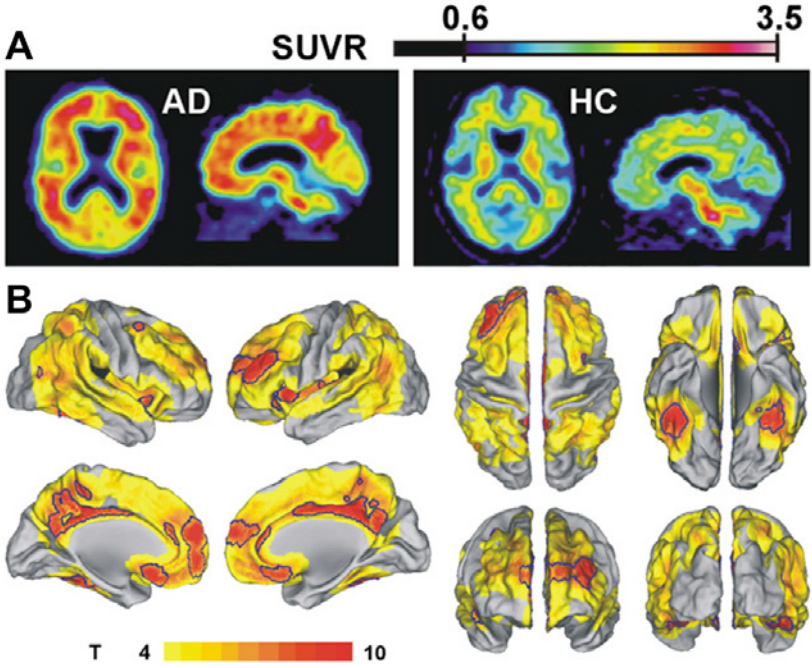

Figure 1.3: Amyloid PET scan with ^{18}F-flutemetamol tracer. (A) On the left side standardized uptake value ratio image of AD patient, on the right side healthy control (HC). (B) Areas with increased amyloid deposition in AD compared with HC. Voxel-level $P_{uncor} = 0.001$. Areas outlined in blue: voxel-level $P = 0.05$ corrected for whole brain volume. Adapted from [66].

analyzed for the presence of Aβ42 peptide by enzyme-linked immunosorbent assay (ELISA). Analysis is usually performed with the commercially available ELISA kits or with in-house developed assays. In principle, amyloid peptide is captured by a first monoclonal antibody, then the sample is incubated with a second biotinylated antibody. The biotinylated antibody is detected by the pereoxidase-labeled streptavidin and after addition of the substrate solution the sample will develop a color, whose intensity is a measure of the target peptide concentration. The high within and between-laboratory variability in the CSF biomarker levels due to assay-related pre-analytical and analytical factors is an important issue [91, 92, 93]. The cut-off values, which are used to dichotomize individuals in the AD or non-AD CSF pattern, are affected by this variability. Several studies have investigated the agreement between CSF Aβ42 assay and amyloid PET, showing that CSF Aβ42 is inversely correlated with cortical uptake of different amyloid tracers in AD, MCI and healthy older adults (with ^{11}C-PIB [94, 95, 96, 97, 50], with ^{18}F-florbetapir [98, 99], and with ^{18}F-flutemetamol [100]). Dichotomization based on ^{11}C-PIB is highly concordant with that based on CSF Aβ42 [101]. When ^{18}F-florbetapir and

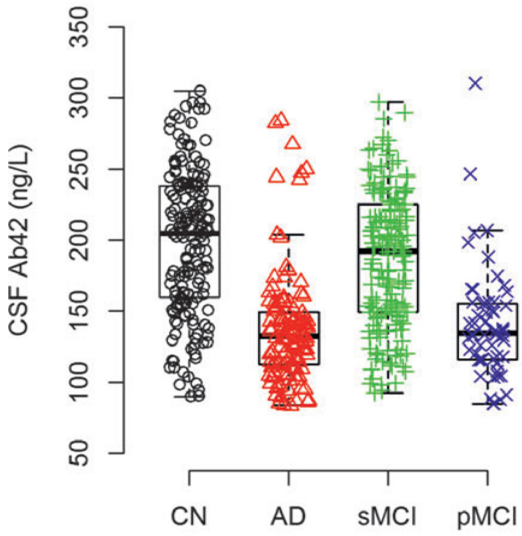

Figure 1.4: Cerebrospinal fluid Aβ42 levels in different populations. Cognitively normal subjects (CN), Alzheimer's disease patients (AD), and individuals with stable and progressive mild cognitive impairment (sMCI and pMCI). Adapted from [99].

CSF Aβ42 were compared, discordance occurred more frequently but overall they were consistent in the majority of subjects [98]. Regardless of the good correlation and similar discriminative power for amyloid positivity, CSF Aβ42 and amyloid PET provide partially independent information and measure different aspects of AD amyloid pathology [102, 103]. In CSF a soluble amyloid β protein is measured [104], whereas PET measures an aggregated (insoluble) form of amyloid β [105]. For a more in-depth discussion of the relationship between soluble Aβ42 in the brain and in CSF refer to *Chapter 7* page 100.

1.4 Genetic effects on amyloid load

The process of Aβ accumulation, as all other biological processes in our body, is influenced by a variety of factors. Except age, genetics is a second main risk factor for increased brain amyloid load in AD, MCI and cognitively intact older subjects. Downstream to the Aβ accumulation, cognitive reserve, environmental factors or brain diseases may influence how one's brain responds to the Aβ pathology [55].

1.4.1 Polymorphism of apolipoprotein E

The strongest genetic factor modulating brain amyloid levels is the apolipoprotein E (APOE) gene. The APOE gene is located on chromosome 19. Its two single nucleotide polymorphisms (SNP) at loci rs429358 and rs7412 cause amino acid substitutions at codons 112 and 158 in the ApoE protein. These SNPs make up three possible alleles: $\varepsilon 2$, $\varepsilon 3$, $\varepsilon 4$. The most common and neutral form is $\varepsilon 3$, $\varepsilon 2$ is less common and may have a protective effect on amyloid accumulation [106]. The APOE $\varepsilon 4$ is a dose-dependent risk factor for late-onset and early-onset AD [107, 108]. The lifetime risk for AD is 30-40% in people with one $\varepsilon 4$ allele, in $\varepsilon 4$ homozygotes it is as high as 90%, and in $\varepsilon 4$ non-carriers it is around 9% [109, 110]. The conversion risk from HC to AD or MCI conferred by the APOE $\varepsilon 4$ is greater in women than in men [111]. In a dose-dependent manner, APOE $\varepsilon 4$ is associated with increased brain amyloid deposition in AD, MCI and healthy older adults as evidenced by amyloid PET scan [112, 113, 114] and Aβ42 in CSF [115, 116, 117, 48]. The majority of neuropathological studies showed that APOE $\varepsilon 4$ AD patients have more pronounced amyloid pathology compared with non-$\varepsilon 4$ patients [118]. The detrimental effect of APOE $\varepsilon 4$ on amyloid deposition is consistent among studies in cognitively intact older adults, however, in clinical AD patients the effect on amyloid load is less consistent [119]. This effect is more pronounced in specific regions, namely in the lateral and medial frontal cortex, temporoparietal cortex, and posterior cingulate-precuneus [112, 113, 114]. Throughout the disease progression this regional pattern remains unchanged, only the amyloid deposition becomes stronger [112, 114]. The mechanism through which the $\varepsilon 4$ variant affects amyloid burden is probably related to the impaired clearance of soluble Aβ. One of the potential mechanisms could be that the $\varepsilon 4$ isoform competes with soluble Aβ peptides for the same receptors/transporters responsible for the metabolism of soluble Aβ species [120, 121].

1.4.2 Other genetic factors

A family history of AD is associated with increased brain amyloid levels and increased risk for developing AD [122, 123], beyond what can be explained by APOE alone. Subjects with a maternal family history of late onset AD in particular, have higher amyloid tracer binding in well-established areas of amyloid deposition, compared with subjects without or with paternal family history [124]. These individuals also manifest decreased CSF Aβ42 levels and this is independent from the effect of APOE $\varepsilon 4$ [125].

Among non-APOE susceptibility genes for AD, several genetic variants identified by genome wide association studies influence brain amyloid levels. For instance, SNP rs6656401 [126] and rs6701713 in the CR1 gene, and two other SNPs in ABCA7 (rs3764650) and CD2AP (rs9349407), plus several newly identified variants [127], were associated with neuritic plaque burden at autopsy. In terms of genetic interactions, the minor allele in BIN1 (rs7561528 or

rs744373) together with the common allele in PICALM (rs7851179) [128], as well as the common allele in CR1 (rs3818361) together with the minor allele in APOE [129], were associated with higher amyloid PET burden. One SNP in an intronic part of the DHCR24 gene (rs7551288) revealed a protective effect against amyloid accumulation [130].

The non-APOE risk genes have small observed effects and they do not explain the whole genetic variation associated with late onset AD [131]. Therefore, new genetic variants explaining the missing heritability remain to be found. For instance, one of the potential candidate genes could be the brain derived neurotrophic factor (BDNF). Given the prominent role of BDNF in neuroplasticity and a failure of neural plasticity as a potential common theme in AD [17], BDNF could theoretically be linked to AD-related processes at the molecular, neuronal or systems level. Thus, BDNF polymorphisms (for instance at SNP rs6265) could influence the resilience against β amyloid related changes.

1.5 Functional brain activity and amyloid load

Task-related fMRI can reveal adaptive changes in cognitive brain circuits during cognitive processing which may provide resilience against the functional impact of amyloid pathology. Brain resilience and functional reorganisation may gain importance in the field as AD therapies may increasingly target multiple facets of AD. To the best of our knowledge, three studies combined amyloid PET and task-related fMRI within the same subjects in MCI or AD.

1.5.1 Language and associative-semantic system

The first study focused on changes in the language circuit in early-stage clinically probable AD and how this is related to amyloid ligand retention [132]. This study built on a preceding study in amnestic MCI. In amnestic MCI, the earliest changes in the language network occur in the posterior part of the left superior temporal sulcus (STS) (Figure 1.5) and these changes correlate with subclinical changes in written word identification speed, in line with the critical role of this region in lexical-semantic retrieval [133]. In early-stage AD hypoactivity is also seen in left posterior temporal cortex during associative-semantic versus visuoperceptual processing. These fMRI changes in the left posterior STS in AD correlate with offline measures of confrontation naming: clinically probable AD subjects with hypoactivity in this region are impaired on confrontation naming [132]. There is no correlation between ^{11}C-PIB levels in this region and the clinical deficit [132]. fMRI activity levels to the homotopical right side show increased activity in those patients who had preserved naming on the confrontation naming, suggestive of a compensatory increase [132].

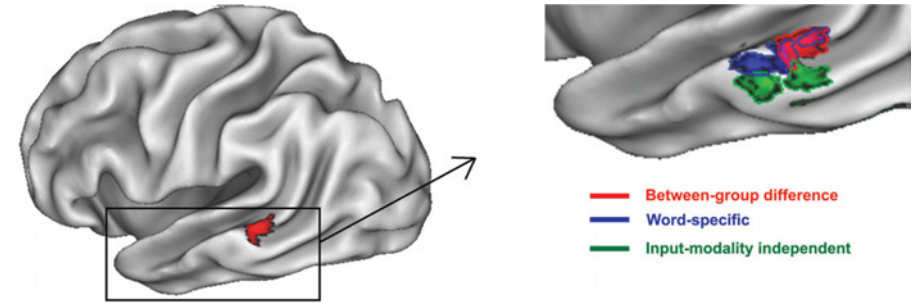

Figure 1.5: **Earliest functional changes in the language system.** Higher activity in the posterior superior temporal sulcus in the associative-semantic task compared with the visuoperceptual task: in controls compared with MCI (red), for words more than pictures (blue), and for words and pictures (green). Uncorrected $P < 0.001$. Adapted from [133].

1.5.2 Memory domain

Other studies focused on the episodic memory domain. In a study with MCI subjects, the effect of a positive amyloid scan on hippocampal fMRI activity, hippocampal volume, and global cognition was evaluated cross-sectionally and longitudinally. At baseline, amyloid-positive MCI subjects had increased hippocampal activation during associative face-name memory encoding task and smaller hippocampal volumes. Longitudinally, these subjects continued to show increased hippocampal activation and decreased hippocampal volumes [134].

A combined ^{11}C-PIB-fMRI studies in healthy older adults revealed that amyloid-positive cases have increased activation in task-positive regions during an episodic memory encoding task of natural scenes, namely in ventrolateral prefrontal, lateral occipital, lateral parietal, posterior inferior temporal cortices, and the right parahippocampal/hippocampus [135, 136]. This increased activity was positively correlated with memory measures [135] and more detailed memory encoding [136]. Amyloid-positive subjects also had decreased deactivation in task-negative regions: posteromedial, medial prefrontal, and lateral temporoparietal cortices [135, 136]. Along the same lines, during encoding of associations between faces and names, the precuneus and temporoparietal cortex, partially overlapping with the posterior nodes of the default mode network, were less deactivated in amyloid-positive subjects compared to amyloid-negative subjects [137]. Deactivation in precuneus-posterior cingulate area is inversely related to hippocampal activation [138].

1.6 Aims of the thesis

In this PhD project we aimed to investigate different effects related to brain amyloid load in the cognitively intact older population. We combined diverse but complementary techniques, such as amyloid imaging- and fluid-biomarkers, functional MRI of the language and associative-semantic system, neuropsychological tests, and genetics to explain the variance in amyloid burden, topography, and effects on brain function.

Aim 1: Influence of BDNF and APOE polymorphisms on brain amyloid load

The first aim of this doctoral research project was to test whether genetic polymorphisms could influence the level of amyloid load in cognitively intact older individuals, and whether they could provide resilience against increased amyloid deposition. In particular, we evaluated if the BDNF *val* carriers were able to compensate for the presence of amyloid in a better way than *met* carriers, and if this was dependent on the APOE status (*Chapter 3*).

Aim 2: Effect of amyloid load on the language and associative-semantic system

The second aim of this doctoral research project was to investigate through which mechanisms cognitively intact volunteers are able to maintain their cognitive status despite a high amyloid load. By means of amyloid imaging and associative-semantic fMRI we investigated whether the increased amyloid load in cognitively intact older adults induced early functional changes in the language and associative-semantic system, and whether these adaptive changes in the language network differed between BDNF *met* carriers and non-carriers (*Chapter 4*).

Aim 3: Comparison of two amyloid imaging biomarkers for preclinical Alzheimer's disease

The third aim of this doctoral research project was to test which amyloid PET tracer was most suitable to identify subjects with abnormal (AD-like) levels of amyloid deposition. More specifically, we evaluated whether the ^{18}F-flutemetamol amyloid ligand was as accurate as its parent molecule ^{11}C-PIB in detecting cognitively intact older subjects with high amyloid load (*Chapter 5*).

Aim 4: Comparison between different CSF Aβ isoforms for detection of preclinical Alzheimer's disease

The fourth aim of this doctoral research project was to evaluate the added value of the various Aβ isoforms and their ratios via the intermediary of ^{18}F-flutemetamol PET and also compared this to the ratio between Aβ42 and total tau. More specifically, we evaluated which of the following, Aβ42, Aβ40, Aβ38 isoforms, total tau, the Aβ42 ratios over Aβ40, Aβ38 and ttau, were most accurate in detecting cognitively intact older subjects with elevated amyloid load defined by a positive ^{18}F-flutemetamol PET (*Chapter 6*).

2 Experimental techniques

2.1 Positron emission tomography

In this project we utilized two positron emission tomography tracers which bind to cortical neuritic plaques [139, 140, 141, 142]: ^{18}F-flutemetamol [66, 65] and ^{11}C-PIB [105]. These and other amyloid tracers are described in *Section 1.3.1.* Basic principles, acquisition, processing, and statistical analysis of a PET scan are described in the following part of this chapter.

2.1.1 Principles, acquisition, and reconstruction

Positron emission tomography is an imaging technique which relies on spatial detection of radioactively labelled molecules. In a cyclotron ^{14}N is bombarded with protons to produce ^{11}C and ^{18}O is bombarded with protons to produce ^{18}F (as fluoride ions). Such unstable radioisotopes (^{11}C, ^{18}F) are later coupled to a molecule of interest. The radio-labelled molecule (tracer) is injected into the blood stream and is distributed according to its physiological function. To reach the steady state a proton inside a radionuclide nucleus is converted into a neutron while releasing a positron and an electron neutrino, this is called a beta+ decay. Within few millimetres the emitted positron collides with an electron. As a consequence their masses annihilate and two photons of 511 keV are produced, which travel in opposite directions at approximately 180 degrees. Photons are detected in the scintilation crystals of a PET camera connected to the photomultipliers, which convert photons into an electric current and then amplify and measure it. An electronic coincidence circuit evaluates timing of the absorbed photons and only the pairs of photons which arrive near simultaneously at the opposite PET camera crystals (coincidence pairs) are passed through. The number and place of origin of the coincident detections along the same line are recorded. It is important to note, that photons interact with the

tissue through which they travel, thereby attenuating their kinetic energy. Usually, a low dose CT scan is acquired before the PET scan to measure densities of different tissues and to estimate a fraction of lost signal. This is used then to correct for the attenuation effects before the PET image is reconstructed. Two other common interactions with tissue are scattered and random coincidences. During a scattered coincidence a travelling photon interacts with an electron and changes its direction. Photons are then detected by two scintilators which are not opposite to each other. A random coincidence occurs when photons from two different annihilation events are picked up by opposite scintilator crystals within the time window of a coincidence. Both scatter and random events lead to wrong predictions of the line of response and place of origin of the true coincidence. This blurs the image and introduces noise to the signal, therefore, images must be corrected for these events before the reconstruction [143].

Measured coincidences (i.e. counts) are assigned to a particular line of response at a particular angle. All coincidences are then placed in 2D images named sinograms, which represent counts measured for all projection lines at each available angle. Sinograms are later reconstructed to visually interpretable images by backprojection algorithms, which as the name says, project back a value measured at a certain line to the whole line, for each angle. Many reconstruction algorithms exist today, such as filtered back projection or iterative reconstruction. One of the often applied iterative algorithms is ordered subsets expectation maximization. This method a priori takes into account information about noise in the signal and includes a non-negativity constraint. These features together with the iterative mode generate superior quality images, however at the cost of longer processing time [143, 144].

2.1.2 Preprocessing

Images corrected for attenuation, scatter, and random coincidences are rebinned into time frames. Depending on the reconstruction method, time frames are either specified in advance or rebinned after the reconstruction. When defining the time frames one should take into account that each frame should have a similar tracer distribution and sufficient counts. In case of a "dynamic" scan, data is acquired from the start of tracer injection, with shorter frames at the beginning gradually extending into longer ones e.g. 4 x 15 s, 4 x 60 s, 2 x 150 s, 12 x 300 s. For a "static" scan, acquisition is started from the point in time when the tracer reaches a stable distribution e.g. after 90 min for ^{18}F-flutemetamol with 6 frames of 5 min. Since the PET scanning time is longer some motion is inevitable and frames should be spatially aligned to correct for potential head motion. Within the same imaging modality rigid transformation (6 parameters: 3 rotation and 3 translation parameters) can be used to align the frames. For further processing of a static scan a sum or an average of the aligned frames is used. In order to perform group analysis, an individual subject's sum or average PET image should be spatially normal-

ized to a common stereotactic space such as the Montreal Neurological Institute (MNI) space. If volumetric T1-weighted MR scan is available, it can be utilized to more precisely transform the PET image into the atlas space. MR images have much higher resolution and contain more detailed information about the anatomy. Also, the transformation will not depend on the tracer uptake, as in the case of PET-based spatial normalization. PET and MR images must be first coregistered to each other. These are two different modalities, therefore, a more detailed method such as an affine transformation with 12 parameters (additionally 3 zoom and 3 skew parameters) is advisable. The coregistered MR is spatially normalized to the T1 template in MNI space. One option to do this, recommended in Statistical Parametric Mapping (SPM) software [145], is to use a unified segmentation approach. This generates three segmentations, grey matter, white matter, and cerebrospinal fluid, and non-linear transformation parameters. The transformation parameters are then applied to the PET scan to bring it to MNI space [144].

2.1.3 Signal quantification

To measure specific tracer retention the PET signal needs to be quantified either by a full kinetic modelling or simplified models applied to each voxel. In the process of kinetic modelling measured data are fitted to a mathematical model to predict tracer behaviour. It requires measuring tracer concentration in arterial blood plasma (input function - reflects the amount of tracer available for binding) and measuring tracer concentration in a target tissue e.g. brain (output function at multiple time points). Tracers often form metabolites outside the brain and the input function needs to be corrected for that. To measure target concentration in the brain across time, a dynamic scan is required. Lastly, a proper mathematical model needs to be selected. Such complex but precise modelling is favoured for new tracers, whose behaviours need to be studied in detail. Often, it is possible to simplify models by making certain assumptions and validating the results versus the original full model. An example of such simplified quantification is a reference tissue model. Instead of an input function it employs a reference region, which contains only non-specifically bound and unbound tracer. A further simplification could be to only use static images at later time points when tracer uptake is considered at steady state. Standard uptake value ratios (SUVR) can be used to create parametric images by dividing the tracer concentration in the tissue of interest e.g. cerebral cortex by the uptake in the reference region e.g. cerebellar grey matter. In this way signal is corrected for the non-specifically bound and unbound tracer [144].

Important confounds that PET images may suffer from are partial volume effects (PVE). They arise from a low spatial resolution of the PET images, which is about 4 to 8 mm of full width at half maximum (FWHM). When the structures of interest are smaller than the sampling resolution, e.g. cerebral grey matter, the measured signal is an average of the tracer uptake in a target

and surrounding tissues. PVE pose a concern especially when the effect of interest is a decrease in tracer binding. For example, a lower signal may stem from a true decreased tracer concentration or from atrophy in the grey matter. One of the common partial volume correction methods uses a volumetric MR image [146]. Grey matter, white matter, and cerebrospinal fluid segmentations are used to estimate different tissue fractions per voxel in order to determine corrected tracer concentration per unit volume of grey matter [144, 146].

2.1.4 Statistical analysis

Before entering the statistical analysis, images should be spatially smoothed. Smoothing improves the signal-to-noise ratio, reduces inter-subject anatomical variability (even after spatial normalization subjects' brains slightly differ in shape and size), and it is required by the Random Field Theory which is used to correct for multiple comparisons during the statistical analysis. The size of the smoothing kernel should correspond to the size of the expected effect.

To explore tracer binding differences or its relationship to different variables between subjects, images must be statistically analysed. Voxel-based analysis will identify which voxels show significant change in tracer binding. SPM performs a statistical test in every voxel of the brain. The dependent variable is the voxel value of the image and independent variables or covariates, such as age or genotype, are the same across all voxels. Since a statistical test is performed in each voxel of the brain, correction for multiple comparisons must be employed to correct for false positive findings. In SPM family-wise error (FWE) correction is used based on Random Field Theory. FWE correction estimates the likelihood of finding a significant group of voxels just by chance, taking into account the number of resolution elements (not voxels) in the whole brain volume. FWE corrected P values are generated for the voxel-level: the highest Z value, for the cluster-level: the cluster of voxels above a certain Z value, and for the set-level: set of clusters above a certain Z value [147]. Significance is often tested at the combined voxel- and cluster-levels [148]. One can also restrict the analysis to a particular volume of interest, hereby reducing number of statistical tests. In another approach, one can calculate a mean value in cerebral cortex or in volumes of interest, and this can be analysed by standard statistics. These values can also be used to dichotomize subjects in tracer positive (increased uptake) or tracer negative (decreased uptake), and they may be used to predict changes in other variables.

2.2 Magnetic resonance imaging

2.2.1 Basic principles

Magnetic resonance imaging is a powerful technique to visualize anatomy and physiology of the human body. It can be used to study anatomical and func-

tional organization of the brain. It measures the protons in tissues (hydrogen atoms), which spin around their axis creating a magnetic dipole. In the absence of an external magnetic field (B0), protons (or spins) are randomly oriented resulting in a net magnetization close to zero. When an external magnetic field is applied during MR scan (the static magnetic field in the MRI scanner is typically 1.5 or 3 Tesla), a small majority of spins aligns with the direction of the magnetic field generating a net magnetization (longitudinal magnetization). The aligned spins precess along the direction of the magnetic field with the Larmor frequency, which is proportional to the strength of B0. The precessing spins are out of phase, therefore the transverse magnetization perpendicular to the direction of the magnetic field is zero. When a radiofrequency (RF) pulse is applied at the Larmor frequency the aligned spins tilt away by 90° (or another flip angle can be used) and they start precessing in phase. Hence, the longitudinal magnetization decreases and transverse magnetization increases. As soon as the RF pulse is terminated spins return to the low energy state and the net magnetisation becomes once again parallel to the B0. This process, which is termed relaxation, is characterized by two time constants. The T1 time constant describes the time point at which longitudinal magnetization recovers to 63% of its original value. A simultaneous but separate time constant is T2, it describes the time point at which transverse magnetization drops to 63% of the original value. T2 depends on the spin-spin interactions in the surrounding microenvironment. Different tissues, such as grey matter, white matter, bone, fat, cerebrospinal fluid, have distinct T1 and T2 time constants. By manipulating the time of read out of the signal, adapted to specific T1 and T2 constants, one can visualize distinct tissue classes. To spatially localize the protons three magnetic gradients are superimposed on the main magnetic field. Gradients change the strength of the magnetic field in different spatial locations, therefore each spin has slightly different precession frequency and can be precisely localized. The transverse magnetization induces alternating current in receiver coils placed around individual's head in the xy-plane. This current is translated into sine (coils along y) and cosine (coils along x) waves. The combination of particular phase and frequency of each wave identifies a spatial location. In the final step frequency spectra are transformed into the spatial domain [143, 149].

2.2.2 Functional MRI principles and acquisition

Functional MRI (fMRI) is used to create images of brain activity in response to a particular task or during rest, indirectly by detecting blood oxygenation changes. Active neurons have increased demand for oxygen supply. To meet this need blood flow and volume in arterioles and venules surrounding active neurons increase. The composition of the blood changes in such a way that the relative amount of oxyhemoglobin to deoxyhemoglobin increases. This hemodynamic response to neuronal activity reaches its peak after around 6 seconds and then comes back to the original state. Oxyhemoglobin is diamagnetic (it has

weak magnetic properties) and deoxyhemoglobin is paramagnetic (it distorts the local magnetic field resulting in a signal decrease). The difference between oxy- and deoxyhemoglobin levels is the source of the blood oxygenation level dependent (BOLD) contrast, which is used in fMRI. Deoxyhemoglobin causes faster dephasing of spins (spin-spin interactions) and combined with field inhomogeneity leads to faster signal loss described by time constant T2*. A higher oxy- to deoxyhemoglobin ratio gives increased signal on the T2*-weighted images. Such images should be acquired by a fast imaging technique as echo planar imaging (EPI). During the EPI sequence a whole xy-plane is acquired after a single RF pulse thanks to rapidly changing gradients. Typically for an fMRI sequence, the time between two RF pulses should be longer (TR, e.g. 3000 ms) and time between RF pulse and data collection should be short (TE, e.g. 30 ms) [149].

2.2.3 Preprocessing

Similarly as for the PET data, fMRI scans need to be preprocessed to correct for some of the noise induced during data acquisition. An fMRI scan usually takes a longer time and is composed of many EPI volumes (images), therefore, to correct for potential head motion volumes are realigned to the first (or any other) acquired volume. The structural T1-weighted image is coregistered to the mean of the realigned fMRI images. This structural scan is then normalized to the T1 template in MNI space by a unified segmentation approach in SPM, producing three segmentations and transformation parameters. The transformation parameters are then applied to the fMRI scans to bring them to MNI space. The spatially normalized fMRI scans are smoothed with a Gaussian kernel, for the reasons explained before in *Section 2.1.2*. Depending on the design of fMRI study, slice-time correction may be necessary (taking into account that not all slices were acquired at the same time point of the hemodynamic response). In this project we used block design, which is considered less sensitive to the slice-time errors. In block design different tasks (conditions) are shown consecutively for few tens of seconds and they are repeated several times. Thus, the signal for a given condition is averaged over a wider time range, and additionally slice-time errors have similar effects on all conditions. The fMRI signal needs to be corrected for non-relevant frequencies coming from physiological or non-physiological sources. Examples of the physiological noise are periodic spin motions, such as breathing, heart beats, blood vessels pulsation. Scanner related drifts are one example of the non-physiological noise. Therefore, low and high-pass filters must be applied to remove too low or too high frequencies [143, 149].

2.2.4 Signal modelling and statistical analysis

In comparison to the PET images, where each voxel contains direct information about a metabolic process, specific brain activity cannot be directly deduced

from the preprocessed fMRI images. To interpret the fMRI signal, a specific question must be asked about a cognitive process and by comparison of the fMRI signal between the condition of interest and a control condition one can obtain meaningful images. Those images are statistical maps which show regions with significant signal change in response to a cognitive task. The analysis of fMRI images is done in two steps.

In the first step, variance in the fMRI signal is modelled at the individual subject level (fixed effects). It is assumed that the measured signal can be explained by a set of explanatory variables and an error term. In SPM the general linear model and standard least squares are used to estimate the contribution of each explanatory variable (condition) to the response variable for each voxel. Technically, an image is created containing a parameter estimate (β) in each voxel, which evaluates the contribution of a given condition to the fMRI signal in that specific voxel, these are β-images. To explore differences between conditions contrast images are created. A contrast image is a difference between β-images weighted for the variance in each voxel. To assess the significance of a contrast a t statistic is applied to each voxel and an image with all t-values is created.

In this project we were interested in specific activations from associative-semantic processing for words and pictures. The associative-semantic task was derived from the Pyramids and Palm Trees test [150], a classical neuropsychological test of associative-semantic processing for words and pictures. We created contrast of interest by comparing the associative-semantic condition with the visuoperceptual control condition. The control and task conditions were matched in terms of difficulty, visual stimulation, and number of right and left button presses. Thus, we believe that this contrast specifically probes associative-semantic language areas.

In the second-level analysis, the individual contrast images are used for a random effects analysis. Hence, it allows for inferences about the population from which the subjects were drawn. Statistical tests as linear regression, two-sample t test, factorial analysis of variance, etc. can be employed at this level. Since the statistical test is applied to each voxel a correction for multiple comparisons must be performed. Different approaches for this are explained in *Section 2.1.2*.

2.3 Neuropsychological tests

2.3.1 Conventional tests

All participants included in this project underwent a conventional neuropsychological protocol which probed several cognitive domains. General cognitive functions, including orientation, memory, attention, language, and calculation, were tested by the Mini Mental State Examination [151], and Clinical Dementia Rating score [152]. Verbal episodic memory was examined by the Rey

Auditory Verbal Learning Test [153]. Language domain was assessed by the Boston Naming Test [154, 155], the Letter Verbal Fluency and the Animal Verbal Fluency [156]. Executive functions were tested with the Raven's Standard Progressive Matrices [157] and the Trail Making Test [158]. We used validated Dutch versions of all the tests.

2.3.2 Experimental language tests

Subjects who participated in the experiments described in *Chapter 3* and *Chapter 4* underwent three experimental neuropsychological tests: confrontation naming [159], lexical decision [160], and speeded word identification [133]. We have chosen these tests since they activate language related temporal areas, some of which are involved in the early language impairment in AD [161, 162, 163, 132]. All the tests were in Dutch. The confrontation naming task tested word-finding abilities. Subjects were asked to read aloud presented words belonging to different categories. The lexical decision task measured lexical-orthographic retrieval. Subjects were asked to decide with a button press if a presented word exists or not. The speeded word and picture identification task examined visual identification and higher-order lexical processes. Subjects were asked to read a word or name a picture, which were presented at various durations. In all 3 tasks we measured subjects' reaction times and accuracies.

3

Polymorphism of brain derived neurotrophic factor influences β amyloid load in cognitively intact apolipoprotein E ε4 carriers

This chapter has been published as:

Katarzyna Adamczuk, An-Sofie De Weer, Natalie Nelissen, Kewei Chen, Kristel Sleegers, Karolien Bettens, Christine Van Broeckhoven, Mathieu Vandenbulcke, Pradeep Thiyyagura, Patrick Dupont, Koen Van Laere, Eric M. Reiman, Rik Vandenberghe. Polymorphism of Brain Derived Neurotrophic Factor influences β amyloid load in cognitively intact Apolipoprotein E ε4 carriers. *Neuroimage Clin* 2013 2:512−520.

3.1 Abstract

Aside from apolipoprotein E (APOE), genetic risk factors for β amyloid deposition in cognitively intact individuals remain to be identified. Brain derived neurotrophic factor (BDNF) modulates neural plasticity, which has been implicated in Alzheimer's disease. We examined in cognitively normal older adults whether the BDNF codon 66 polymorphism affects β amyloid burden and the relationship between β amyloid burden and cognitive scores, and how this relates to the effect of APOE. Amyloid load was measured by means of ^{18}F-flutemetamol PET in 64 community-recruited cognitively intact individuals (mean age 66, S.D. 5.1). Recruitment was stratified according to a factorial design with APOE (ε4 allele present vs absent) and BDNF (*met* allele at codon 66 present vs absent) as factors. Individuals in the four resulting cells were matched by the number of cases, age, and gender. Among the APOE ε4 carriers, BDNF *met* positive subjects had a significantly higher amyloid load than BDNF *met* negative subjects, while BDNF *met* carrier status did not

have an effect in APOE $\varepsilon 4$ non-carriers. This interaction effect was localized to precuneus, orbitofrontal cortex, gyrus rectus, and lateral prefrontal cortex. In the APOE $\varepsilon 4$/BDNF *met* carriers, a significant inverse relationship existed between episodic memory scores and amyloid burden but not in any of the other groups. This hypothesis-generating experiment highlights a potential role of BDNF polymorphisms in the preclinical phase of β amyloid deposition and also suggests that BDNF codon 66 polymorphisms may influence resilience against β amyloid-related effects on cognition.

3.2 Introduction

In a variable proportion of cognitively intact older subjects, in vivo amyloid imaging has revealed increased cerebral Aβ deposition, sometimes to a degree identical to that seen in patients with clinically probable Alzheimer's disease (AD) [164, 165, 166, 132, 167, 168, 169]. This finding has attracted a lot of interest as it may be a possible marker for preclinical Alzheimer's disease [55]. The only genetic risk factor proven to be associated with increased amyloid load in a cognitively intact population is the apolipoprotein E (APOE) $\varepsilon 4$ allele [114, 166, 113, 117, 43], which is also a strong risk factor for Alzheimer's disease [107, 170]. Beyond what can be explained by APOE alone, a family history of AD is associated with increased brain amyloid levels in cognitively intact older adults [125]. According to a recent study, polymorphisms of complement component (3b/4b) receptor-1 (*CR1*) modulate the effect of APOE $\varepsilon 4$ on brain amyloid levels [129]. These findings suggest a complex interaction between genetic variants and brain amyloid deposition in preclinical AD [55].

A failure of neural plasticity has been put forward as a unifying theme spanning across the multiple pathways that lead to clinical AD [171, 172, 17, 173, 174]. Brain derived neurotrophic factor (BDNF), a neurotrophin with high affinity for tyrosine kinase B receptors (TrkB), has been implicated in neural plasticity [175, 176] as well as in memory, both in humans [177] and in animal models [178, 179, 180]. In humans, a common single nucleotide polymorphism (SNP) in the 5' prodomain of the BDNF gene which results in valine to methionine substitution at codon 66 (*val*66*met*), affects memory function [181, 182, 183, 184, 185, 186, 187], hippocampal volume and fMRI responses [183, 188]. The *met* allele occurs in approximately 35% of the Caucasian population [189]. Given the prominent role of BDNF in neuroplasticity and a failure of neural plasticity as a potential common theme in AD [17], the BDNF-TrkB pathway could theoretically be linked to a host of AD-related processes at the molecular, neuronal or systems level.

The original hypothesis underlying the design of our study was that BDNF polymorphisms might influence the resilience against β amyloid related changes [132]. We hypothesized that BDNF *val* carriers would be able to compensate for the presence of β amyloid in a better way than *met* carriers. Such resilience might be manifest as a difference between genetic strata in how Aβ load affects

cognitive scores and also as a difference in compensatory mechanisms at the brain systems level [132]. As a first step, we examined whether there were any direct effects of the BDNF codon 66 polymorphism on amyloid retention in cognitively intact older adults, measured by means of ^{18}F-flutemetamol positron emission tomography (PET) [65, 66, 73, 190].

3.3 Subjects and methods

3.3.1 Subjects

The main cohort consisted of 64 community-recruited older adults between 50 and 75 years of age (mean age = 66, S.D. = 5.1, range 53-74) (Table 3.1). The study exclusion criteria were a Mini Mental State Examination [151] score lower than 27, a Clinical Dementia Rating score [152] higher than 0, significant neurological or psychiatric history, significant brain lesions on structural MRI, and below-normal test scores on conventional neuropsychological assessment (Table 3.1). Inclusion was stratified per age bin (50-59, 60-64, 65-69, 70-75) for two genetic factors: BDNF (*met* allele present or absent) and APOE (ε4 allele present or absent). The cells of this 2 x 2 factorial design were prospectively matched for number of cases, gender, age, education and handedness (Edinburgh Handedness Inventory) (Table 3.1). BDNF and APOE variants were genotyped by sequencing at the Genetic Service Facility (GSF, www.vibgeneticservicefacility.be) of the VIB Department of Molecular Genetics.

The genetic distribution among all subjects who underwent screening, was 10% BDNF *met* +ve/APOE ε4 +ve, 16% BDNF *met* -ve/APOE ε4 +ve, 33% BDNF *met* +ve/APOE ε4 -ve, and 41% BDNF *met* -ve/APOE ε4 -ve. After genetic stratification, the genetic distribution of the final cohort (n = 64) was as follows: 25% were BDNF *met* +ve/APOE ε4 +ve, 23% BDNF *met* -ve/APOE ε4 +ve, 25% BDNF *met* +ve/APOE ε4 -ve, and 27% were BDNF *met* -ve/APOE ε4 -ve.

The protocol was approved by the Ethics Committee University Hospitals Leuven (EudraCT: 2009-014475-45) and written informed consent was obtained from all subjects in accordance with the Declaration of Helsinki.

3.3.2 Image acquisition

^{18}F-flutemetamol PET imaging for the main cohort was performed at the University Hospitals Leuven. The acquisition procedure has been described before [65, 66, 73, 190]. Images were acquired on a 16-slice Siemens Biograph PET/CT scanner (Siemens, Erlangen, Germany). The PET tracer was injected intravenously as a bolus (mean activity 150.6 MBq, S.D. 8 MBq, range 137.9-192.5 MBq) in an antecubital vein. Image acquisition started 90 min after tracer

Demographic data and neuropsychological test scores

	Genetic groups				*P*
	BDNF *met* +ve APOE ε4 +ve	BDNF *met* -ve APOE ε4 +ve	BDNF *met* +ve APOE ε4 -ve	BDNF *met* -ve APOE ε4 -ve	
Gender (M/F)	7/9	9/6	8/8	10/7	0.8
Age (years)	65.4 (5.5)	66.5 (4.3)	65.3 (5.5)	65.8 (5.4)	0.9
Education (years)	13.3 (3.0)	12.5 (2.2)	13.9 (2.2)	14.7 (3.6)	0.2
Handedness (%)	95.0 (14.5)	100.0 (0.0)	96.7 (7.7)	100.0 (0.0)	0.2
MMSE (/30)	29.0 (0.9)	28.7 (1.1)	29.3 (0.6)	28.9 (0.9)	0.3
AVLT DR (/15)	11.4 (2.4)	10.3 (3.6)	11.3 (2.8)	10.6 (2.2)	0.6
AVLT TL (/75)	48.9 (7.8)	50.1 (8.6)	51.1 (12.3)	49.0 (9.1)	0.9
BNT (/60)	53.1 (5.4)	51.9 (6.5)	52.6 (4.8)	54.2 (3.2)	0.6
AVF (# words)	18.6 (4.7)	19.9 (5.3)	21.8 (5.5)	21.2 (4.2)	0.3
LVF (# words)	33.5 (11.8)	31.1 (8.1)	33.6 (9.9)	37.4 (9.8)	0.4
RPM (/60)	39 (8.6)	42.1 (9.2)	44.3 (7.3)	46.5 (7.5)	0.07
TMT B/A	2.9 (1.0)	2.5 (0.6)	2.6 (1.0)	2.5 (1.1)	0.5

Table 3.1: Values represent means and standard deviations (in parenthesis) unless stated otherwise; gender is expressed in number of individuals. Abbreviations: M = male; F = female; MMSE = Mini Mental State Examination; AVLT = Rey Auditory Verbal Learning Test; DR = delayed recall; TL = total learning; BNT = Boston Naming Test; AVF = Animal Verbal Fluency Test; LVF = Letter Verbal Fluency Test; RPM = Raven's Progressive Matrices; TMT = Trail Making Test part B divided by part A.

injection and lasted for 30 min. Prior to the PET scan, a low-dose computed tomography (CT) scan was performed for attenuation correction. Random and scatter corrections were also applied. Images were reconstructed using Ordered Subsets Expectation Maximization (OSEM; 4 iterations x 16 subsets).

A high-resolution T1-weighted structural MRI was obtained on a 3T Philips Intera system equipped with an 8-channel receive-only head coil (Philips SENSitivity Encoding head coil), using a 3D turbo field echo sequence (coronal inversion recovery prepared 3D gradient-echo images, inversion time 900 ms, TR = 9.6 ms, TE = 4.6 ms, flip angle 8°, field of view = 250 x 250 mm, 182 slices; voxel size 0.98 x 0.98 x 1.2 mm^3).

3.3.3 Image analysis

All analyses were performed using Statistical Parametric Mapping 8 (SPM8, http://www.fil.ion.ucl.ac.uk/spm). The PET data were reconstructed as 6 frames of 5 minutes and realigned to the first frame to correct for potential head motion. Subsequently, the 6 frames were summed to create one summed image. The individual's T1-weighted structural image was then co-registered to his/her PET summed image. This MR image was subsequently normalized to the SPM8 T1 template in Montreal Neurological Institute (MNI) space using a unified segmentation approach. Next, this normalization matrix was applied to the individual's co-registered PET summed image.

From the spatially normalized images (voxel size 2 x 2 x 2 mm^3) standardized uptake value ratios (SUVR) were calculated with cerebellar grey matter as reference region, resulting in SUVR images. The cerebellar grey matter reference region was defined as areas 91 to 108 of the Automated Anatomical Labelling atlas (AAL) [191]. The cerebellar reference region was resliced to each individual's normalized PET summed image. In order to exclude white matter (WM) content, it was masked by the normalized and modulated subject-specific grey matter (GM) map, with the threshold for masking set at 0.3.

We also defined a composite cortical volume of interest. This was composed of 5 bilateral cortical areas, i.e. frontal, parietal, anterior cingulate, precuneus/posterior cingulate and lateral temporal defined as AAL areas 3-10, 13-16, 23-28, 31-32, 35-36, 57-70, 81-82, 85-90. The composite cortical VOI was resliced to each individual's normalized PET summed image. In order to exclude WM content, it was masked by the normalized and modulated subject-specific GM map, with the threshold for masking set at 0.3.

In one of the subjects the structural T1 image was missing due to a contraindication for MRI. This individual's PET summed image was normalized to the group mean normalized PET summed image created from the 63 remaining subjects. The AAL-derived cerebellar and composite cortical VOIs were co-registered to this normalized PET summed image and were masked with the mean normalized modulated GM map (thresholded at 0.3) created out of the 63 normalized modulated GM maps. This individual's SUVR image was calculated based on this normalized PET summed image with the cerebellar grey matter reference region.

As a secondary measure we also worked on partial volume corrected (PVC) data. PVC was based on the MRI using the modified Müller-Gärtner method [146]. This method determines tracer concentration per unit volume of GM. In the modified method, we use probabilistic segmentation instead of binary maps. The normalized unmodulated GM and WM segmentations were used to estimate different tissue fractions per voxel. PVC was applied to the normalized PET summed images. The remaining of the procedures were identical to those outlined above.

We also tested for any group differences in tracer retention in the cerebellar reference region, as this could cause spurious differences in cortical SUVR values. We calculated the standardized uptake values (SUV) in the cerebellar grey matter region. SUV values were defined as the ratio of mean activity concentration in cerebellar grey matter in the normalized PET summed image [MBq] to the injected activity concentration [MBq/kg] per total body weight [kg].

Lastly, we evaluated whether similar results could be obtained when pons was used as reference region for the SUVR images[1]. For this purpose pons was manually drawn on the SPM8 T1-template (13 axial slices of 2 mm) and then

[1]The analyses with pons as reference region were added to the thesis after publication of the article.

for each individual it was corrected to match the subject-specific anatomical boundaries of the pons based on the subject's spatially normalized MR image.

3.3.3.1 Statistical analysis

We statistically analyzed all SUVR images using two approaches: one was based on the global composite cortical VOI, the other was voxel-based. In the global composite cortical analysis our primary outcome measure was mean SUVR value calculated in the composite cortical VOI ($SUVR_{comp}$). We used $SUVR_{comp}$ as the dependent variable and performed a factorial ANOVA with BDNF (2 levels: *met* allele present vs absent) and APOE (2 levels: $\varepsilon 4$ allele present vs absent) as between-subjects factors. In addition, we performed a confirmatory non-parametric Kruskal-Wallis ANOVA on the 4 genetic groups with $SUVR_{comp}$ as the dependent variable.

In the voxel-based analysis, using SPM8, we analysed SUVR images by means of a factorial ANOVA with BDNF (2 levels: *met* allele present vs absent) and APOE (2 levels: $\varepsilon 4$ allele present vs absent) as between-subjects factors. The significance threshold was set at a cluster-level of $P < 0.05$ family-wise error (FWE) corrected for the entire brain search volume, with the voxel-level threshold set at uncorrected $P < 0.001$.

The composite cortical and voxel-based analyses were also performed using pons as reference region.

The partial-volume corrected data were analyzed using a factorial ANOVA with BDNF (2 levels: *met* allele present vs absent) and APOE (2 levels: $\varepsilon 4$ allele present vs absent) as between-subjects factors.

Differences in the SUV values in the cerebellar grey matter VOI were analysed by a factorial ANOVA with 2 between-subjects factors: BDNF (2 levels: *met* allele present vs absent) and APOE (2 levels: $\varepsilon 4$ allele present vs absent).

3.3.4 Relationship to episodic memory test scores

To assess the relationship between ^{18}F-flutemetamol retention and episodic memory measures, we conducted a linear regression analysis with either AVLT delayed recall score (DR) or total learning score (TL) as dependent variable and $SUVR_{comp}$ as independent variable. This analysis was performed across the entire group as well as within each genetic group separately. To evaluate whether the relationship was specifically observed with episodic memory scores, we also performed a linear regression analysis with other tests from our cognitive battery: Boston Naming Test (BNT), Animal Verbal Fluency Test (AVF) and total score on Raven's Progressive Matrices (RPM).

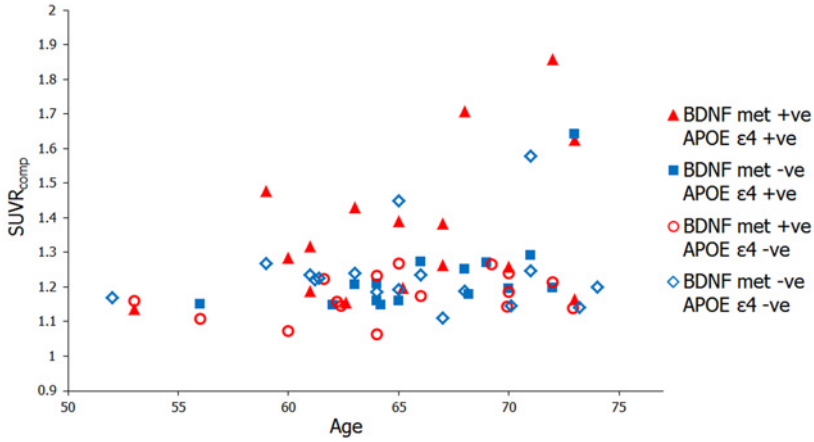

Figure 3.1: Distribution of ^{18}F-flutemetamol retention levels for the different genetic groups. X axis: age in years; Y axis: SUVR$_{comp}$.

3.4 Results

The four genetic groups did not differ in age, gender, years of education or neuropsychological test scores (Table 3.1).

3.4.1 Effect of APOE and BDNF polymorphisms on SUVR

3.4.1.1 Global composite cortical analysis

Our primary outcome measure, SUVR$_{comp}$, differed significantly between the four genetic groups ($F(3,60) = 5.37$, $P = 0.002$) (Figure 3.1). The main effect of APOE was significant: APOE $\varepsilon 4$ carriers had significantly higher ligand retention than APOE $\varepsilon 4$ non-carriers ($F(1,60) = 7.14$, $P = 0.01$). The main effect of BDNF genotype was not significant ($F(1,60) = 1.02$, $P = 0.32$). The interaction between BDNF and APOE on ligand retention was significant ($F(1,60) = 7.94$, $P = 0.007$): BDNF *met* +ve/APOE $\varepsilon 4$ +ve carriers had significantly higher ligand retention (mean SUVR$_{comp}$ = 1.37, S.D. = 0.21) than BDNF *met* -ve/APOE $\varepsilon 4$ +ve carriers (mean SUVR$_{comp}$ = 1.23, S.D. = 0.12) ($P = 0.01$), while amyloid ligand retention in APOE $\varepsilon 4$ non-carriers did not differ between BDNF *met* +ve (mean SUVR$_{comp}$ = 1.17, S.D. = 0.06) and BDNF *met* -ve cases (mean SUVR$_{comp}$ = 1.24, S.D. = 0.11) ($P = 0.2$) (Figure 3.2 A and B).

Non-parametric analysis confirmed these results. The four genetic groups differed significantly in SUVR$_{comp}$ (H(df 3, N 64) = 11.35, $P = 0.01$). The main effect of APOE was significant: APOE $\varepsilon 4$ carriers had significantly higher ligand retention than APOE $\varepsilon 4$ non-carriers (H(df 1, N 64) = 5.25, $P = 0.02$). The main effect of BDNF genotype was not significant (H(df 1, N 64) = 0.04,

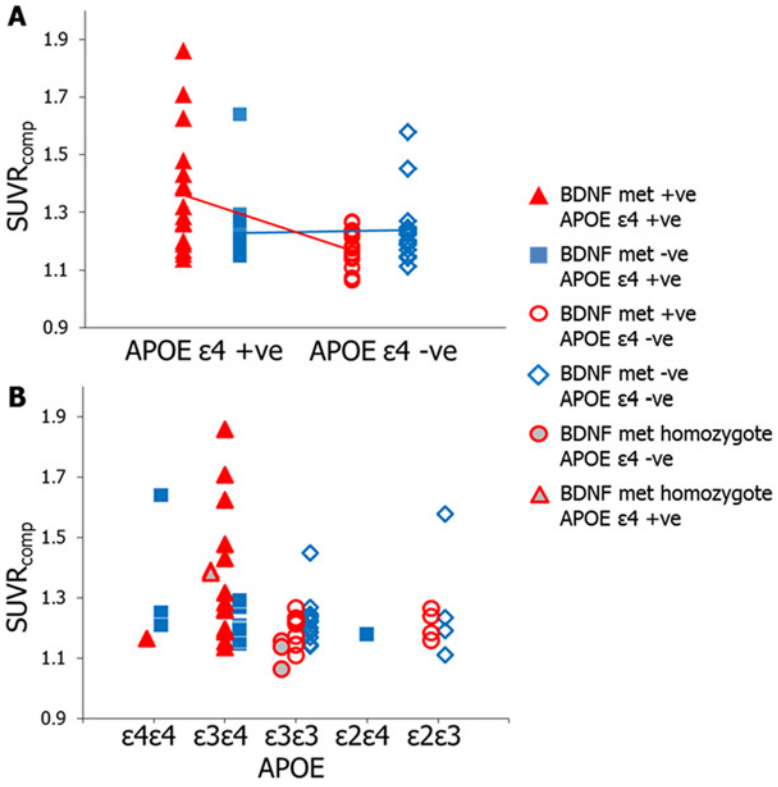

Figure 3.2: Effects of BDNF and APOE genotypes on amyloid deposition measured by $SUVR_{comp}$. (A) $SUVR_{comp}$ in the different genetic subgroups. (B) Further differentiation depending on APOE and BDNF subgroups.

$P = 0.85$). Planned comparisons revealed that BDNF *met* +ve/APOE $\varepsilon 4$ +ve carriers exhibited higher ligand retention (mean rank = 19.1) than BDNF *met* -ve/APOE $\varepsilon 4$ +ve carriers (mean rank = 12.6) ($P = 0.048$). Amyloid ligand retention also tended to be higher in BDNF *met* +ve (mean rank = 13.8) than in BDNF *met* -ve (mean rank = 19.9) APOE $\varepsilon 4$ non-carriers ($P = 0.07$).

Analysis of partial volume corrected data confirmed these results. PVC $SUVR_{comp}$ was significantly different between the four genetic groups ($F(3,59) = 4.64$, $P = 0.006$). The main effect of APOE was significant: APOE $\varepsilon 4$ carriers had significantly higher ligand retention than APOE $\varepsilon 4$ non-carriers ($F(1,59) = 6.96$, $P = 0.01$). The main effect of BDNF genotype was not significant ($F(1,59) = 0.55$, $P = 0.46$). The interaction between BDNF and APOE on ligand retention was significant ($F(1,59) = 6.7$, $P = 0.01$): BDNF *met* +ve/APOE $\varepsilon 4$ +ve carriers had significantly higher ligand retention (mean $SUVR_{comp} = 1.56$, S.D. = 0.39) than BDNF *met* -ve/APOE $\varepsilon 4$ +ve carriers (mean $SUVR_{comp}$ =

1.36, S.D. = 0.24) ($P = 0.02$), while amyloid ligand retention in APOE $\varepsilon 4$ non-carriers did not differ between BDNF *met* +ve (mean $SUVR_{comp} = 1.24$, S.D. = 0.09) and BDNF *met* -ve cases (mean $SUVR_{comp} = 1.35$, S.D. = 0.18) ($P = 0.19$).

SUV values in cerebellar grey matter did not differ between genetic groups ($F(3,60) = 0.54$, $P = 0.66$). There was no difference between APOE $\varepsilon 4$ carriers and non-carriers ($F(1,60) = 0.21$, $P = 0.65$), between BDNF *met* carriers and non-carriers ($F(1,60) = 0.55$, $P = 0.46$) and neither was there any interaction ($F(1,60) = 0.79$, $P = 0.38$).

3.4.1.2 Voxel-based analysis

The whole-brain voxel-wise analysis confirmed the findings from the composite cortical analysis. There was a significant main effect of APOE: APOE $\varepsilon 4$ carriers had significantly higher ^{18}F-flutemetamol retention than APOE $\varepsilon 4$ non-carriers in the posterior cingulate (cluster peak -14, -20, 40, $Z = 4.26$, extent of voxels (ext.) 178 mm^3, corr. cluster-level $P = 0.025$) (Figure 3.3A). There was no main effect of BDNF genotype (corr. cluster-level $P > 0.7$). The interaction effect of APOE and BDNF was significant in precuneus (cluster peak 10, -40, 42, $Z = 4.71$, ext. 437 mm^3, corr. cluster-level $P = 0.0001$), left orbitofrontal cortex (cluster peak -8, 64, -14, $Z = 4.69$, ext. 387 mm^3, corr. cluster-level $P = 0.0003$), right orbitofrontal cortex (cluster peak 16, 68, -2, $Z = 4.37$, ext. 240 mm^3, corr. cluster-level $P = 0.006$), left gyrus rectus (cluster peak -8, 22, -18, $Z = 4.62$, ext. 252 mm^3, corr. cluster-level $P = 0.004$), right gyrus rectus (cluster peak 16, 28, -28, $Z = 4.35$, ext. 209 mm^3, corr. cluster-level $P = 0.012$), right middle frontal gyrus (cluster peak 34, 46, 28, $Z = 4.14$, ext. 316 mm^3, corr. cluster-level $P = 0.001$) and right inferior frontal sulcus (cluster peak 50, 38, 6, $Z = 3.88$, ext. 281 mm^3, corr. cluster-level $P = 0.002$) (Figure 3.3 B). Simple effects revealed that BDNF *met* +ve/APOE $\varepsilon 4$ +ve carriers had higher ligand retention than BDNF *met* -ve/APOE $\varepsilon 4$ +ve carriers in posterior cingulate (cluster peak at 2, -32, 42, $Z = 4.25$, ext. 388 mm^3, corr. cluster-level $P = 0.0003$), gyrus rectus (cluster peak at -4, 34, -26, $Z = 4.44$, ext. 196 mm^3, corr. cluster-level $P = 0.016$), insula (cluster peak at 36, 8, -12, $Z = 4.89$, ext. 311 mm^3, corr. cluster-level $P = 0.001$) and posterior middle temporal cortex (cluster peak at 62, -62, 4, $Z = 4.23$, ext. 168 mm^3, corr. cluster-level $P = 0.03$). There was no difference between BDNF *met* +ve/APOE $\varepsilon 4$ -ve carriers and BDNF *met* -ve/APOE $\varepsilon 4$ -ve carriers (corr. cluster-level $P > 0.9$).

3.4.1.3 Relationship between β amyloid load and episodic memory

Across the entire sample, $SUVR_{comp}$ did not correlate with AVLT DR ($P = 0.38$) or TL ($P = 0.16$). When analysed per genetic group, a highly significant and negative correlation was seen only in the group of BDNF *met* +ve/APOE $\varepsilon 4$ +ve carriers (DR $r = -0.62$, $P = 0.01$, and TL $r = -0.58$, $P = 0.02$) (Figure 3.4 A and B, red lines). In the other groups the correlation remained far

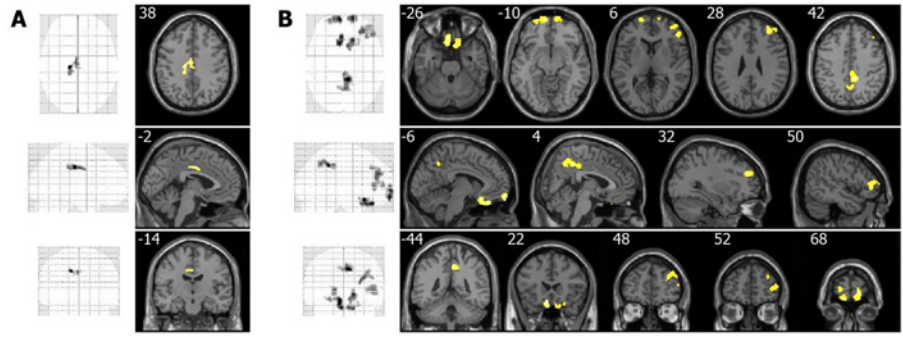

Figure 3.3: Statistical parametric map of the main effect of APOE (A) and the interaction effect between APOE and BDNF (B). (A) Main effect of APOE genotype: increased ^{18}F-flutemetamol retention in APOE $\varepsilon 4$ +ve carriers compared to APOE $\varepsilon 4$ -ve carriers in the posterior cingulate. (B) Interaction effect between BDNF and APOE: increased ^{18}F-flutemetamol retention in the precuneus, orbitofrontal cortex, gyrus rectus, middle frontal gyrus, and inferior frontal sulcus. Images are displayed at voxel-level $P < 0.001$, only clusters that reached corrected cluster-level $P < 0.05$ are shown. SPM t maps are projected onto axial, sagittal, and coronal sections of the SPM8 standard single subject T1 template and as SPM8 glass brain views.

below significance ($P > 0.49$) (Table 3.2). A formal pairwise comparison however of the regression slopes between groups did not reach significance ($P > 0.05$) [192].

None of the other cognitive test scores showed any correlation with β amyloid when tested across the entire sample ($P > 0.17$) or per group (Table 3.2).

3.4.1.4 Analyses with pons as reference region[2]

With pons as reference region, similar results were obtained. SUVR_{comp} differed significantly between the four genetic groups ($F(3,60) = 5.68$, $P = 0.0017$). The main effect of APOE was significant: APOE $\varepsilon 4$ carriers had significantly higher ligand retention than APOE $\varepsilon 4$ non-carriers ($F(1,60) = 8.60$, $P = 0.005$). The main effect of BDNF genotype was not significant ($F(1,60) = 2.33$, $P = 0.13$). The interaction between BDNF and APOE on ligand retention was significant ($F(1,60) = 6.04$, $P = 0.017$): BDNF *met* +ve/APOE $\varepsilon 4$ +ve carriers had significantly higher ligand retention (mean $\text{SUVR}_{comp} = 0.65$, S.D. $= 0.11$) than BDNF *met* -ve/APOE $\varepsilon 4$ +ve carriers (mean $\text{SUVR}_{comp} = 0.58$, S.D. $= 0.04$) ($P = 0.0074$), while amyloid ligand retention in APOE $\varepsilon 4$ non-carriers

[2]The analyses with pons as reference region were added to the thesis after publication of the article.

did not differ between BDNF *met* +ve (mean $SUVR_{comp}$ = 0.56, S.D. = 0.04) and BDNF *met* -ve cases (mean $SUVR_{comp}$ = 0.58, S.D. = 0.05) (P = 0.51).

The voxelwise analysis with pons as reference region also yielded identical results as the main analysis.

The linear regression analysis between AVLT DR or TL and $SUVR_{comp}$ with pons as reference region yielded the same results as when cerebellar cortex was used as reference region.

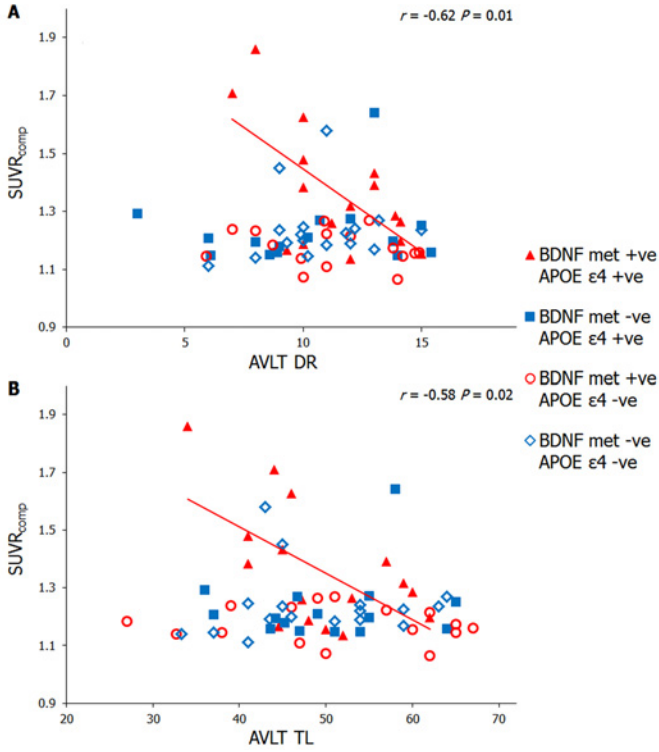

Figure 3.4: Correlation between amyloid ligand retention and AVLT delayed recall (DR) and total learning (TL) scores. (A) Negative correlation between $SUVR_{comp}$ values and AVLT DR scores in the BDNF *met* +ve/APOE ε4 +ve group (red line). (B) Negative correlation between $SUVR_{comp}$ values and AVLT TL scores in the BDNF *met* +ve/APOE ε4 +ve (red line). $SUVR_{comp}$ (Y axis) plotted by AVLT DR or TL scores (X axis): BDNF *met* +ve/APOE ε4 +ve (red triangles), BDNF *met* -ve/APOE ε4 +ve (blue squares), BDNF *met* +ve/APOE ε4 -ve (red circles) and BDNF *met* -ve/APOE ε4 -ve (blue diamonds). When the correlation does not reach significance, no regression line is shown.

Linear regression between $SUVR_{comp}$ and cognitive test scores in each of the four genetic groups.

	BDNF *met* +ve APOE ε4 +ve		BDNF *met* -ve APOE ε4 +ve		BDNF *met* +ve APOE ε4 -ve		BDNF *met* -ve APOE ε4 -ve	
	r	P	r	P	r	P	r	P
AVLT DR	**-0.62**	**0.01**	0.14	0.61	-0.19	0.49	0.15	0.56
AVLT TL	**-0.58**	**0.02**	0.18	0.51	-0.12	0.65	0.02	0.95
BNT	-0.18	0.49	-0.03	0.91	-0.06	0.81	-0.07	0.78
AVF	0.04	0.88	0.21	0.44	0.11	0.69	-0.42	0.09
RPM	-0.36	0.17	0.00	1.00	0.03	0.92	0.10	0.72

Table 3.2: Values represent correlation coefficient (r) and statistical significance (P). Abbreviations: AVLT = Rey Auditory Verbal Learning Test; DR = delayed recall; TL = total learning; BNT = Boston Naming Test; AVF = Animal Verbal Fluency Test; RPM = Raven's Progressive Matrices.

3.5 Discussion

Our study revealed two key novel findings. First, APOE ε4 carriers exhibited a higher β amyloid load in the presence of one or two BDNF *met* alleles compared to BDNF *met* non-carriers (Figure 3.1, 3.2). Second, an inverse relationship between Aβ load and episodic memory exists in BDNF *met*/APOE ε4 carriers but not in any of the other subgroups.

The interaction effect between BDNF and APOE on β amyloid load was unexpected and needs further confirmation by independent studies. The genetic stratification for APOE and BDNF prior to recruitment for scanning is a unique feature of our cohort that was probably critical for obtaining this novel finding. In the group of individuals volunteering for this study, after applying all non-genetic criteria for in/exclusion, the proportion of BNDF *met* +ve/APOE ε4 +ve subjects was only 10%. After stratification this was raised to 25%. It is this genetic combination that drives the interaction. Had we not strived for a balanced factorial design with cells matched for numbers at recruitment, the interaction effect would almost certainly have been missed. This means that we had to genotype much higher numbers of subjects than were actually able to enter the scanning phase of the study. Replication of the interaction effect will probably also have to be based on samples enriched for the naturally least frequent combination of BNDF *met* and APOE ε4 carriers.

Most of the subjects with raised amyloid were APOE ε4 carriers with BDNF *met* allele at codon 66 (Figure 3.1). The number of subjects with raised amyloid is relatively low but impacts relatively strongly on the statistical outcome. Non-parametric testing confirmed that BDNF *met* carriage affected Aβ load. Our findings were obtained in a cohort stratified at recruitment for APOE and BDNF polymorphisms according to a balanced factorial design with demographically matched subjects. The stratification, the balanced design and the fact that we only tested these two gene polymorphisms, reduces the risk of

a false-positive. As a relatively low number of the 64 healthy subjects had a raised Aβ load, the power of our study to determine an influence of genetics is limited and any negative findings should be interpreted with caution. The proportion of subjects with raised amyloid increases with age [166]. Further studies in a higher age range will be needed to confirm whether the interaction is present also in an older population.

We used the volumetric MRI scan for normalisation and the segmented gray matter maps for definition of the cerebellar gray matter and the composite cortical volume. The method we applied differs from the purely PET-based method applied in the phase 2 study of ^{18}F-flutemetamol [73]. As a consequence, we cannot simply use the cut-off from the phase 2 study to discriminate positive from negative cases in a binary manner. Furthermore, in a cognitively intact population of older adults, a significant minority exhibits intermediary values. While categorical discrimination between positive and negative individuals is relevant for clinical purposes, a binary division in positive and negative cases is not essential for the current scientific question.

The interaction effect was seen in frontobasal cortex, precuneus, and lateral prefrontal cortex, which are well-established areas of predilection for amyloid deposition in the initial phase of the disease [164, 193, 114, 165, 167, 168]. For posterior cingulate and precuneus this has been linked to their status as a network hub [194, 195], including their centrality in the connections from the hippocampal formation to parietal cortex [196, 197]. Why orbitofrontal cortex regularly recurs as an area of predilection, is less clear. In any case, numerous studies of the earliest changes in amyloid load in AD have reported increased amyloid load in this region [10, 198, 199, 193, 114]. Orbitofrontal cortex also shows hypometabolism on ^{18}F-deoxyglucose PET early in the AD disease course [200].

The original purpose of our factorial design was to evaluate the effect of BDNF on functional reorganisation and plasticity [132] in response to β amyloid related injury. We predicted that compared to BDNF *met* carriers BDNF *val* status would confer a higher compensatory capacity for functional reorganisation in the face of increased Aβ amyloid [132]. Given ample evidence for a relationship between BDNF polymorphism and episodic memory [181, 182, 183, 184, 185, 186, 187] and given the prominent role of episodic memory decline in the earliest clinical stages of Alzheimer's disease, we primarily evaluated whether BDNF affected the relationship between Aβ deposition and episodic memory. We found a strong negative correlation between Aβ deposition and episodic memory encoding and recall in the BDNF *met* +ve/APOE ε4 +ve carriers but not in any of the three other groups (Figure 3.4, Table 3.2). This finding is in line with our a priori hypothesis that BDNF polymorphism may influence resilience against Aβ related injury. A formal pairwise comparison however of the regression slopes of β amyloid load versus episodic memory scores between the groups did not reach significance, possibly due to the relatively small sample size. The relationship between cognitive test scores in cognitively intact individuals and Aβ deposition is still a

topic of active research, with some studies reporting an inverse relationship and others an absence of any relationship [199, 201, 167, 202, 203]. Our findings offer one possible explanation for this divergence between studies: if the genetic composition differs between cohorts, this may cause differences in how β amyloid load relates to episodic memory scores (Figure 3.4 A, B). The effect of Aβ load on episodic memory scores in the BDNF *met* +ve/APOE ε4 +ve group highlights the behavioural relevance of our findings.

Previous studies have shown the negative effect of BDNF codon 66 *val* to *met* substitution on a number of parameters: It is associated with worse memory function [181, 183, 184, 185, 186, 187], lower fMRI responses in hippocampi during both encoding and retrieval [183, 184], smaller volumes of hippocampi [204, 205, 186, 188, 206], lateral prefrontal cortex [207, 188, 208], temporal neocortex, cingulate, and insula [208], and amygdalae [209, 210], as well as age-related volume reduction of other cortical areas which may be gender-dependent [207]. The BDNF codon 66 *met* allele also affects white matter connectivity [211]. Interestingly, a recent study reported effects of BDNF *val*66*met* polymorphism on brain metabolism in healthy controls, MCI and AD cases [212]. To the best of our knowledge our study is the first to directly examine how the well-studied negative effects of BDNF *met* relate to subclinical Aβ amyloid and its relationship to episodic memory.

An interaction effect between BDNF and APOE on amyloid ligand retention has not been reported in previous genome-wide association studies (GWAS) of clinically probable Alzheimer's disease patients. In their conventional form, GWAS make use of massively univariate single-locus tests. Such tests are designed to search for single disease-associated polymorphisms [213] where each gene variant is tested individually for association with a specific phenotype (cases versus controls) [214]. GWAS in their classical form will miss interaction effects between genes.

Apart from amyloid load, it is currently unknown how the interaction between BDNF and APOE polymorphisms affects other contributors to the pathogenesis of AD, such as synapse loss, cholinergic depletion, or neurofibrillary tangle formation. For this reason, it remains to be seen whether the interaction effect between BDNF and APOE on amyloid burden we observed in cognitively intact subjects can be extrapolated to genetic comparisons between clinically probable AD and controls.

Studies in animal models of AD offer us with several putative mechanisms through which BDNF and the amyloid cascade may interact. Intrahippocampal injections of Aβ(1-42) in rats reduce the expression of BDNF and also result in decreased BDNF levels in prefrontal cortex [215]. In amyloid precursor protein (APP) double transgenic mice with both the Swedish and the Indiana APP mutations, BDNF gene delivery to entorhinal cortex reverses synapse loss and improves cell signalling, partially normalizes APP-related alterations in hippocampal and entorhinal gene expression, and restores learning and memory [216]. In AD postmortem samples, BDNF protein expression as

well as mRNA levels are decreased in hippocampi and other cortical areas [217, 218, 219, 220, 221]. During the course of AD, BDNF serum concentration levels correlate with the severity of dementia: levels are increased in early stages of AD and decreased in the advanced stages [222, 223]. It however is difficult to speculate on the exact mechanism through which BDNF may interact with APOE to increase amyloid burden as the relationship between APOE and increased amyloid aggregation itself is still relatively poorly understood. Both genes have been implicated in neural plasticity. This concept encompasses widely diverse processes [17]. Possibly, the efficacy with which neurons dispose of toxic forms of Aβ may depend on pathways that are linked to lipid metabolism and neuronal survival in which APOE and BDNF, respectively, play pivotal roles.

In conclusion, we demonstrate an association between BDNF *met* allele and PET measures of amyloid deposition in cognitively normal older adult APOE ε4 carriers. This finding provides empirical evidence for a role of the BDNF-TrkB pathway not only in neural plasticity but also in the pathogenesis of Alzheimer's disease [17]. It underscores the opportunity to use brain imaging measurements to help characterize the individual and epistatic effects of putative genetic risk factors in the predisposition to AD. We however would like to emphasize that the current study is hypothesis-generating and needs further replication.

4

Functional changes in the language network in response to increased amyloid deposition in cognitively intact older adults

This chapter has been published as:

Katarzyna Adamczuk, An-Sofie De Weer, Natalie Nelissen, Patrick Dupont, Stefan Sunaert, Karolien Bettens, Kristel Sleegers, Christine Van Broeckhoven, Koen Van Laere, Rik Vandenberghe. Functional changes in the language network in response to increased amyloid deposition in cognitively intact older adults. *Cereb Cortex* 2014 doi:10.1093/cercor/bhu286.

4.1 Abstract

Word finding symptoms are frequent early in the course of Alzheimer's disease and relate principally to functional changes in left posterior temporal cortex. In cognitively intact older adults, we examined whether amyloid load affects the network for language and associative-semantic processing. Fifty-six community-recruited subjects (52-74 years), stratified for Apolipoprotein E and Brain Derived Neurotrophic Factor genotype, received a neurolinguistic assessment, ^{18}F-flutemetamol PET, and a functional MRI of the associative-semantic system. The primary measure of amyloid load was the cerebral-to-cerebellar grey matter standardized uptake value ratio in a composite cortical volume of interest ($SUVR_{comp}$). The primary outcome analysis consisted of a whole-brain voxelwise linear regression between $SUVR_{comp}$ and fMRI response during associative-semantic versus visuoperceptual processing. Higher activity in one region, the posterior left middle temporal gyrus, correlated positively with increased amyloid load. The correlation remained significant when only the word conditions were contrasted but not for pictures. According to a stepwise lin-

ear regression analysis, offline naming reaction times correlated positively with $SUVR_{comp}$. A binary classification into amyloid-positive and amyloid-negative cases confirmed our findings. The left posterior temporal activity increase may reflect higher demands for semantic control in the presence of a higher amyloid burden.

4.2 Introduction

Modern techniques such as amyloid positron emission tomography (PET) allow one to detect hallmark lesions related to Alzheimer's disease (AD) directly in vivo [224, 225, 226, 31, 69]. Depending on mainly age and Apolipoprotein E (APOE) genotype, 10-30% of cognitively intact older adults have a positive amyloid scan, which can be indistinguishable from what is seen in clinically probable AD (for review see [37]). Longitudinally, increased Aβ load is associated with greater risk of cognitive decline [227, 203, 43, 79] and grey matter volume loss [44]. Amyloid PET has become one of the principal ways to define the 'preclinical' stage of AD, a term that refers to the AD-related pathogenetic processes that happen before clinical symptoms become apparent [55]. In this study we used ^{18}F-flutemetamol [73] as our ligand. Previous studies have revealed a high correlation between the cortical retention levels obtained with this ligand and those obtained with ^{11}C-Pittsburgh Compound B [73, 228] as well as with neuritic plaque density based on Bielschowsky silver staining [229].

Word finding difficulties are frequent in clinically probable AD, even at a pre-dementia stage [230, 231, 232, 133, 233, 234, 235]. The first language area to become dysfunctional in early-stage AD and amnestic mild cognitive impairment (MCI) is the left posterior superior temporal sulcus (STS) [132, 133]. Functional magnetic resonance imaging (fMRI) activity is lower in this region during associative-semantic compared with visuoperceptual processing in mild cognitive impairment (MCI) [133] and in clinically probable AD [132] compared to controls. In these populations, fMRI activity levels positively correlate with Boston Naming test scores [132] and with word identification speed [133]. Furthermore, in AD patients in whom naming is preserved, fMRI activity in the homotopical right-sided STS is increased compared to controls [132]. Accordingly, we hypothesized that posterior temporal cortex may show adaptive changes in the presence of increased amyloid burden also in cognitively intact individuals. The study of functional changes related to amyloid burden in cognitively intact subjects is important because it could explain why some brains appear to be more resilient against Aβ related injury than others. This factor may determine which individuals show clinical manifestations of underlying Alzheimer pathology and which remain cognitively intact despite the presence of Alzheimer pathology in the brain [34, 35, 236, 19, 36, 237, 164]. Even during the initial stages of neurodegenerative disease, the brain retains a potential for plasticity [238, 239, 240, 241, 17, 242, 243, 162].

One of the genes that have been implicated in functional plasticity [175, 176]

is Brain Derived Neurotrophic Factor (BDNF), both in humans [177] and in animal models [179, 178, 180]. The presence of one or two *met* alleles on codon 66 is often considered to reduce the capacity for functional reorganisation. As our second hypothesis, we examined whether adaptive changes occurring in the language network in response to amyloid load differ between BDNF *met* carriers and non-carriers and how this interacts with APOE $\varepsilon 4$ genotype [244].

4.3 Materials and methods

The protocol was approved by the Ethics Committee University Hospitals Leuven (EudraCT: 2009-014475-45) and written informed consent was obtained from all subjects in accordance with the latest version of the Declaration of Helsinki.

4.3.1 Participants

Subjects were recruited from the community via advertisement in local newspapers and via a website for seniors, asking for healthy volunteers between 50 and 75 years of age for participation in a scientific study at the University Hospital Leuven, Belgium, involving brain imaging. The relationship between genotype (APOE versus BDNF) and amyloid levels in the present cohort has been described by [244].

At screening, subjects underwent blood sampling for genotyping, Mini Mental State Examination (MMSE), Clinical Dementia Rating score (CDR), and a structured interview about medical history. Inclusion was stratified per age bin (50-59, 60-64, 65-69, 70-75) for two genetic factors: BDNF (*met* allele present or absent) and APOE ($\varepsilon 4$ allele present or absent). The cells of this 2 x 2 factorial design were prospectively matched for number of cases, gender, age, education and handedness (Edinburgh Handedness Inventory) [244]. BDNF and APOE variants were genotyped by sequencing at the Genetic Service Facility (GSF, www.vibgeneticservicefacility.be) of the VIB Department of Molecular Genetics. The study exclusion criteria were an MMSE score below 27, a CDR score above 0, neurological or psychiatric history, brain lesions on structural MRI, left-handedness, non-native Dutch speaker, and below-normal test scores on conventional neuropsychological assessment (< 1.9 SD on published norms adapted for age, gender, and education) (Table 4.1). The conventional neuropsychological test protocol consisted of the Rey Auditory Verbal Learning Test, Boston Naming Test, Letter Verbal Fluency and Animal Verbal Fluency, Raven's Standard Progressive Matrices and the Trail Making Test (Table 4.1).

Fifty-six healthy, right-handed adults between 50 and 75 years of age (mean age = 65, SD = 5.5, range 52-74) who fulfilled all criteria were included in the study.

Demographic data and neuropsychological test scores

	Genetic groups				*P*
	BDNF *met* +ve APOE ε4 +ve	BDNF *met* -ve APOE ε4 +ve	BDNF *met* +ve APOE ε4 -ve	BDNF *met* -ve APOE ε4 -ve	
Gender (M/F)	7/7	7/4	7/7	10/7	0.9
Age (years)	64.7 (5.9)	66.5 (4.7)	64.5 (6.0)	64.9 (5.5)	0.83
Education (years)	13.1 (2.7)	12.7 (1.8)	13.8 (2.2)	14.4 (3.6)	0.47
Handedness	94.3 (15.5)	100.0 (0.0)	96.2 (8.2)	100.0 (0.0)	0.24
MMSE (/30)	28.9 (0.9)	28.7 (1.1)	29.3 (0.6)	28.9 (0.9)	0.47
AVLT TL (/75)	48.7 (8.0)	47.5 (8.4)	51.2 (12.4)	50.0 (8.4)	0.79
AVLT DR (/15)	11.6 (2.2)	9.0 (3.3)	11.4 (2.7)	10.8 (2.1)	0.07
BNT (/60)	53.6 (4.6)	50.9 (7.4)	53.4 (3.9)	54.0 (3.3)	0.39
AVF (# words)	18.6 (4.7)	19.7 (5.2)	21.9 (5.8)	21.3 (4.3)	0.30
LVF (# words)	32.4 (12.1)	29.8 (7.9)	34.1 (10.3)	37.1 (10.0)	0.33
RPM (/60)	39.1 (9.2)	39.8 (8.7)	45.7 (6.6)	46.5 (7.5)	0.03
TMT B/A	2.9 (1.1)	2.4 (0.6)	2.5 (0.9)	2.5 (1.1)	0.50

Table 4.1: Values represent means and standard deviations. Gender is expressed in number of individuals. M = male; F = female; MMSE = Mini Mental State Examination; AVLT = Rey Auditory Verbal Learning Test; TL = total learning; DR = delayed recall; BNT = Boston Naming Test; AVF = Animal Verbal Fluency Test; LVF = Letter Verbal Fluency Test; RPM = Raven's Progressive Matrices; TMT = Trail Making Test B divided by A. Last column represents *P*-values for one-way between groups ANOVA. Bonferroni corrected threshold for significance $P < 0.006$ corresponding to $P_{corrected} < 0.05$.

4.3.2 Experimental language tests

Given our a priori hypothesis of early involvement of left posterior STS and given its possible role in lexical-semantic retrieval [133], the experimental language tests conducted outside the fMRI scanner consisted of confrontation naming, lexical decision and speeded word identification (Table 4.2). Each of these tests was presented by Presentation 14.8 (NeuroBehavioural Systems, Albany, CA, USA) and was displayed on a 19-inch cathode ray tube monitor (resolution 1024 x 768 pixels, refresh rate 75 Hz) 60 cm from subjects' eyes.

4.3.2.1 Confrontation naming task

In a computerized version of the picture naming task from Laiacona and Capitani [159], 60 white line drawings of concrete entities were presented on a black background (picture size 9.68 deg x 7.74 deg [245]). The 60 items comprised 3 living (10 animals, 10 fruits and 10 vegetables) and 3 non-living (10 tools, 10 pieces of furniture, 10 vehicles) categories. Item order was randomized for each individual. A trial started with the appearance of a fixation point displayed for 2 s before stimulus onset. A warning sound (177 ms duration) was presented 500 ms before stimulus onset. The stimulus was on the screen until the subject provided a response, for a maximum duration of one minute.

Reaction times (RT) were measured for the correct responses from the onset of the stimulus to the onset of the naming response. Voice recordings were manually analysed in the WavePad Sound Editor version 4.57 (http://www.nch.com.au/wavepad). Accuracy was measured as percentage correct responses. Responses were considered correct if they were the picture's dominant name, a synonym, the name of a subordinate to the entity designated by the dominant name, or else if it occurred in at least 3 out of 30 other healthy controls viewing the picture for 2 s. Spontaneous, immediate auto-corrections were allowed.

4.3.2.2 Lexical decision task

In a computerized version of the visual lexical decision test from the Dutch version of the Psycholinguistic Assessment of Language Processing in Aphasia (PALPA 24 [160]), words and non-words were presented as white letters (letter height: 1 deg) on a black background. Stimuli consisted of 40 words with high imageability (20 high and 20 low frequency words), 40 words with low imageability (20 high and 20 low frequency words) and 80 non-words, randomly divided into 4 blocks (literal transcription of PALPA 24 paper version). Each stimulus was preceded by a fixation point for 1 s. Subjects were instructed to use their dominant hand and respond by key press whether the stimulus was a word or non-word. The stimulus was on the screen until the subject responded, for a maximum duration of stimulus presentation of 30 s.

RTs were measured for correct responses from the onset of the stimulus to the time of the button press. A' was used as our accuracy measure [246].

4.3.2.3 Speeded word and picture identification

The purpose of the speeded word and picture identification task was to analyse written word and picture identification under varying time constraints [133]. We derived a time-accuracy curve for stimulus presentation durations varying between 30, 60, 90, 150, 200, 500, 800 or 2000 ms. Subjects were instructed to read the word or name the picture. A trial consisted of a warning sound, a forward mask (200 ms duration, 9.68 deg x 7.74 deg), followed by either a word (letter height 1 deg) or a picture (9.68 deg x 7.74 deg [245]), which was immediately followed by a backward mask (200 ms duration, 9.68 deg x 7.74 deg), and a fixation point for 3 s. For each individual subject, the onset (a), steepness of the curve (b), and asymptote (c) of the time-accuracy function for words and pictures were calculated by means of the equation: $accuracy = c*(1\text{-}e^{(a-\Delta t)/b})$ for $\Delta t \geq a$ [247, 133]. Goodness of fit was estimated as the sum of squared differences between the measured and calculated values (sum of the squared errors).

Experimental test scores

		Genetic groups				*P*		
	BDNF	*met* +ve	*met* -ve	*met* +ve	*met* -ve			
	APOE	$\varepsilon 4$ +ve	$\varepsilon 4$ +ve	$\varepsilon 4$ -ve	$\varepsilon 4$ -ve	BDNF	APOE	int
Conf naming	RT (ms)	1595 (288)	1507 (237)	1471 (333)	1450 (317)	0.27	0.50	0.68
	Accu (%)	93.0 (3.3)	91.2 (8.1)	92.4 (5.3)	90.7 (5.0)	0.70	0.24	0.96
Lexical decision	RT (ms)	1033 (146)	1118 (238)	1138 (211)	1154 (352)	0.29	0.44	0.60
	Accu (A')	0.99 (0.01)	0.99 (0.01)	0.99 (0.01)	0.98 (0.02)	0.95	0.38	0.45
Speeded id W	*a* (ms)	25.2 (17.5)	21.2 (9.7)	21.6 (12.2)	19.9 (9.1)	0.48	0.42	0.75
	b (ms)	17.4 (8.3)	25.5 (13.5)	22.7 (10.1)	19.2 (10.7)	0.85	0.42	0.05
	c (%)	99.1 (1.3)	98.2 (1.8)	99.6 (0.6)	99.0 (1.7)	0.09	0.05	0.77

Table 4.2: Values represent means and standard deviations. Conf naming = confrontation naming task; Speeded id W = speeded identification task for words; RT = reaction times; Accu = accuracy. Last three columns represent significance values for the main effect of BDNF, APOE, and interaction between them. Bonferroni corrected threshold for significance $P < 0.007$ corresponding to $P_{corrected} < 0.05$.

4.3.3 Functional MRI

4.3.3.1 Stimuli and tasks

Stimuli were projected onto a screen (resolution of 1024 x 768 pixels, refresh rate 60 hz) using Presentation 14.8 (NeuroBehavioural Systems, Albany, CA, USA). The fMRI paradigm has been described in detail before [248, 249, 250, 132, 133, 251, 252]. In summary, the experimental design was factorial [248]. The first factor, task, had two levels: associative-semantic (Figure 4.1 blue and purple) versus visuoperceptual judgement (Figure 4.1 cyan and yellow). The second factor, input modality, also had two levels: printed words (Figure 4.1 blue and cyan) versus pictures (Figure 4.1 purple and yellow). The associative-semantic condition was derived from the Pyramids and Palm Trees test [150], a classical neuropsychological test of associative-semantic processing for words and pictures. During a trial, a triplet of stimuli was presented for 5250 ms, one stimulus on top (the sample stimulus) and one in each lower quadrant (the test stimuli) at 4.6 deg eccentricity (mean picture size was 3.7 deg and mean letter size 1.2 deg), followed by a 1500 ms interstimulus interval. Subjects were asked to press a left- or right-hand key depending on which of the two test stimuli matched the sample stimulus more closely in meaning. A given triplet was presented in either the picture or the word format and this was counterbalanced across subjects. In the visuoperceptual control condition, a picture or word stimulus was presented in three different sizes (mean picture size was 3.7 deg and mean letter size 1.2 deg). Subjects had to press a left- or right-hand key depending on which of the two test stimuli matched the sample stimulus more closely in size on the screen. An epoch, i.e. a block of trials belonging to the same condition, consisted of four trials (total duration 27 s). The fifth condition consisted of a resting baseline condition during which a fixation point was presented in the centre of the screen (Figure 4.1 red). During each fMRI run (5 runs in total), a series of the 5 epoch types, was replicated

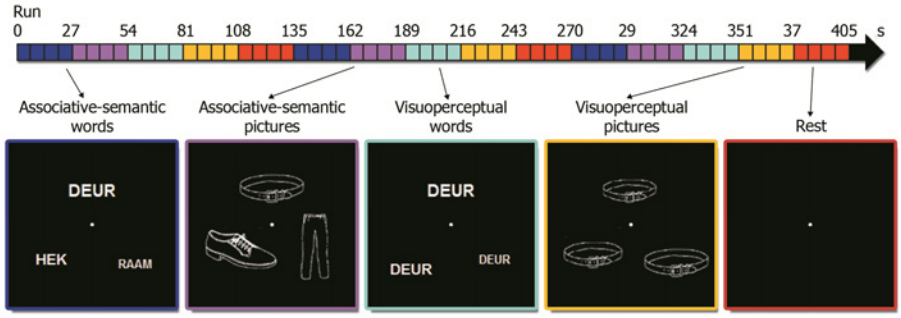

Figure 4.1: Stimuli and tasks in fMRI experiment. Associative-semantic task with words (*blue*) and with pictures (*purple*). Visuoperceptual task with words (*cyan*) or pictures (*yellow*). Resting baseline with fixation point (*red*). Subjects were asked to press a left- or right-hand key depending on which of the two lower stimuli matched the upper stimulus more closely in meaning (*blue, purple*) or in size on the screen (*cyan, yellow*). A given concept triplet was presented in either the word or the picture format and this was counterbalanced across subjects. Arrow in the top of the figure shows a timeline of one fMRI run, with each condition indicated in its respective colour. The order of conditions was randomized for each run and subject. Translation: deur = door, hek = fence, raam = window.

3 times (Figure 4.1 timeline). The order of conditions was pseudorandom and differed across runs of the same subject.

Prior to the fMRI session, visual acuity was tested in each participant. Subjects were asked to read aloud a text written in font 12 at 40 cm distance from their eyes. In case a correction to normal vision was necessary, subjects received MR compatible glasses with lenses matched to the subjects' sight defect. Following this, subjects performed an offline practice session of fMRI task. In this session we determined which size difference (9%, 6%, 3%, or 1%) for the visuoperceptual conditions was needed for each individual subject to obtain comparable accuracies as for the associative-semantic conditions.

4.3.3.2 Image acquisition

Twenty-eight subjects were scanned on a 3T Philips Intera system equipped with an 8-channel receive-only head coil (Philips SENSitivity Encoding head coil). Twenty-eight subjects could not undergo the fMRI in the Intera system because their body in the scanner lumen obstructed the beam from the projector to the screen. These subjects were scanned on a 3T Philips Achieva system equipped with a 32-channel receive-only head coil (Philips SENSitivity Encoding head coil) which used a screen placed behind the individual's head for the projection. There were no statistically significant differences of sex ($P = 0.79$)

(*chi*-square test), genetic groups ($P = 0.17$), age ($P = 0.49$), or MMSE ($P = 0.92$) (Kolmogorov-Smirnov comparison of two datasets) between subjects scanned on the Intera versus the Achieva system. Scanner type was included as a covariate of no interest for all analyses.

Sequence parameters were the same for both scanners. A high-resolution T1-weighted structural scan was obtained using a 3D turbo field echo sequence (coronal inversion recovery prepared 3D gradient-echo images, inversion time 900 ms, TR = 9.6 ms, TE = 4.6 ms, flip angle 8°, field of view = 250 x 250 mm, 182 slices; voxel size 0.98 x 0.98 x 1.2 mm^3). Functional MRIs were acquired using T2* echo-planar images (50 transverse slices, voxel size 2.5 x 2.5 x 2.5 mm^3 ; TR = 3000 ms, TE = 30ms, flip angle 90°, field of view 200 x 200 mm).

4.3.3.3 Image analysis

All analyses were performed using Statistical Parametric Mapping 8 (SPM8, http://www.fil.ion.ucl.ac.uk/spm). Functional MR scans of each subject were realigned to correct for potential head motion. The structural MR image was coregistered to the average of the realigned fMRI images. The structural MR image was then normalized to the SPM8 T1 template in Montreal Neurological Institute (MNI) space. The same normalization matrix was applied to the coregistered fMRI scans. The normalized fMRI images (voxel size 3 x 3 x 3 mm^3) were smoothed using a 6 x 6 x 6 mm^3 Gaussian kernel. A high-pass filter with a Full Width at Half Maximum of 270 s and a low-pass filter consisting of a canonical hemodynamic response function (HRF) were applied. The epoch-related response was modeled by a canonical HRF convolved with a boxcar.

4.3.4 Flutemetamol PET

4.3.4.1 Image acquisition

As described before [65, 66, 73, 190], images were acquired on a 16-slice Siemens Biograph PET/CT scanner (Siemens, Erlangen, Germany). The PET tracer was injected intravenously as a bolus (mean activity 151.2 MBq, SD 8.3, range 137.9 - 192.5 MBq) in an antecubital vein. Image acquisition started 90 min after tracer injection and lasted for 30 min. Prior to the PET scan, a low-dose computed tomography scan was performed for attenuation correction. Random and scatter corrections were also applied. Images were reconstructed using Ordered Subsets Expectation Maximization (4 iterations x 16 subsets).

4.3.4.2 Image analysis

The PET data were reconstructed as 6 frames of 5 minutes and realigned to the first frame to correct for potential head motion. Subsequently, the 6 frames were summed to create one summed image. The individual's T1-

weighted structural image was then coregistered to this PET summed image. This MR image was subsequently normalized to the SPM8 T1 template. The same normalization matrix was then applied to the individual's coregistered PET summed image. From the spatially normalized PET images (voxel size 2 x 2 x 2 mm^3), standardized uptake value ratios (SUVR) were calculated in a voxelwise manner with cerebellar grey matter (GM) as reference region. The cerebellar grey matter reference region was defined as areas 91 to 108 of the Automated Anatomical Labelling atlas (AAL) [191]. The cerebellar reference region was resliced to each individual's normalized PET summed image. In order to exclude most of the white matter (WM) content, it was masked by the normalized and modulated subject-specific GM map, with the threshold for masking set at > 0.3.

Our primary PET outcome measure was the mean SUVR in a composite cortical volume of interest (VOI) ($SUVR_{comp}$). This composite VOI consisted of 5 bilateral cortical regions: frontal (AAL areas 3-10, 13-16, 23-28), parietal (AAL 57-70), anterior cingulate (AAL 31-32), posterior cingulate (AAL 35-36) and lateral temporal (AAL 81-82, 85-90). The composite cortical VOI was resliced to each individual's normalized PET summed image. In order to exclude most of the WM content, it was masked by the normalized and modulated subject-specific GM map, with the threshold for masking set at $>$ 0.3.

While we used $SUVR_{comp}$ as a continuous variable in our primary analysis, we also conducted a secondary analysis where amyloid load was treated as a binary variable and cases were classified as amyloid-positive versus -negative based on an $SUVR_{comp}$ cut-off. Such a binary approach is closer to the way in which Sperling et al. (2011) conceptualized preclinical AD. The $SUVR_{comp}$ cut-off for binary classification was derived from an independent dataset [73] which contained 27 scans from AD patients (mean age 70, SD 7.0) and 15 scans from healthy older controls (HC) (mean age 69, SD 7.6). ^{18}F-flutemetamol scans from the Vandenberghe et al. (2010) study were re-analyzed using the MRI-informed PET analysis method described above. The cut-off was defined based on the statistical distance between the AD group and the HC as described in Vandenberghe et al. (2010). This gave a $SUVR_{comp}$ cut-off equal to 1.38. Note that this cut-off is lower than the cut-off defined by Vandenberghe et al. (2010) or Thurfjell et al. (2014) for a purely PET-based approach, probably due to exclusion of more white matter signal in the MRI-informed method in the amyloid-negative cases. Because of this difference, we also verified our binary case classification using the PET-based method and cut-off from Thurfjell et al. (2014) (cut-off equal to 1.57).

We verified our findings using partial volume corrected (PVC) data. PVC was based on the MRI using the modified Müller-Gärtner method [146, 244]. This method makes use of probabilistic segmentation and determines tracer concentration per unit volume of GM. The normalized unmodulated GM and WM segmentations were used to estimate different tissue fractions per voxel. PVC was applied to the normalized PET summed images. The remaining

procedures were identical to those outlined above.

4.3.5 Statistical analysis

4.3.5.1 Analysis of behavioural data obtained during fMRI

RTs and accuracies (% correct responses) were analyzed by means of a four-factor repeated-measures ANOVA, with stimulus modality (2 levels: pictures vs words) and task (2 levels: associative-semantic vs visuoperceptual) as within-subject factors and, as between-subject factors, BDNF (2 levels: codon 66 *met* carriers vs non-carriers) and APOE (2 levels: $\varepsilon 4$ carriers vs non-carriers) genotype (Table 4.3). Pairwise comparisons were performed using Bonferroni post hoc tests.

4.3.5.2 Whole-brain voxelwise analysis

All voxelwise analyses were performed using SPM8. For each subject, parameter estimates were generated modelling each of the 5 conditions. We then created the following contrast images, averaging across runs:

1. (Associative-semantic task with words + Associative-semantic task with pictures) - (Visuoperceptual task with words + Visuoperceptual task with pictures)
2. Associative-semantic task with words - Visuoperceptual task with words
3. Associative-semantic task with pictures - Visuoperceptual task with pictures
4. (Associative-semantic task with words - Visuoperceptual task with words) - (Associative-semantic task with pictures - Visuoperceptual task with pictures) and inversely.
5. (Associative-semantic task with words + Associative-semantic task with pictures) - baseline
6. (Visuoperceptual task with words + Visuoperceptual task with pictures) - baseline.
7. Visuoperceptual task with words - baseline.
8. Visuoperceptual task with pictures - baseline.

The first-level contrast images were then used for second-level whole-brain analysis.

Our primary outcome analysis consisted of a whole-brain voxelwise linear regression analysis with SUVR_{comp} as independent variable, and fMRI response in contrast 1 (main effect of task) as dependent variable. The statistical map was thresholded at a significance threshold of voxel-level $P_{uncorrected} < 0.001$ combined with a cluster-level $P_{corrected} < 0.05$, family-wise error (FWE) corrected for the whole brain volume.

As a secondary outcome analysis, we examined for each of the 10 regions that constitute the composite cortical VOI, the correlation between regional SUVR and the main effect of task (contrast 1) across the whole brain.

Furthermore, we examined whether any significant correlations with amyloid load were found for contrasts 2-8.

As a further secondary outcome analysis, we performed a whole-brain voxel-by-voxel linear regression between SUVR images and fMRI images representing associative-semantic minus visuoperceptual activity (contrast 1) using Biological Parametric Mapping (BPM) [253]. The BPM is a toolbox for multimodal image analysis which is based on a voxel-wise use of the SPM's general linear model. This allows comparison of different imaging modalities within voxels.

As a further secondary analysis, we categorized the cases into amyloid-positive versus amyloid-negative and compared the main effect of task between the two groups (contrast 1) using a two-sample t test.

We also tested if there was any difference in fMRI response between the four genetic groups by means of a factorial ANOVA with BDNF (2 levels: *met* allele present vs absent) and APOE (2 levels: $\varepsilon 4$ allele present vs absent) as between-subject factors and the main effect of task (contrast 1) as dependent variable.

All whole-brain voxelwise analyses were thresholded at a significance threshold of voxel-level $P_{uncorrected} < 0.001$ combined with a cluster-level $P_{corrected} < 0.05$, FWE corrected for the whole brain volume. In the BPM analysis we used threshold of voxel-level $P_{uncorrected} < 0.001$ combined with cluster size of at least 10 voxels.

4.3.5.3 Relationship to offline measures of linguistic performance

When our primary analysis revealed clusters of significant correlation between SUVR_{comp} and fMRI response during associative-semantic versus visuoperceptual processing (contrast 1), we examined in further detail whether mean fMRI response in these clusters correlated with a pre-specified set of offline measures of linguistic performance. Clusters of voxels exhibiting a significant correlation between SUVR_{comp} and fMRI response (contrast 1) were extracted using the MarsBaR 0.43 toolbox (http://marsbar.sourceforge.net/). Given the proposed role of the posterior STS in lexical-semantic retrieval [133], the principal measures that we selected a priori were 1) Reaction times during the confrontation naming task, 2) Reaction times during the lexical decision task, 3) The b parameter from the speeded word identification task. For each of these parameters, we performed a stepwise linear regression analysis with this parameter as dependent variable and the independent variables: fMRI response during the associative-semantic minus the visuoperceptual condition (contrast 1), SUVR_{comp}, age, education level, BDNF genotype, and APOE genotype. Probability to enter the model was set at $P < 0.05$ with probability to remove set to $P > 0.1$. This analysis was performed outside SPM in a VOI-based

manner using STATISTICA 11 (http://www.statsoft.com/) as SPM software does not include stepwise linear regression.

In an additional, binary approach, we examined which of these neurolinguistic measures differed between the amyloid-positive and the amyloid-negative class (two-sample t test).

4.4 Results

4.4.1 Analysis of behavioral scores during fMRI

The main effect of task was significant: subjects responded more accurately during the associative-semantic conditions than during the visuoperceptual conditions ($F(1,52) = 17.4$, $P = 0.0001$), albeit with longer RTs ($F(1,52) = 24.9$, $P = 0.000007$) (Table 4.3). The main effect of modality was also significant: subjects responded more slowly ($F(1,52) = 21.3$, $P = 0.00003$) and less accurately ($F(1,52) = 5.7$, $P = 0.02$) for pictures than for words (Table 4.3). The interaction between task and modality was significant ($F(1,52) = 11$, $P = 0.002$): the associative-semantic task was performed more accurately with words than with pictures ($P = 0.00008$), while there was no difference between words and pictures for the visuoperceptual task ($P = 1$). There was no main effect of BDNF and APOE genotypes on accuracy or RT ($P > 0.2$) (Table 4.3). The three-way interaction between task, modality and APOE genotype was significant for accuracies ($F(1,52) = 8.2$, $P = 0.006$) (Table 4.3). According to a posthoc analysis, APOE $\varepsilon 4$ non-carriers performed the associative-semantic task more accurately with words than with pictures ($P = 0.0006$), while there was no difference between the two input-modalities for the visuoperceptual task ($P = 0.35$). No such difference was seen in the APOE $\varepsilon 4$ carriers ($P = 0.23$). We did not find any significant interactions for reaction times ($P > 0.05$).

Performance during fMRI experiment

	Reaction time (ms)					Accuracy (% correct)				
BDNF	*met*+	*met*-	*met*+	*met*-	all	*met*+	*met*-	*met*+	*met*-	all
APOE	$\varepsilon 4$+	$\varepsilon 4$+	$\varepsilon 4$-	$\varepsilon 4$-	groups	$\varepsilon 4$+	$\varepsilon 4$+	$\varepsilon 4$-	$\varepsilon 4$-	groups
Sem W	2653	2852	2679	2725	2717	88.8	85.5	90.7	89.0	88.8
	(395)	(326)	(300)	(449)	(376)	(7.4)	(4.7)	(4.2)	(9.0)	(7.0)
Sem P	2885	2839	2771	2858	2840	80.2	83.5	82.6	81.3	81.7
	(530)	(332)	(293)	(462)	(417)	(8.7)	(7.9)	(9.5)	(9.0)	(8.7)
Visuo W	2343	2570	2474	2457	2451	81.2	75.7	75.1	80.7	78.5
	(404)	(407)	(381)	(357)	(382)	(10.3)	(15.8)	(16.0)	(15.6)	(14.4)
Visuo P	2633	2765	2534	2647	2636	76.3	71.7	81.2	85.0	79.3
	(611)	(447)	(426)	(382)	(468)	(13.9)	(17.8)	(15.2)	(14.5)	(15.5)

Table 4.3: Values represent means and standard deviations. Sem W = associative-semantic task with words; Sem P = associative-semantic task with pictures; Visuo W = visuoperceptual task with words; Visuo P = visuoperceptual task with pictures.

4.4.2 Whole-brain voxelwise analysis

4.4.2.1 Univariate contrast between fMRI conditions

The contrast between the associative-semantic minus the visuoperceptual conditions (main effect of task, contrast 1) revealed a distributed semantic network consistent with previous findings [248, 133, 132] (Figure 4.2A). The interaction between task and input modality (contrast 4) revealed word-specific activation during the semantic compared to the visuoperceptual task in left STS, extending from posterior to more anterior portions of the STS (cluster peak coordinates -66, -36, 9, extent (ext) = 113 voxels, cluster level $P_{corrected}$ = 0.0001) (Figure 4.2B). Picture-specific semantic activation (inverse of contrast 4) occurred bilaterally in ventral occipitotemporal cortex extending to superior occipital gyrus (right cluster peak coordinates 33, -45, -21, ext = 1756 voxels, cluster level $P_{corrected} < 0.0001$ and left cluster peak coordinates -39, -51, -15, ext = 1286 voxels, cluster level $P_{corrected} < 0.0001$) and in right inferior frontal gyrus (cluster peak coordinates 48, 12, 27, ext = 141 voxels, cluster level $P_{corrected} < 0.0001$) (Figure 4.2C).

4.4.2.2 Linear regression between fMRI response and amyloid load

In a whole-brain analysis, the posterior third of the left middle temporal gyrus (MTG) (Figure 4.3A) exhibited a significant positive correlation between fMRI response during the associative-semantic versus the visuoperceptual task (contrast 1) and $SUVR_{comp}$: activity levels were higher with a higher amyloid load (-57, -45, 9, ext = 64 voxels, cluster level $P_{corrected} = 0.006$) (Figure 4.3A-E). No other regions showed a correlation, even when we lowered the significance threshold to cluster-level $P_{corrected} < 0.25$. The MTG belonged to the amodal network, as evidenced by the conjunction analysis of contrast 2 and 3 (Figure 4.4A versus B and C).

When we restricted the contrast between the associative-semantic and the visuoperceptual task to the words (contrast 2) and examined the correlation with amyloid load in the whole-brain analysis, $SUVR_{comp}$ correlated positively with fMRI response during the associative-semantic minus visuoperceptual control condition for words in the same region (-60, -48, 9, ext = 49 voxels, cluster level $P_{corrected} = 0.02$). For pictures, there was no correlation (contrast 3) (cluster-level $P_{corrected} > 0.6$). No other regions showed a correlation, even when we lowered the significance threshold to cluster-level $P_{corrected} < 0.10$. Neither were any correlations with $SUVR_{comp}$ found for contrast 4-8.

Analysis of partial volume corrected data confirmed these results. PVC $SUVR_{comp}$ positively correlated with fMRI response during the associative-semantic minus the visuoperceptual condition (contrast 1) in the posterior third of the left MTG (-54, -39, 12, ext = 87 voxels, cluster level $P_{corrected} = 0.001$). Analysis restricted only to the word conditions showed that $SUVR_{comp}$ correlated positively with fMRI response during the associative-semantic minus

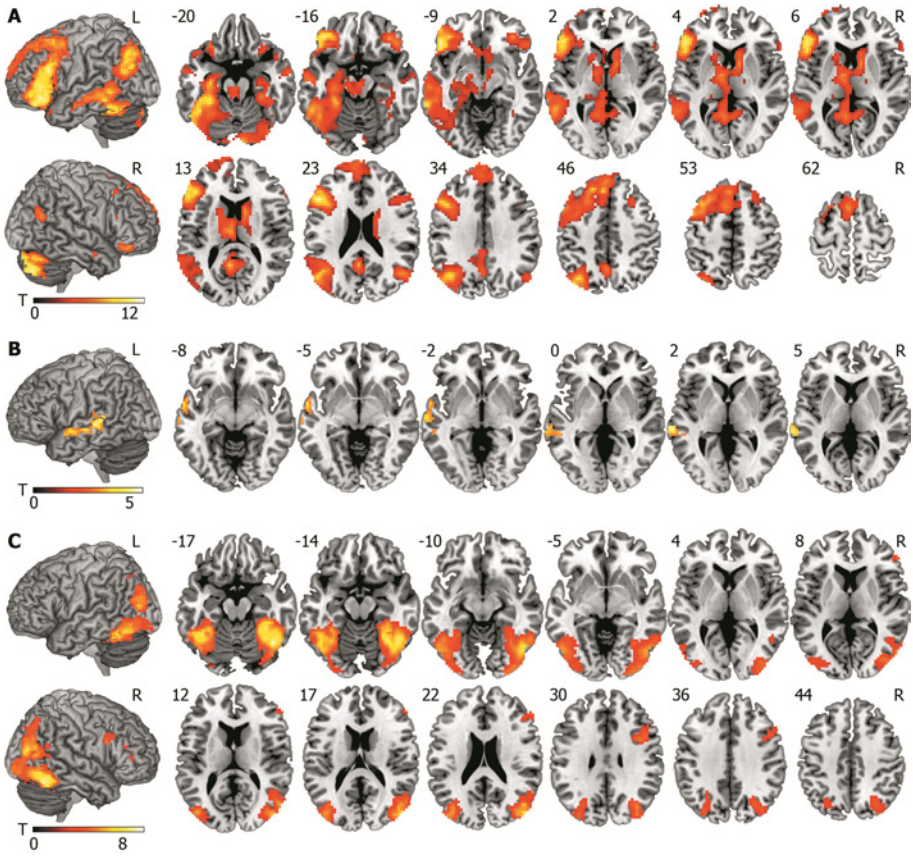

Figure 4.2: fMRI activity during associative-semantic processing. (A) Main effect of associative-semantic task minus visuopercetual task (contrast 1). (B) Interaction effect of task and modality: effect of semantic words (contrast 4, i.e. (associative-semantic task with words - visuoperceptual task with words) - (associative-semantic task with pictures - visuoperceptual task with pictures)). (C) Interaction effect of task and modality: effect of semantic pictures (inverse of contrast 4, i.e. (associative-semantic task with pictures - visuoperceptual task with pictures) - (associative-semantic task with words - visuoperceptual task with words)). Shown activations are significant at the threshold of voxel level $P_{uncorrected} = 0.001$ combined with cluster level $P_{corrected} = 0.05$. The colour scales indicate the T-values for the contrasts. MNI coordinates are indicated in the left upper corner and orientation of the brain in the right upper corner.

visuoperceptual control condition for words (contrast 2) in the same region (-54, -36, 9, ext = 45 voxels, cluster level $P_{corrected} = 0.028$). No correlation was found between SUVR_{comp} and the fMRI response during the associative-

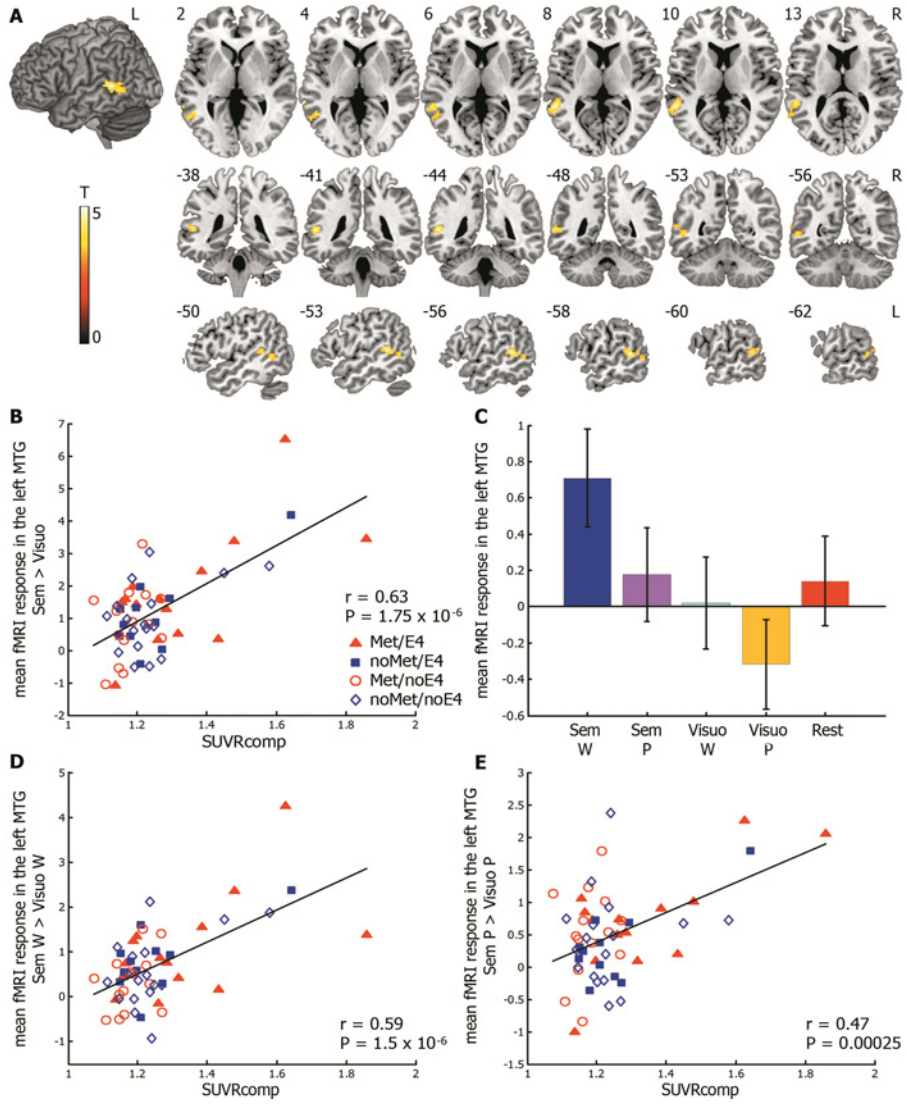

Figure 4.3: Correlation between fMRI response during associative-semantic processing and amyloid load. (A) Area in the left posterior MTG of significant correlation between SUVR_{comp} and fMRI response during associative-semantic minus visuoperceptual condition (contrast 1) (cluster peak -57, -45, 9, ext = 64 voxels, cluster level $P_{corrected} = 0.006$). The colour scale indicates the T-values. MNI coordinates are indicated in the left upper corner and orientation of the brain in the right upper corner. (B) Plot of correlation between SUVR_{comp} (X axis) and mean fMRI contrast values in the left MTG VOI during associative-semantic minus visuoperceptual condition (contrast 1) (Y axis) ($r = 0.63$, $P < 0.0001$). (C) Bar plot depicting mean fMRI contrast values (Y axis) in the left posterior MTG during each condition (X axis). Error bars: standard error;

Sem W: associative-semantic task with words (*blue*); Sem P: associative-semantic task with pictures (*purple*); Visuo W: visuoperceptual task with words (*cyan*); Visuo P: visuoperceptual task with pictures (*yellow*); Rest: resting baseline condition (*red*). (D) Correlation of $SUVR_{comp}$ (X axis) with mean fMRI contrast values during associative-semantic word processing (contrast 2) in the left MTG VOI (Y axis) ($r = 0.59$, $P < 0.0001$). (E) Correlation of $SUVR_{comp}$ (X axis) with mean fMRI contrast values during associative-semantic picture processing (contrast 3) in the left MTG VOI (Y axis) ($r = 0.47$, $P = 0.00025$). Black lines: linear regressions; *red triangles*: BDNF *met* +ve/APOE $\varepsilon 4$ +ve; *blue squares*: BDNF *met* -ve/APOE $\varepsilon 4$ +ve; *red circles*: BDNF *met* +ve/APOE $\varepsilon 4$ -ve; *blue diamonds*: BDNF *met* -ve/APOE $\varepsilon 4$ -ve.

semantic minus visuoperceptual condition when only pictures were used (contrast 3) (cluster level $P_{corrected} > 0.07$).

Among the regions which constituted the composite cortical VOI, average SUVR in each of the regions besides the left and right anterior cingulate and left lateral frontal region contributed to the correlation of fMRI response during contrast 1 and $SUVR_{comp}$ (cluster level $P_{corrected} < 0.038$).

Biological parametric mapping indicated a significant correlation within-voxels between fMRI activity and SUVR in the posterior left MTG (cluster peak coordinates -60, -54, 12, ext = 18 voxels, voxel level $P_{uncorrected} = 0.0001$, $Z = 3.65$, $r = 0.50$).

4.4.2.3 Binary classification

We evaluated whether similar results would be obtained had we used a binary approach: amyloid-positive versus amyloid-negative group (Figure 4.5). Eight subjects (14%) were classified as positive (Figure 4.5). fMRI performance parameters did not differ between the amyloid-positive and the amyloid-negative group (Table 4.4). In a whole-brain voxelwise analysis, the amyloid-positive group exhibited a higher fMRI response compared to the amyloid-negative group during the associative-semantic minus visuoperceptual conditions (contrast 1) in the posterior third of the MTG (-54, -42, 9, ext = 55 voxels, cluster-level $P_{corrected} = 0.013$) (Figure 4.5B red cluster). This was also true for the contrast between the associative-semantic minus visuoperceptual task presented as words (contrast 2) (-57, -45, 6, ext = 59 voxels, cluster-level $P_{corrected} = 0.008$) (Figure 4.5B green cluster). Overlap between clusters is shown in dark orange (Figure 4.5B). We did not find any significant differences elsewhere and neither did we find any significant between-group differences for other contrasts. When we applied the Thurfjell et al. (2014) method and cut-off for binary classification, 4 cases were positive. The between-group differences remained essentially the same: the amyloid-positive group had higher fMRI response compared to the amyloid-negative group during the associative-semantic versus

visuoperceptual condition (-60, -48, 9, ext = 54 voxels, cluster-level $P_{corrected}$ = 0.014).

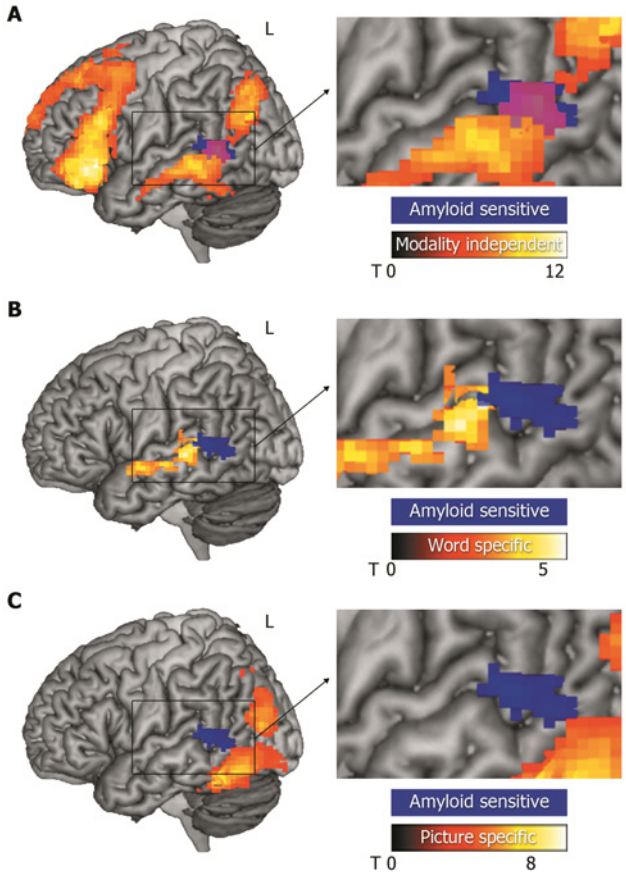

Figure 4.4: Modality specificity of amyloid sensitive VOI (left MTG). (A) Functional left MTG VOI belongs to the amodal associative-semantic network (conjunction of contrast 2 and 3) (MTG cluster pick -63, -45, 3, ext = 51 voxels, voxel level $P_{corrected}$ = 0.000002). Overlap is shown in *purple*. (B) Left MTG VOI did not belong to the word specific associative-semantic areas (contrast 4) (voxel level $P_{corrected} > 0.16$) and (C) neither to the picture specific semantic areas (inverse of contrast 4) (voxel level $P_{corrected} > 0.18$). The left MTG VOI is shown in *blue*. The hot colour scales indicate the T-values of associative-semantic network (A), word specific associative-semantic regions (B), and picture specific associative-semantic regions (C). Orientation of the brain is indicated in the right upper corner. All P-values were FWE corrected for multiple comparisons in a small volume.

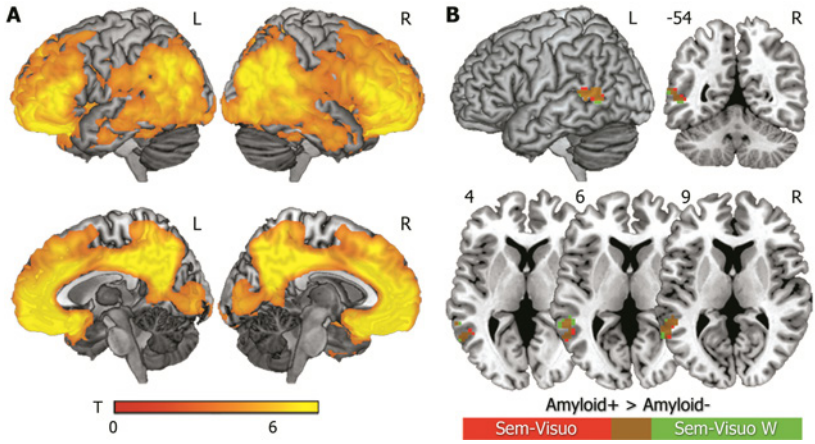

Figure 4.5: Amyloid-positive versus amyloid-negative group. (A) Older healthy amyloid-positive subjects had higher amyloid deposition compared to amyloid-negative subjects in typical regions for increased amyloid load (precuneus, anterior and posterior cingulate, lateral prefrontal, lateral parietal, and lateral temporal, ext = 39779 voxels, cluster level $P_{corrected} < 0.0001$). The hot colour scale indicates the T-values for the differences. (B) Older healthy amyloid-positive subjects had increased fMRI response compared to amyloid-negative subjects during the associative-semantic minus visuoperceptual conditions (contrast 1) in the posterior third of the MTG (-54, -42, 9, ext = 55 voxels, cluster level $P_{corrected} = 0.013$; in *red*), and during the associative-semantic minus visuoperceptual task presented as words (contrast 2) also in the MTG (-57, -45, 6, ext = 59 voxels, cluster level $P_{corrected} = 0.008$; in *green*). Overlap between clusters is shown in *dark orange*. Results are thresholded at voxel level $P_{uncorrected} = 0.001$ combined with cluster level $P_{corrected} = 0.05$. MNI coordinates are indicated in the left upper corner and orientation of the brain in the right upper corner.

4.4.3 Genotype effect on fMRI response and relationship between fMRI response and SUVR

BDNF and APOE genotype did not affect the activity patterns during the associative-semantic versus visuoperceptual conditions (cluster level $P_{corrected} > 0.8$). Nor was there an effect of BDNF or APOE genotype on the correlation between mean fMRI response in the left posterior MTG (contrast 1) and SUVR_{comp} ($P > 0.1$) (BDNF *met* carriers $r = 0.64$, $P = 0.0002$; BDNF non-carriers $r = 0.61$, $P = 0.0005$; APOE $\varepsilon 4$ carriers $r = 0.71$, $P = 0.00006$; APOE $\varepsilon 4$ non-carriers $r = 0.40$, $P = 0.03$) (Figure 4.6).

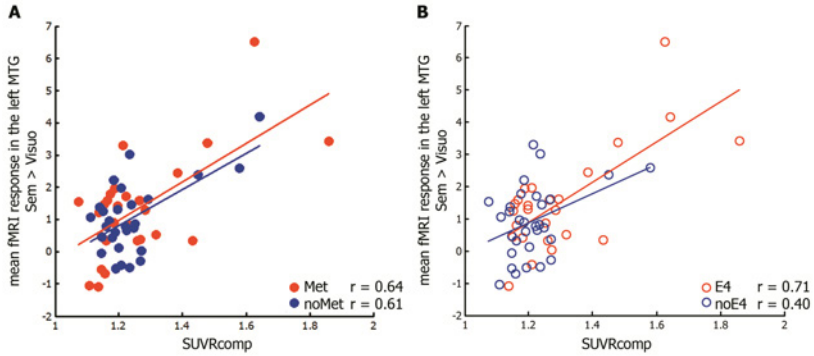

Figure 4.6: Effect of BDNF and APOE genotype on fMRI response. (A) The difference between correlations for BDNF *met* carriers (*red full circles*) and non-carriers (*blue full circles*) ($P = 0.86$). (B) The difference between correlations for APOE $\varepsilon 4$ carriers (*red empty circles*) and non-carriers (*blue empty circles*) ($P = 0.11$). Y axes: mean fMRI response during the associative-semantic minus the visuoperceptual condition (contrast 1) in functional left MTG VOI. X axes: SUVR_{comp}. Lines show linear regressions.

4.4.4 Relationship with offline language measures

According to a stepwise regression analysis, variance in RT during the confrontation naming task was partly explained by SUVR_{comp} ($r = 0.27$, $P = 0.04$), rather than fMRI response (contrast 1; $P = 0.62$), age ($P = 0.34$), education ($P = 0.57$), BDNF ($P = 0.21$), or APOE status ($P = 0.42$) (Figure 4.7).

Response latencies during confrontation naming were longer in the amyloid-positive compared to the amyloid-negative group ($P = 0.047$) (Table 4.4). There were no differences for any of the other experimental language tests and neither did the conventional neuropsychological test scores differ between the amyloid-positive and -negative class (Table 4.4).

4.5 Discussion

In cognitively intact older adults, a higher amyloid burden was associated with subclinical alterations of the network for language and associative-semantic processing. Activity in left posterior middle temporal gyrus was higher with a higher amyloid load (Figure 4.3A, B). Higher amyloid levels were correlated with slower confrontation naming (Figure 4.7). Our posterior temporal findings are based on a whole-brain search without prior restriction of the search volume. They were in agreement with our a priori hypothesis about posterior temporal cortex, although the exact location was in the amodal posterior MTG (Figure 4.4A) adjacent to the word-specific posterior STS found before in MCI

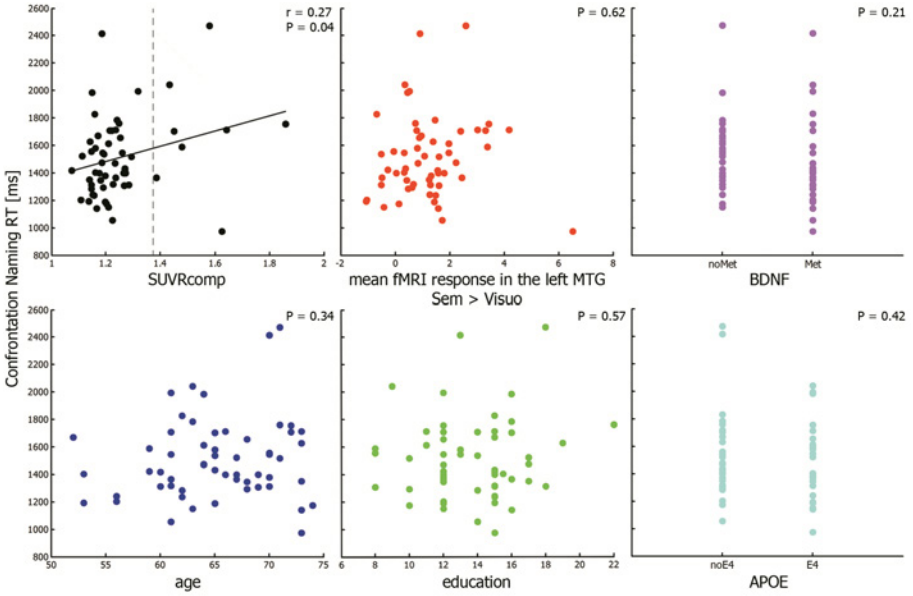

Figure 4.7: Results of a stepwise regression analysis. RT during the confrontation naming task (Y axis) was best predicted by the $SUVR_{comp}$ (*black circles*) ($r = 0.27$, $P = 0.04$), and not by fMRI response from contrast 1 (*red circles*) ($P = 0.62$), age (*blue circles*) ($P = 0.34$), education (*green circles*) ($P = 0.57$), BDNF (*purple circles*) ($P = 0.21$), or APOE (*cyan circles*) ($P = 0.42$) status. X axis represents values of the predictor variables. Grey dashed line = $SUVR_{comp}$ cut-off of 1.38.

[133] and AD [132] patients.

While we used the $SUVR_{comp}$ as a continuous variable for the primary outcome analysis, we also conducted a secondary analysis where amyloid load was treated as a binary variable and cases were classified as amyloid-positive versus -negative based on an $SUVR_{comp}$ cut-off. Such a binary approach is closer to the way in which Sperling et al. (2011) conceptualize preclinical AD. The findings based on a binary approach were entirely in line with the findings obtained with the linear regression approach (Figure 4.5).

During the visuoperceptual control conditions subjects engaged in an active comparison of the size-on-the-screen of a picture or a word. It is highly plausible that the meaning of this word or picture is automatically activated to some degree during the visuoperceptual condition too. A lower-level control condition with consonant letter strings or scrambled pictures [254] would have been necessary had we wanted to isolate the regions activated during word and picture processing in the visuoperceptual condition. In any case, we did not find a correlation between amyloid load and the activity pattern during the visuoper-

ceptual control conditions minus fixation baseline. This could suggest that the network underlying activation of word and picture meaning during the visuoperceptual condition is relatively intact in preclinical AD and that the principal changes are at the level of explicit associative-semantic processing.

Our findings are based on observational cross-sectional data, analyzed by means of correlational analysis and between-group comparisons. One therefore has to be careful in drawing conclusions about a causal link between the increase in amyloid burden, the increase in left posterior temporal activity, and the decrease in confrontation naming latencies. To adequately resolve this fundamental limitation, one would need to conduct interventional studies. This is difficult since there are no proven amyloid-lowering interventions available. Transcranial magnetic stimulation targeting the left posterior temporal cortex could be an option to examine how altering activity within a subject affects naming latencies and whether this depends on amyloid load.

We also observed right-hemispheric inferior frontal activation during the associative-semantic versus the visuoperceptual task (Figure 4.2A), and this was particularly pronounced for the pictures (Figure 4.2C). The right inferior frontal activation could be related to the older age range of our individuals, in line with the Hemispheric Asymmetry Reduction in Older Adults model [255, 256]. However, one would need fMRI data over a wider age range including also young adults to confirm this. In any case, no increase in right-hemispheric activation was found as a consequence of increasing amyloid load in our dataset, contrary to our original hypothesis [132].

Previous studies have investigated changes in task-related fMRI in AD principally within the episodic memory domain. AD patients consistently show lower hippocampal activation in episodic memory encoding tasks in comparison to controls and/or MCI subjects [257, 258, 259, 260, 138, 261]. Subjects with late MCI also have decreased hippocampal activity during episodic memory encoding [258, 262] while subjects with early MCI compared to controls show an increase in hippocampal activity during memory encoding [263, 264]. Young healthy presenilin 1 mutation carriers destined for early-onset AD exhibit higher activity in the hippocampal formation in comparison to the non-carrier controls [265, 266]. Subjects with a higher risk for AD due to family history and APOE $\varepsilon 4$ carrier status also have higher hippocampal activation during encoding compared to non-carrier controls [267]. These studies led to a model where the direction of functional changes in medial temporal cortex is stage-dependent: in the preclinical AD stage and the early MCI stage, activity during memory encoding in the hippocampus is increased compared to controls, while in the late MCI and the clinically probable AD stage activity is decreased compared to controls. Our findings indicate that a similar sequence may occur in the language domain in left posterior temporal cortex. The current data show increased activity during associative-semantic processing in preclinical AD according to the National Institute on Aging and Alzheimer's Association criteria [55]. In a previous study in amnestic MCI, activity in left posterior STS was decreased and correlated with the speed of written word identification [133]. In

clinically probable AD, the same region also showed lower activity levels [132]. Our study is the first to report an increase in left posterior temporal cortex in a stage that has been referred to as preclinical AD (Figure 4.3), similarly to what has been described in the hippocampal formation for episodic memory [261]. Taken together, this series of studies may suggest a similar sequence of increased activity in posterior temporal cortex followed by activity decreases as Alzeimer's disease progresses to the clinical stages.

Initial functional imaging studies of language and semantic memory in clinically probable AD have emphasized prefrontal increases which correlated positively with task performance [240, 242, 268]. These AD-related prefrontal increases generalized across episodic and semantic memory tasks [268] and presumably reflect general adaptive strategic processes [240, 268]. A series of studies revealed functional changes also in temporal cortex, most notably left inferior temporal cortex [161, 162], left and right middle temporal gyrus [161, 162, 163] and left posterior superior temporal sulcus [132, 133]. Functional differentiation exists within left temporal cortex even within nearby areas. For instance, the posterior third of the left STS is activated during semantic processing specifically for words [248, 133]. It has been principally implicated in lexical-semantic [133] or lexical-phonological retrieval [269, 270]. In contrast, an adjacent more inferior region, the posterior third of the left MTG, is activated during semantic processing for both words and pictures (Figure 4.4A versus B and C, Figure 4.3D-E). The left posterior middle temporal gyrus is one of the most consistent hubs in the associative-semantic network [271, 252]. It has been implicated in amodal semantic processing [248, 133] as well as in semantic control [272, 273]. In the current study the correlation principally occurred within the amodal posterior MTG region rather than the word-specific STS (Figure 4.3A, Figure 4.4A). Our findings can be readily integrated in current hypotheses that attribute to posterior MTG a role in cognitive control: regions involved in semantic control may be the prime candidates for compensatory processes in response to increases in amyloid load. Increased amyloid burden in cortical areas may hamper normal neuronal functioning due to its neurotoxic effects. In order to cope with such functional changes at the neuronal level, demands for cognitive control may increase and this may account for the increase in MTG activity levels. Cognitively normal older persons may have increased Aβ levels yet intact neuropsychological performance [237, 164], possibly due to ongoing compensatory processes. As the disease advances, mechanisms responsible for maintaining constant level of increased activation may become exhausted, resulting in the first cognitive symptoms. Thus early word finding difficulties in the course of AD might arise due to failure of semantic control processes, followed by a gradual activity decrease in other language areas, e.g. areas directly involved in word processing like posterior STS.

We did not find any effect of genetic polymorphisms of APOE or BDNF on the language network in our cohort. In AD, APOE $\varepsilon 4$ status has been associated more closely with episodic memory deficits than with language symptoms [274, 275, 276, 277]. Healthy older controls with a family history of Alzeimer's

disease and at least one APOE $\varepsilon 4$ allele, have increased fMRI activation during a semantic memory task (famous versus unfamiliar names) in bilateral temporoparietal areas, posterior cingulate and precuneus, posterior middle and superior temporal regions, and left hippocampal complex [278]. It is not that we did not find any effect of APOE. As reported before, APOE genotype exerted an effect on the amyloid burden in our cohort: a higher amyloid load in APOE $\varepsilon 4$ carriers was present in posterior cingulate, a region outside the network that our paradigm is activating [244].

As of yet, the relationship between BDNF and language has been principally studied during development and early adulthood [279, 280, 281] and in schizophrenia [282]. Contrary to our hypothesis, the regression between fMRI response and amyloid load was not influenced by BDNF status. In the same cohort we previously reported that BDNF exerted a direct effect on amyloid load in interaction with APOE: BDNF *met* carriers had increased levels of Aβ in typical regions of predilection in comparison to the BDNF *met* non-carriers with APOE $\varepsilon 4$ [244]. In summary, contrary to our prediction, the effect of BDNF in our cohort is situated at the level of amyloid aggregation rather than at the level of fMRI response.

Our findings highlight the critical role of left posterior temporal cortex in AD-related processes. Changes in left posterior superior temporal sulcus lead to lexical-semantic retrieval deficits which may explain the word finding difficulties in clinical AD [132] and the subclinical slowing in word identification speed in MCI [133]. The changes we observed in this study in the posterior middle temporal gyrus may reflect higher demands for semantic control in those subjects who are cognitively intact despite a high amyloid burden.

To conclude, our cross-sectional data indicate that a higher amyloid load in cognitively intact individuals has functional consequences for the network mediating language and associative-semantic processing. The converging evidence obtained in cognitively intact older adults, amnestic MCI and AD may suggest a sequence of events similar to that proposed for the hippocampal formation in episodic memory. The initial compensatory role of increased neuronal activity may precede later deterioration.

Differences between amyloid-positive and amyloid-negative subjects

	Age (yr)	Gender (M/F)	Education (yr)	MMSE (/30)	AVTL TL (/75)	AVLT DR (/15)	BNT (/60)	AVF (# words)	LVF (# words)	RPM (/60)
Amyloid+	67.9 (5.2)	3/5	13.1 (3.5)	28.5 (0.9)	44.1 (6.8)	10.5 (1.8)	52.8 (4.1)	18.4 (4.2)	30.0 (13.8)	39.3 (12.1)
Amyloid−	64.8 (5.5)	28/20	13.8 (2.7)	29.1 (0.9)	50.0 (9.7)	10.8 (2.8)	53.3 (4.9)	20.8 (5.1)	34.5 (9.7)	43.7 (7.7)
P	0.14	0.27	0.55	0.10	0.10	0.81	0.78	0.21	0.26	0.17
	BDNF	*APOE*	Conf naming		Lexical decision			Speeded id W		
	met+/met-	*ε4+/ε4-*	RT (ms)	Accu (%)	RT (ms)	Accu (A')	*a* (ms)	*b* (ms)	*c* (ms)	
Amyloid+	5/3	6/2	2203 (441)	92.3 (0.0)	1109 (322)	98.0 (0.0)	21.3 (9.9)	21.4 (10.9)	98.6 (1.3)	
Amyloid−	23/25	19/29	1978 (258)	91.9 (0.1)	1106 (231)	98.9 (0.0)	22.4 (13.4)	20.7 (10.8)	99.1 (1.5)	
P	0.45	0.06	**0.047**	0.84	0.97	0.11	0.83	0.86	0.42	
	Sem W		Sem P		Visuo W		Visuo P			
	RT (ms)	Accu (%)	RT (ms)	Accu (%)	RT (ms)	Accu (%)	RT (ms)	Accu (%)		
Amyloid+	2885 (416)	89.4 (4.0)	2883 (564)	83.5 (9.3)	2571 (443)	82.3 (11.0)	2856 (686)	74.8 (15.7)		
Amyloid−	2689 (367)	88.7 (7.4)	2833 (395)	81.4 (8.7)	2431 (372)	77.9 (14.9)	2599 (420)	80.1 (15.5)		
P	0.17	0.79	0.76	0.53	0.34	0.43	0.15	0.38		

Table 4.4: Values represent means and standard deviations. Gender, APOE, and BDNF genotypes are expressed in number of individuals. Abbreviations are explained in Table 1, 2, and 3. *P*-values represent significance for two-sample *t*-test or *chi*-square test (gender, APOE, BDNF).

5

Amyloid imaging in cognitively normal older adults: Comparison between ^{18}F-flutemetamol and ^{11}C-Pittsburgh Compound B

This chapter has been published as:

Katarzyna Adamczuk, Jolien Schaeverbeke, Natalie Nelissen, Veerle Neyens, Mathieu Vandenbulcke, Karolien Goffin, Johan Lilja, Kelly Hilven, Patrick Dupont, Koen Van Laere, Rik Vandenberghe. Amyloid imaging in cognitively normal older adults: Comparison between ^{18}F-flutemetamol and ^{11}C-Pittsburgh Compound B. *Eur J Nucl Med Mol Imaging* 2015 doi:10.1007/s00259-015-3156-9.

5.1 Abstract

Preclinical, or asymptomatic, Alzheimer's disease (AD) refers to the presence of positive AD biomarkers in the absence of cognitive deficits. This research concept is being applied to define target populations for clinical drug development. In a prospective community-recruited cohort of cognitively intact older adults, we compared two amyloid imaging markers within subjects: ^{18}F-flutemetamol to ^{11}C-Pittsburgh compound B (^{11}C-PIB).

In 32 community-recruited cognitively intact older adults aged between 65 and 80 years, we determined the concordance between binary classification based on ^{18}F-flutemetamol versus ^{11}C-PIB according to semiquantitative assessment (standardized uptake value ratio in composite cortical volume, $SUVR_{comp}$) and, alternatively, according to visual reads. We also determined the correlation between ^{18}F-flutemetamol and ^{11}C-PIB SUVR and evaluated how this was affected by the reference region chosen (cerebellar grey matter versus pons) and the use of partial volume correction (PVC) in this popula-

tion.

Binary classification based on semiquantitative assessment was concordant between ^{18}F-flutemetamol and ^{11}C-PIB in 94% of cases. Concordance of blinded binary visual reads between tracers was 84%. The Spearman correlation between ^{18}F-flutemetamol and ^{11}C-PIB SUVR$_{comp}$ with cerebellar grey matter as reference region, was 0.84, with a slope of 0.98. Correlations in neocortical regions were significantly lower with pons as reference region. PVC improved the correlation in striatum and medial temporal cortex.

For the definition of preclinical AD based on ^{18}F-flutemetamol, concordance with ^{11}C-PIB was highest using semiquantitative assessment with cerebellar grey matter as reference region rather than pons.

5.2 Introduction

Biomarkers for Aβ accumulation in the brain play a central role in the National Institute on Ageing and Alzheimer's Association (NIA-AA) research definition of preclinical Alzheimer's disease (AD) [55]. Preclinical AD, also termed asymptomatic AD, refers to the presence of AD-related pathophysiological processes, such as amyloid aggregation, in individuals who do not have cognitive deficits [55, 56]. Cognitively intact individuals who are amyloid-positive are at increased risk for cognitive decline [57, 58]. Recent methods for defining amyloid-positivity include positron emission tomography (PET) amyloid imaging and Aβ42 in cerebrospinal fluid assay. It is still largely unknown how the choice of a particular amyloid biomarker may affect the discrimination between amyloid-positive and amyloid-negative healthy subjects. This is important since an amyloid-positive status may define potential candidates for experimental (e.g. anti-amyloid) therapies in clinical drug development.

^{18}F-labeled tracers currently approved by the Food and Drugs Administration (FDA) and European Medicines Agency (EMA) for estimation of amyloid plaques in patients evaluated for cognitive decline are ^{18}F-flutemetamol [65, 66], ^{18}F-florbetaben [67], and ^{18}F-florbetapir [68]. The cortical retention of ^{18}F-flutemetamol has been compared to ^{11}C-Pittsburgh compound B (^{11}C-PIB) [105] in clinical populations such as amnestic mild cognitive impairment (aMCI) patients together with clinically probable AD patients [73], or aMCI and clinically probable AD together with healthy controls [228], but not in cohorts consisting exclusively of cognitively intact older adults. This is crucial since the discriminative value of a tracer may also depend on the population under study. The concordance between two tracers may be better in a mixed sample of patients and controls then in a group consisting exclusively of cognitively normal controls. In cognitively intact older adults ligand retention values may lie closer to threshold than in patients with probable AD and it has been hypothesized that ^{11}C-PIB could potentially outperform ^{18}F-labelled tracers under such conditions [283]. Other ^{18}F-labelled amyloid tracers (^{18}F-florbetaben [67], ^{18}F-florbetapir [68], ^{18}F-AZD4694 [76]) have also been

compared with ^{11}C-PIB within subjects, again mostly in clinical patient populations combined with cognitively intact older adults [31, 72]. For these tracers, no direct comparisons have been performed in cohorts consisting exclusively of cognitively intact older adults. Cognitively intact older adults who are amyloid-positive constitute the target population for a number of current clinical drug development programmes. The success of targeted molecular therapies may critically depend on the presence of the drug target. Accurate ascertainment of amyloid-positivity prior to inclusion may constitute one of the factors that determines the success of trials in preclinical AD (importance of high specificity), as well as the cost of screening for eligible subjects (importance of high sensitivity). Moreover, in cognitively intact older adults where amyloid levels are slightly to markedly elevated, the precise analysis method is essential. This may be less of an issue in patients with clinically probable AD who are well within the abnormal range. None of the studies comparing ^{18}F-flutemetamol and ^{11}C-PIB have evaluated the effect of reference region, magnetic resonance image (MRI) versus PET-based normalization or partial volume correction on the concordance between those tracers in cognitively normal older adults.

Therefore, the aim of this study was to directly compare ^{18}F-flutemetamol to ^{11}C-PIB within the same subjects in a prospective community-recruited cohort of cognitively intact older adults. We evaluated concordance between ^{18}F-flutemetamol versus ^{11}C-PIB binary classifications based on semiquantitative assessment and visual reads, as well as the correlations between the semiquantitative measures. We also estimated the impact of different image analysis methods on amyloid quantification.

5.3 Materials and methods

5.3.1 Participants

Thirty-two cognitively intact older controls (mean age 72 years, SD 5) participated in this study (Table 5.1). They were recruited through advertisement in local newspapers and through websites for seniors as part of a larger longitudinal study, asking for healthy volunteers between 65 and 80 years of age for participation in a scientific study at the University Hospital Leuven, Belgium, involving brain imaging. At screening, subjects underwent a detailed interview about medical history, a Mini Mental State Examination, a Clinical Dementia Rating, general physical and neurological examination, blood sampling, and a conventional neuropsychological assessment. Inclusion criteria were age between 65 and 80 years, MMSE $\geq$ 27, CDR = 0, and normal test scores on neuropsychological assessment. Inclusion was stratified for two genetic factors: BDNF (*met* allele present or absent) and APOE (ε4 allele present or absent), as this cohort was part of a larger ^{18}F-flutemetamol study in healthy controls of the interactions between these polymorphisms [244, 284]. Exclusion criteria were neurological or psychiatric history and brain lesions on structural MRI.

Demographic and neuropsychological characteristics		
Gender (male/female)	21/11	
ApoE $\varepsilon 4$	13 (41%)	
Age (years)	72 (4.5)	65-80
Education (years)	12.6 (3.2)	8-20
MMSE (/30)	29.1 (1.1)	27-30
AVLT TL (/75)	44.4 (7.1)	33-69
AVLT DR (/15)	8.8 (2.3)	5-13
AVLT %DR	78.5 (12.5)	55-100
BNT (/60)	54.3 (4.1)	41-60
AVF (# words)	24.6 (5.2)	16-40
LVF (# words)	35.0 (11.9)	14-61
RPM (/60)	35.5 (10.0)	15-54
TMT B/A	2.3 (0.6)	1.3-3.8

Table 5.1: Second column: Mean (SD). Third column: Range. MMSE = Mini Mental State Examination; AVLT = Rey Auditory Verbal Learning Test; TL = total learning; DR = delayed recall; BNT = Boston Naming Test; AVF = Animal Verbal Fluency Test; LVF = Letter Verbal Fluency Test; RPM = Raven's Progressive Matrices; TMT = Trail Making Test part B divided by part A.

The protocol (EudraCT: 2009-014475-45) was approved by the Ethics Committee University Hospitals Leuven. Written informed consent was obtained from all subjects in accordance with the Declaration of Helsinki.

5.3.2 Amyloid PET

PET scans were acquired on a 16-slice Siemens Biograph PET/CT scanner (Siemens, Erlangen, Germany). Tracers were injected as a bolus in an antecubital vein (^{18}F-flutemetamol mean activity 150 MBq, SD 5 MBq, range 134-162 MBq; ^{11}C-PIB mean activity 363 MBq, SD 33 MBq, range 255-420 MBq). The ^{18}F-flutemetamol scan acquisition started 90 min after tracer injection and lasted for 30 min [66, 73, 244, 284]. The ^{11}C-PIB scan was obtained within 30 days from the ^{18}F-flutemetamol scan (mean 2 days, median 0 days, range -22 to 21 days). Three subjects could not come to the clinic within the 30 days period due to personal or health reasons and they received a ^{11}C-PIB scan within 32, 39, and 118 days from the ^{18}F-flutemetamol scan. Dynamic ^{11}C-PIB scan acquisition extended from 0 to 70 min post tracer injection. Prior to PET acquisition, a low-dose computed tomography scan of the head was performed for attenuation correction. Random and scatter correction were applied. The ^{18}F-flutemetamol measurement was rebinned into 6 frames of 5 min and the ^{11}C-PIB measurement between 40 and 70 min post injection was also rebinned into 6 frames of 5 min each. Images were reconstructed using Ordered Subsets Expectation Maximization (4 iterations x 16 subsets). A structural T1-weighted MRI was acquired on a 3T Philips Achieva scanner (3D

turbo field echo sequence, 32-channel Philips SENSitivity Encoding head coil: coronal inversion recovery prepared 3D gradient-echo images, inversion time 900 ms, TE/TR 4.6/9.6, flip angle 8°, voxel size 0.98 x 0.98 x 1.2 mm^3 [284]).

The ^{18}F-flutemetamol and the ^{11}C-PIB scans were preprocessed using Statistical Parametric Mapping 8 (SPM8, http://www.fil.ion.ucl.ac.uk/spm). The individual images of the 6 frames were realigned and summed for both data sets separately. The individual's ^{18}F-flutemetamol and ^{11}C-PIB PET summed images were co-registered to the subject's T1-weighted MRI. ^{18}F-flutemetamol and ^{11}C-PIB PET summed images were spatially normalized to the Montreal Neurological Institute (MNI) space using MRI. This was done in two steps. First, the MR image was spatially normalized to the SPM8 T1 template in MNI space using a unified segmentation approach. This generated the non-linear transformation parameters, as well as grey matter (GM), white matter (WM) and cerebrospinal fluid images. Next, these transformation parameters were applied to the individual's co-registered ^{18}F-flutemetamol and ^{11}C-PIB PET summed images to spatially normalize them to MNI space.

5.3.2.1 Semiquantitative analysis of amyloid PET

To measure specific tracer retention, standardised uptake value ratio (SUVR) images were calculated from the spatially normalized summed ^{18}F-flutemetamol images and from the spatially normalized summed ^{11}C-PIB images (voxel size 2 x 2 x 2 mm^3) with the cerebellar GM used as reference region. The spatially standardised volumes of interest (VOIs) were identical for ^{18}F-flutemetamol and for ^{11}C-PIB image analysis. The cerebellar GM was defined based on the automated anatomical labelling (AAL) atlas (areas 91-108) and masked inclusively with subject-specific GM maps, with the threshold for masking set at $>$ 0.3 [244, 284]. This reference region was used both for ^{18}F-flutemetamol and for ^{11}C-PIB images. As a secondary analysis, we also used pons as a reference region: this region was manually drawn on the SPM8 T1-template (13 axial slices of 2 mm) and then for each individual it was corrected to match the subject-specific anatomical boundaries of the pons based on the subject's spatially normalized MR image.

Our primary PET outcome measure was the mean SUVR in the composite cortical VOI (SUVR$_{comp}$) with cerebellar GM as reference region. The composite VOI consisted of 5 bilateral cortical areas [244, 284]. The spatially standardised VOIs were based on the AAL template. We also calculated mean SUVR in each of these regions separately and additionally in medial temporal (AAL 37-42), and occipital cortex (AAL 43-54), and striatum (AAL 71-74). The AAL VOIs were masked inclusively with subject-specific GM maps, with the threshold for masking set at $>$ 0.3 [244, 284]. Mean SUVR was also estimated in subcortical WM (SWM), which was defined based on subject-specific WM maps thresholded at $>$ 0.5.

The cut-offs for SUVR$_{comp}$ for binary classification were defined based on

independent datasets re-analyzed using the MRI-based PET analysis method described above. The cut-offs were defined based on the statistical distance between the AD group and the HC as described in Vandenberghe et al. (2010), that is: $factor = \frac{Mean\ SUVR_{comp}\ AD\ -\ Mean\ SUVR_{comp}\ HC}{SD\ SUVR_{comp}\ AD\ +\ SD\ SUVR_{comp}\ HC}$, $SUVR_{comp}$ cut-off $= Mean\ SUVR_{comp}\ AD - factor \times SD\ SUVR_{comp}\ AD$. ^{18}F-flutemetamol cut-off was estimated based on the Vandenberghe et al. (2010) dataset [73], and was equal to 1.38. The ^{11}C-PIB cut-off was calculated based on 37 clinically probable AD subjects and 23 age-matched healthy controls (datasets from Nelissen et al. (2007) [132], Vandenberghe et al. 2010 [73], and Ahmad et al. 2014 [285]) and was equal to 1.22. Note that the used 1.38 ^{18}F-flutemetamol cut-off is lower than the cut-off defined by Vandenberghe et al. (2010) or Thurfjell et al. (2014) for a purely PET-based approach, probably due to exclusion of more white matter signal by the current MRI-based method in the amyloid-negative cases. We also verified our binary case classification using the purely PET-based method with narrow VOIs and SUVR cut-offs with reference to cerebellar GM as used by Thurfjell et al. (2014). For this method, the cut-off with the neuropathological modified Consortium to Establish a Registry for Alzheimer's Disease score as standard-of-truth was 1.57 [229].

In addition, we evaluated how cut-offs and concordance changed when we defined the cut-off of one tracer based on receiver operating characteristic (ROC) analysis with the categorization by the other tracer as standard-of-truth (SoT)[1]. We did this with the categorization based on ^{11}C-PIB as SoT and, separately, with the categorization based on ^{18}F-flutemetamol as SoT.

As a further secondary analysis, we performed a semiquantitative analysis based on partial volume corrected (PVC) data. PVC was based on the MRI using the modified Müller-Gärtner method [146, 244, 284].

5.3.2.2 Visual reads

^{18}F-flutemetamol and ^{11}C-PIB scans were visually evaluated by 3 independent readers blinded to all subject information: two certified nuclear medicine physicians (reader 1 K.V.L, reader 2 K.G.) and a certified psychiatrist (reader 3 M.V.), experienced in reading amyloid scans. All readers had successfully completed the GE Healthcare electronic reader training program for ^{18}F-flutemetamol images. The visual read was done on summed orthogonal PET images in native space, scaled to the image maximum intensity value and displayed with a modifiable rainbow (NIH) colour scale. Each reader received an individually randomized list of ^{18}F-flutemetamol and ^{11}C-PIB images which were evaluated in separate sessions. Readers were asked to assign scans as positive or negative and to rate their overall confidence in classifying the image on a scale from 1 to 5 (5 being the highest confidence). The final assignment was based on a majority verdict.

[1]The ROC analyses were added to the thesis after publication of the article.

5.3.3 Statistical analysis

The primary analyses were intended to evaluate in cognitively intact older adults:

1. The concordance between binary classification based on ^{18}F-flutemetamol versus ^{11}C-PIB according to semiquantitative SUVR$_{comp}$ assessment.
2. The concordance of binary visual reads of ^{18}F-flutemetamol versus ^{11}C-PIB.
3. The correlation between ^{18}F-flutemetamol and ^{11}C-PIB SUVR$_{comp}$. Normality of data distribution was tested using the Shapiro-Wilk test. Correlations were evaluated using (a) Spearman rank correlation coefficients ρ if distributions deviated from normality, and (b) using slopes of linear regression m. The agreement between ^{18}F-flutemetamol and ^{11}C-PIB SUVR$_{comp}$ was tested by a Bland-Altman analysis [286].

The secondary analyses evaluated in cognitively intact older adults:

1. The agreement between readers of the visual classification. This was analysed by means of Fleiss' Kappa (κ).
2. Readers' confidence in visual binary classification of the PET scans. This was analysed by three-factor repeated measures ANOVA, with reader (3 levels: reader 1 vs 2 vs 3) and tracer (2 levels: ^{18}F-flutemetamol vs ^{11}C-PIB) as within-subject factors, and concordance of binary visual reads (2 levels: concordant vs discordant) as between-subject factor.
3. The correlation between ^{18}F-flutemetamol and ^{11}C-PIB SUVR in a set of 9 separate regions.
4. The correlation between ^{18}F-flutemetamol and ^{11}C-PIB SUVR values using the pons as reference region.
5. The correlation between PVC-corrected ^{18}F-flutemetamol and PVC-corrected ^{11}C-PIB SUVR values.

Statistical analyses were performed in Statistica 11 (http://www.statsoft.com/) and Matlab R2013b (http://www.mathworks.com).

5.4 Results

Regional and composite SUVR values of ^{18}F-flutemetamol ($W = 0.68$-0.86, $P < 0.002$) and ^{11}C-PIB ($W = 0.69$-0.87, $P < 0.006$) were not normally distributed. Therefore in the subsequent analyses we used Spearman ρ coefficient.

Binary classification based on semiquantitative cut-offs was concordant between ^{18}F-flutemetamol versus ^{11}C-PIB in 94% of the cases (Figure 5.1A). Based on ^{18}F-flutemetamol SUVR$_{comp}$ 5 out of 32 subjects (16%) were assigned to the amyloid-positive category (Figure 5.1A, 5.2). Based on ^{11}C-PIB SUVR$_{comp}$, 7 out of 32 subjects (22%) were assigned to the amyloid-

positive category (Figure 5.1A, 5.2). Two cases were discordant between ^{18}F-flutemetamol and ^{11}C-PIB (cases 8 and 31, Figure 5.1A, 5.2). These subjects were assigned to the amyloid-negative category based on ^{18}F-flutemetamol and to the amyloid-positive category based on ^{11}C-PIB.

Concordance of binary visual reads between tracers was 84% (Figure 5.1B). Based on ^{18}F-flutemetamol scans 3 out of 32 subjects (9%) were assigned to the amyloid-positive category (Figure 5.1B, 5.2). According to ^{11}C-PIB scans, 6 out of 32 subjects (19%) were assigned to the amyloid-positive category (Figure 5.1B, 5.2). Out of 5 discordant cases, one subject was read as positive for ^{18}F-flutemetamol but negative for ^{11}C-PIB (case 24, Figure 5.1B, 5.2, 5.3), and 4 were read as positive for ^{11}C-PIB but negative for ^{18}F-flutemetamol (cases 17, 19, 29, 31, Figure 5.1B, 5.2). Fleiss' κ for inter-reader agreement was 0.86 for ^{18}F-flutemetamol, and 0.93 for ^{11}C-PIB.

When we analysed readers' confidence in visual classification of ^{18}F-flutemetamol and ^{11}C-PIB scans we found a significant main effect of reader ($F_{2,62} = 12.3$, $P = 0.00003$): reader 1 (r1) and 3 (r3) were more confident than reader 2 (r2) (r1 > r2 $P = 0.0001$, r3 > r2 $P = 0.0006$) (Figure 5.4A). We also found a significant main effect of concordance of visual classification: readers were more confident when classifying concordant cases compared with discordant cases ($F_{1,30} = 5.1$, $P = 0.03$) (Figure 5.4B). No other effects were found.

^{18}F-flutemetamol and ^{11}C-PIB SUVR values were highly correlated in the composite cortical VOI, in all neocortical VOIs and in subcortical white matter (Table 5.2; Figure 5.5). The correlations in striatum and medial temporal cortex were weaker (Table 5.2; Figure 5.5). The slopes of linear regression

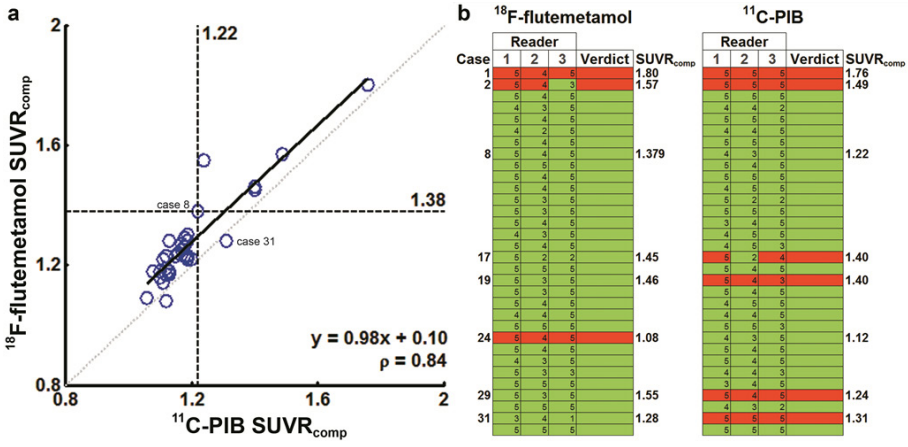

Figure 5.1: Concordance between binary semiquantitative (A) and visual (B) classifications of ^{18}F-flutemetamol and ^{11}C-PIB scans. (A) Dashed lines = SUVR cut-offs. (B) Red = positive scan; green = negative scan. Values in red and green cells = confidence levels of the readers.

were close to 1 in all neocortical regions and subcortical white matter (Table 5.2; Figure 5.5). Slopes in striatum and medial temporal cortex were lower (Table 5.2; Figure 5.5). The Bland-Altman analysis [286] showed a good agreement between ^{18}F-flutemetamol and ^{11}C-PIB SUVR$_{comp}$, with a systematic bias towards higher ^{18}F-flutemetamol SUVR values (Figure 5.6).

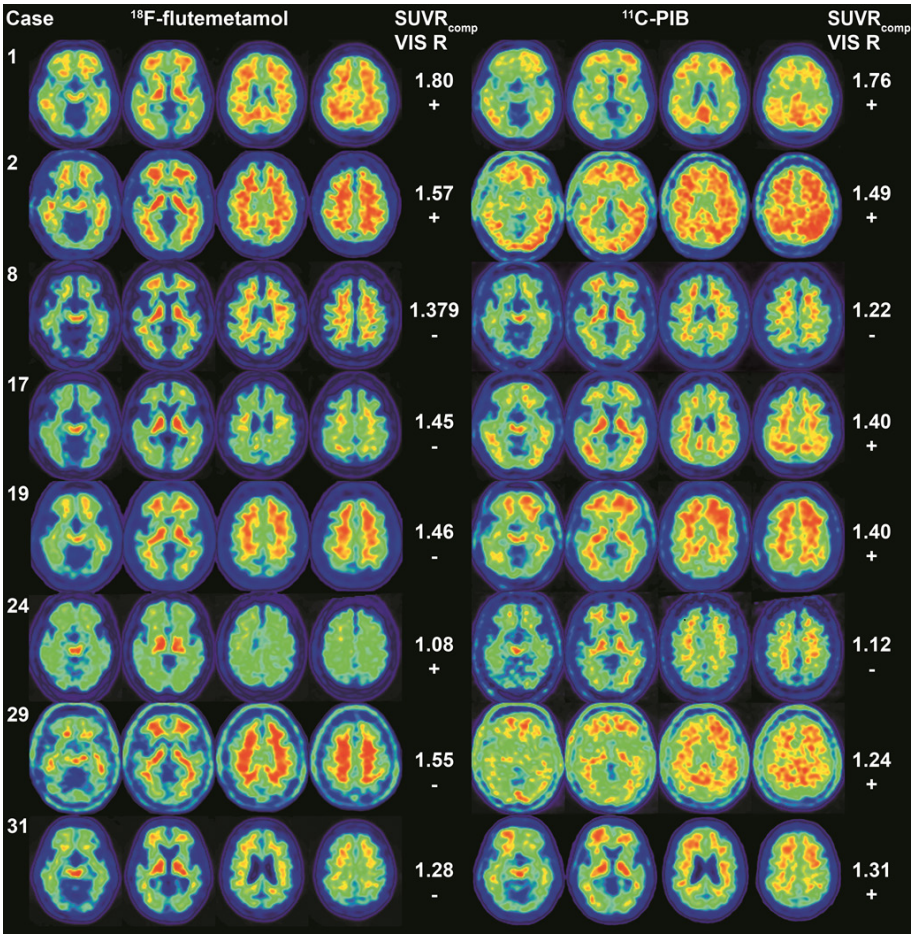

Figure 5.2: Representative summed PET images of the discordant cases between ^{18}F-flutemetamol and ^{11}C-PIB scans based on semiquantitative and visual classification. For the sake of comparison we also displayed two positive cases who were concordantly classified by semiquantitative and visual approach. Brain sections show axial slices at -4, 10, 24, 38 MNI z coordinates. On the right side of the brain sections SUVR$_{comp}$ values (at the top) and results of visual reads (VIS R, at the bottom, + positive scan, - negative scan) are shown. Images are scaled to a maximum intensity in an image.

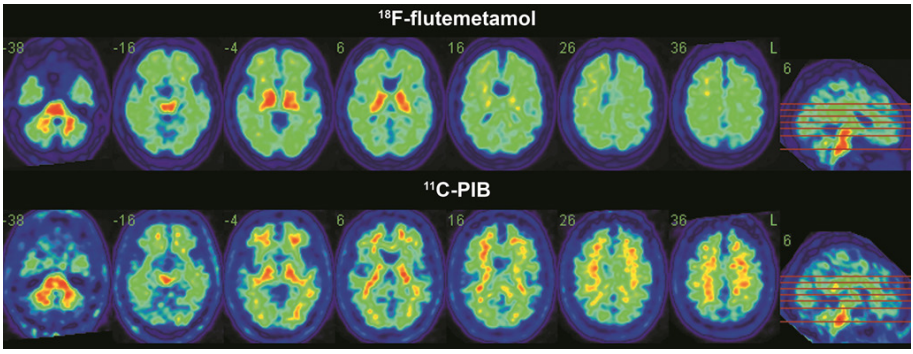

Figure 5.3: Detailed view on case 24. Left upper corners show MNI coordinates. Right upper corners show brain orientation. Images are scaled to a maximum intensity in an image.

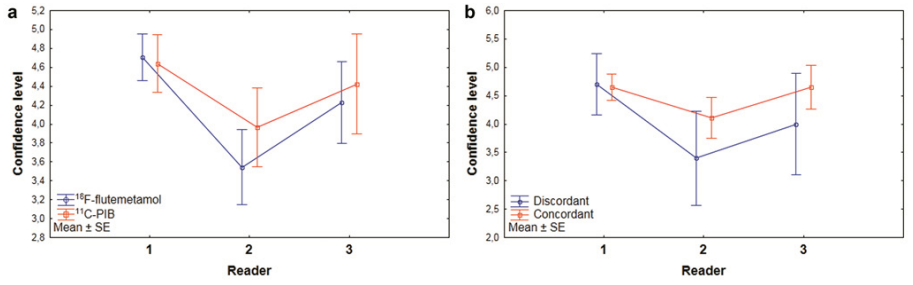

Figure 5.4: Analysis of readers' confidence in visual binary classification of ^{18}F-flutemetamol and ^{11}C-PIB scans. (A) Main effect of reader. (B) Main effect of concordantly versus discordantly classified cases.

When we applied the Thurfjell et al. (2014) PET-based processing method and autopsy derived SUVR cut-off with reference to cerebellar GM, 4 out of 32 ^{18}F-flutemetamol scans (13%) were classified as amyloid-positive. In three cases, the MRI-informed and the purely PET-based processing methods yielded discordant classification: two subjects were classified as amyloid-negative based on the PET-based method and as amyloid-positive based on the MRI-informed method (case 19 and 29, Figure 5.1B, 5.2, $SUVR_{comp}$ based on purely PET-based processing method 1.45 and 1.47 respectively), one subject showed the inverse pattern (case 31, Figure 5.1B, 5.2, $SUVR_{comp}$ based on purely PET-based processing method 1.61). The correlation between ^{18}F-flutemetamol and ^{11}C-PIB scans analysed by the purely PET-based processing method was high in composite cortical VOI and in all neocortical VOIs (Table 5.2).

We also performed an ROC analysis to evaluate whether a different cut-off was obtained when one of the tracers was evaluated against the categorization

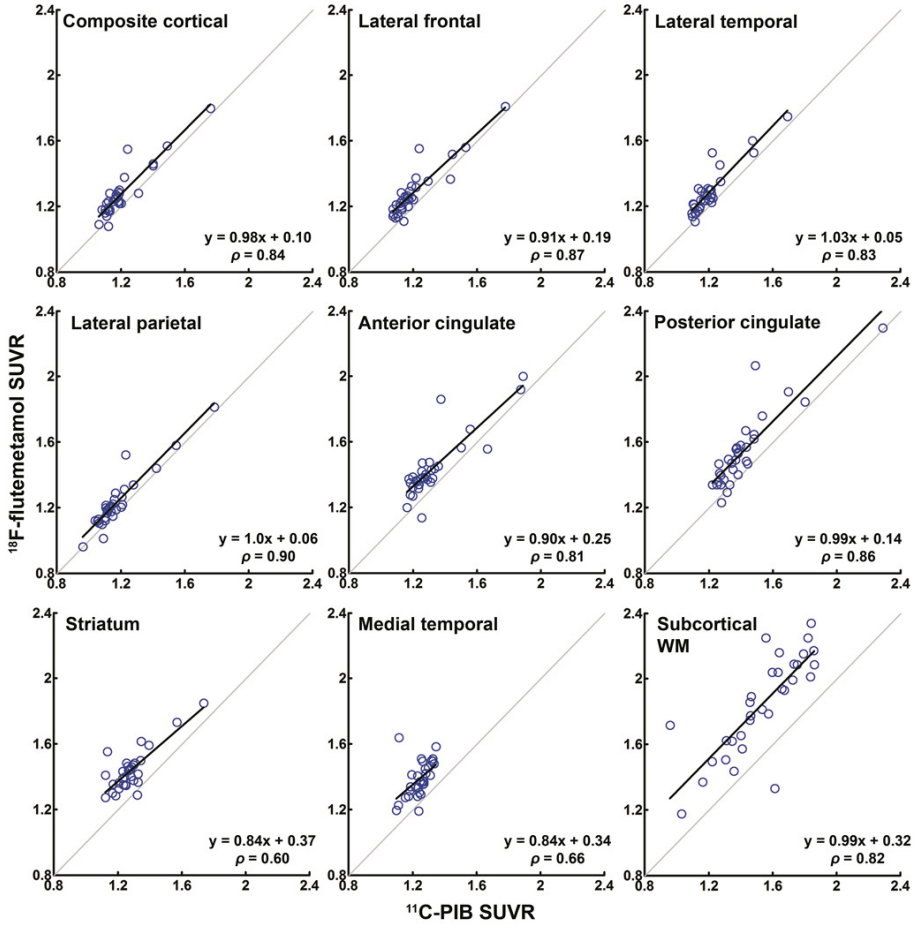

Figure 5.5: Regional correlations between ^{18}F-flutemetamol and ^{11}C-PIB SUVRs. WM = white matter.

Region-wise correlations between ^{18}F-flutemetamol and ^{11}C-PIB SUVRs for different analysis methods

	MRI-informed method						PET-based method	
	Cerebellar GM		Pons		Cerebellar GM & PVC		Cerebellar GM	
Region	m	ρ	m	ρ	m	ρ	m	ρ
Composite cortical	0.98	0.84	**0.49**	0.69	0.96	0.90	**0.72**	0.86
Lateral frontal	0.91	0.87	**0.49**	0.76	0.91	0.89	**0.72**	0.85
Lateral temporal	1.03	0.83	**0.47**	0.70	1.03	0.87	**0.73**	0.75
Lateral parietal	1.00	0.90	**0.50**	**0.63**	0.97	0.92	**0.74**	0.92
Anterior cingulate	0.90	0.81	**0.54**	0.79	0.89	0.90	**0.73**	0.82
Posterior cingulate	0.99	0.86	**0.56**	0.78	0.98	0.83	**0.72**	0.92
Lateral occipital	1.03	0.77	**0.43**	0.72	0.94	0.86	**0.67**	0.84
Striatum	0.84	0.60	**0.52**	0.81	**0.95**	**0.87**	-	-
Medial temporal	0.84	0.66	**0.53**	0.79	**0.99**	0.68	**0.76**	0.70
Subcortical WM	0.99	0.82	0.90	**0.96**	0.98	**0.95**	-	-

Table 5.2: GM = grey matter; WM = white matter; PVC = partial volume correction; m = slope of linear regression; ρ = Spearman correlation coefficient. All correlations reached $P \leq 0.0001$, except for the correlation in striatum with cerebellar GM as reference region $P = 0.0003$. Bold font shows significant differences at $P < 0.05$ for comparison of m and ρ with columns 2-3, respectively. Not corrected for multiple comparisons.

by the other tracer as standard-of-truth. The SUVR_{comp} cut-offs for optimal agreement between the tracers defined based on ROC analysis were 1.3 for ^{18}F-flutemetamol (Area under the ROC curve (AUC) 0.983, 95% CI 0.861 - 1.0, sensitivity 86%, specificity 100%) and 1.22 for ^{11}C-PIB (AUC 0.993, 95% CI 0.877 - 1.0, sensitivity 100%, specificity 96%)[2]. Seven cases were defined as amyloid-positive based on ^{18}F-flutemetamol cut-off and also based on ^{11}C-PIB cut-off. There were two discordant cases between ^{18}F-flutemetamol and ^{11}C-PIB classifications: one classified as amyloid-negative based on ^{18}F-flutemetamol and as amyloid-positive based on ^{11}C-PIB (case 31) and one in an opposite fashion (case 16). The obtained cut-off values were essentially the same as those derived from the independent datasets.

When pons was used as reference region, the correlation between ^{18}F-flutemetamol and ^{11}C-PIB SUVRs was weaker in the composite cortical VOI and in neocortical VOIs. This difference was statistically significant in the lateral parietal VOI ($P = 0.007$) (Table 5.2). The correlation however was stronger in striatum, medial temporal cortex, and subcortical WM when pons was used as reference region than when cerebellar GM was used. This difference was statistically significant in subcortical WM ($P = 0.004$) (Table 5.2). With pons as reference region, the slopes of linear regression were close to 0.5 and were significantly less steep than with cerebellar GM as reference region in all VOIs ($P < 0.0001$) except for subcortical WM where slope was 0.9 (Table 5.2). When pons was used as reference region for ^{18}F-flutemetamol and cerebellar grey matter was used as reference region for ^{11}C-PIB, correlations

[2]The ROC analyses were added to the thesis after publication of the article.

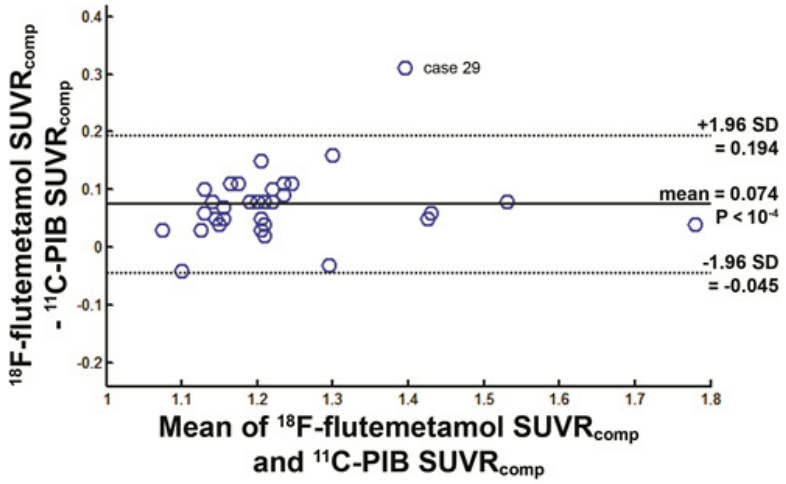

Figure 5.6: Agreement between ^{18}F-flutemetamol and ^{11}C-PIB SUVRs based on Bland-Altman analysis.

between SUVRs in all VOIs were weaker than when either pons or cerebellar grey matter were used for both of the tracers[3]. Statistically significant differences were found in medial temporal ($P = 0.006$) and subcortical WM ($P = 0.02$) VOIs, compared with correlations with pons as reference region for both tracers.

PVC did not significantly alter ρ and slopes for the correlation between ^{18}F-flutemetamol and ^{11}C-PIB SUVR values in the composite cortical VOI or any of the neocortical VOIs (Table 5.2). In striatum, medial temporal cortex and subcortical WM, PVC improved ρ or slope significantly (Table 5.2).

5.5 Discussion

To our knowledge this is the first study comparing ^{18}F-flutemetamol to ^{11}C-PIB in a cohort consisting exclusively of cognitively intact older adults, without patients with cognitive deficits. Our results provide evidence for a close correspondence between the two amyloid tracers even at this preclinical stage.

We detected a few more amyloid-positive cases with ^{11}C-PIB scan (7 out of 32) than with ^{18}F-flutemetamol scan (5 out of 32). This differs from previous comparisons that included only AD and MCI [73] or AD, MCI, together with HC [228], where concordance between ^{18}F-flutemetamol and ^{11}C-PIB was 100%. In the Hatashita et al. study [228] the cut-offs for semiquantitative assessment were not defined independently from the test sample and this may

[3]These analyses were added to the thesis after publication of the article.

also have contributed to this complete concordance. In our study the cut-offs were based on independent datasets. One of the discordant subjects (case 8) lay within 1.5% test-retest variability of $SUVR_{comp}$ values [73], therefore only case 31 should be considered meaningfully discordant.

The values in the discordant cases in our study were around the cut-off, except for case 24 (see below). Near-threshold values may render the binary division between amyloid-positive and -negative cases in cognitively normal individuals more difficult. Amyloid accumulation is a progressive process and the amyloid-positive cases are distributed over range of continuous values rather than bimodally. Hence, among cognitively normal controls a binary classification into positive and negative subjects is somewhat artificial. Individuals with the intermediate amyloid levels may either remain at this level or may be heading towards further pathological amyloid aggregation [287]. Subjects around the cut-off may be accumulating amyloid at a higher rate than those subjects who are further removed from the cut-off [287] and in this sense may be of special interest for potentially disease-modifying drug trials. To investigate the prevalence and the meaning of these cases with sufficient power a joint longitudinal approach including different centres would be necessary. In such an approach a standardized quantification of amyloid deposition, such as centiloid scale [288], would facilitate the comparison. Values close to threshold probably explain the higher rate of discordance in visual reads in our study compared to what has been found in AD and MCI [73, 228]. We however met one exception: in case 24, ^{18}F-flutemetamol SUVR was far removed from the cut-off and nevertheless the ^{18}F-flutemetamol scan was read as positive by all 3 readers with relatively high confidence. When evaluating this scan in retrospect, the outcome of the read may have been determined by the fact that tracer retention was similarly low in white matter and in neocortex. As a consequence, the pattern of gyral indentation was lost and the cortical surface relatively even. This was not true for the ^{11}C-PIB scan. The similarity in ^{18}F-flutemetamol retention between neocortex and white matter and the even appearance of the surface may have led to the positive read despite the low neocortical SUVR. This underscores the usefulness of semiquantitative measures when evaluating normal control ^{18}F-flutemetamol scans. The overall confidence of readers in visual evaluation of scans was high, however, the confidence of all readers was lower when evaluating discordant cases compared with concordant cases. This indicated that a subset of scans in this population is particularly difficult to read.

As a further difference with previous comparative studies [73], the correlation between ^{18}F-flutemetamol and ^{11}C-PIB SUVR values in subcortical white matter (Table 5.2) was higher than previously observed (in [73] $r = 0.36$). The definition of the white matter VOI may have been more accurate in the current study as it was based on the MRI. A white matter VOI that is defined based on PET may be affected by spill-over between grey and white matter and this may differ between ^{18}F-flutemetamol and ^{11}C-PIB, yielding lower correlations in previous studies [73].

We also evaluated how differences in the analysis method affected the concordance and the correlation with ^{11}C-PIB. PVC did not substantially alter correlations between ^{18}F-flutemetamol and ^{11}C-PIB in neocortical VOIs, but affected the correlation in striatum and medial temporal cortex in a positive sense. The latter area is known to be particularly susceptible to partial volume effects. Second, using pons as a reference region resulted in substantially lower correlations between ^{18}F-flutemetamol and ^{11}C-PIB in neocortical regions (Table 5.2). Only in striatum, medial temporal cortex, and subcortical WM did pons as a reference region yield better correlations (Table 5.2). Finally, the correlations of SUVRs were the same when ^{18}F-flutemetamol and ^{11}C-PIB scans were analysed with a purely PET-based method [229] compared to our MRI-based method [244] (Table 5.2). It however is worth noting that the slopes for the correlations between ^{18}F-flutemetamol and ^{11}C-PIB were substantially lower for the purely PET-based method than when MRI was used to independently define the regions to be used for analysis of the two PET modalities.

Practical implications

The FDA and EMA approvals of amyloid imaging are for visual reads and are restricted to patients with cognitive decline. For research use in cognitively intact individuals, our findings suggest that semiquantitative assessment would be preferable above visual reads. In cognitively intact older individuals cerebellar grey matter would be the preferred reference region compared with pons. PVC would be advantageous for evaluation of medial temporal cortex and subcortical regions. Concordance between ^{18}F-flutemetamol and ^{11}C-PIB was better when regions were based on MRI rather than for PET based regions.

5.5.1 Conclusion

Our study of amyloid markers in asymptomatic older adults provides evidence that semiquantitative measures of ^{18}F-flutemetamol with cerebellar grey matter as a reference are closely similar to what one would obtain if ^{11}C-PIB was used, in particular if MRI is used to define the regions of interest. Concordance for visual reads tended to be less convincing in this population.

6

Diagnostic value of cerebrospinal fluid Aβ ratios in preclinical Alzheimer's disease

This chapter has been submitted for publication:

Katarzyna Adamczuk, Jolien Schaeverbeke, Hugo MJ Vanderstichele, Johan Lilja, Natalie Nelissen, Koen Van Laere, Patrick Dupont, Kelly Hilven, Koen Poesen, Rik Vandenberghe. Diagnostic value of cerebrospinal fluid Aβ ratios in preclinical Alzheimer's disease. *Under revision.*

6.1 Abstract

In this study of preclinical Alzheimer's disease (AD) we assessed the added diagnostic value of using cerebrospinal fluid (CSF) Aβ ratios rather than Aβ42 in isolation for detecting individuals who are positive on amyloid positron emission tomography (PET).

Thirty-eight community-recruited cognitively intact older adults (mean age 73, range 65-80 years) underwent ^{18}F-flutemetamol PET and CSF measurement of Aβ1-42, Aβ1-40, Aβ1-38, and total tau (ttau). ^{18}F-flutemetamol retention was quantified using standardized uptake value ratios in a composite cortical region (SUVR$_{comp}$) with reference to cerebellar grey matter. Based on a prior autopsy validation study, the SUVR$_{comp}$ cut-off was 1.57. Sensitivities, specificities and cut-offs were defined based on receiver operating characteristic analysis with CSF analytes as variables of interest and ^{18}F-flutemetamol positivity as the classifier. We also determined sensitivities and CSF cut-off values at fixed specificities of 90% and 95%.

Seven out of 38 subjects (18%) were positive on amyloid PET. Aβ42/ttau, Aβ42/Aβ40, Aβ42/Aβ38, and Aβ42 had the highest accuracy to identify amyloid-positive subjects (area under the curve (AUC) $\geq$ 0.908). Aβ40 and Aβ38

had significantly lower discriminative power (AUC = 0.571). When specificity was fixed at 90% and 95%, Aβ42/ttau had the highest sensitivity among the different CSF markers (85.71% and 71.43%, respectively). Sensitivity of Aβ42 alone was significantly lower under these conditions (57.14% and 42.86%, respectively).

For the CSF-based definition of preclinical AD, if a high specificity is required, our data support the use of Aβ42/ttau rather than using Aβ42 in isolation.

6.2 Introduction

Preclinical [55, 58], or asymptomatic [63], Alzheimer's disease (AD) is characterized by the presence of AD-related pathophysiological processes in the absence of cognitive deficits. Evidence of brain amyloidosis is a requirement common to all 3 National Institute on Ageing and Alzheimer's Association (NIA-AA) stages of preclinical AD [55]. This can be detected directly in vivo by means of either β-amyloid (Aβ) protein quantification in cerebrospinal fluid (CSF) or positron emission tomography (PET) amyloid imaging [55, 100, 102].

Apart from Aβ1-42, other Aβ isoforms (e.g. Aβ1-40, Aβ1-38) have evoked interest from a clinical-diagnostic perspective, as either a separate biomarker tool or when combined (ratio) with Aβ1-42 [289, 290, 291]. Using ratios of Aβ isoforms (Aβ1-42/Aβ1-38, Aβ1-42/Aβ1-40) may have added value for the discriminaton between AD and normal pressure hydrocephalus [292], cerebral amyloid angiopathy [293], frontotemporal dementia [294], and Lewy body dementia [295], and also between mild cognitive impairment (MCI) due to AD and non-AD MCI [296]. In cognitively intact individuals, Aβ38 or Aβ40 do not correlate with amyloid PET positivity, in contrast with Aβ42 [101, 102].

In this study of preclinical AD, we assessed the added value of using ratios of Aβ42 to other C-terminal Aβ isoforms or to total tau for discriminating amyloid-positive versus amyloid-negative cognitively intact healthy controls, with an autopsy-validated ^{18}F-flutemetamol cut-off score [229] as standard-of-truth. The cut-off value was derived from the ^{18}F-flutemetamol phase 3 study using a binarized measure of postmortem brain neuritic plaque density [297] (overall mean Bielschowsky score below or above 1.5 [229]).

6.3 Methods

6.3.1 Participants

Thirty-eight cognitively intact older controls (mean age 73 years, SD 5 years, Table 6.1) were recruited, from 10/09/2012 until 04/04/2014, through advertisement in local newspapers and through websites for seniors, asking for

healthy volunteers between 65 and 80 years of age for participation in a scientific study at the University Hospital Leuven, Belgium, involving brain imaging. At screening, subjects underwent a detailed interview about medical history, a Mini Mental State Examination (MMSE), a Clinical Dementia Rating (CDR), blood sampling, and a conventional neuropsychological assessment. Inclusion criteria were age 65 - 80 years, MMSE $\geq$ 27, CDR = 0, and normal test scores on neuropsychological assessment according to the published norms adapted for age, gender, and education. Inclusion was stratified per age bin (65-69, 70-74, 75-80) for two genetic factors: Brain-Derived Neurotrophic Factor (BDNF) (*met* allele present or absent) and Apolipoprotein E (APOE) ($\varepsilon 4$ allele present or absent). The cells of this 2 x 2 factorial design were prospectively matched for number of cases, age, sex, and education. This cohort was part of a larger ^{18}F-flutemetamol study in healthy controls about the interaction between BDNF and APOE [244, 284]. Among the exclusion criteria were a neurological or psychiatric history and focal brain lesions on structural magnetic resonance image (MRI). Subjects who fulfilled all criteria underwent ^{18}F-flutemetamol PET and lumbal puncture. The protocol (EudraCT: 2009-014475-45) was approved by the Ethics Committee University Hospitals Leuven. Written informed consent was obtained from all subjects in accordance with the Declaration of Helsinki.

6.3.2 Amyloid PET

^{18}F-flutemetamol PET was acquired on a 16-slice Siemens Biograph PET/CT scanner (Siemens, Erlangen, Germany). The tracer was injected as a bolus in an antecubital vein (mean activity 150 MBq, SD 5 MBq, range 134-162 MBq). Scan acquisition started 90 min after tracer injection and lasted for 30 min [66, 73, 244, 284]. Three adverse events were reported within 24 hours after the scan. This includes 2 mild headaches, which were resolved the same and the next day after the scan. One subject reported a rising heartbeat and a warm feeling immediately after injection, which were resolved within 2 min. Prior to PET acquisition, a low-dose computed tomography scan of the head was performed for attenuation correction. Random and scatter correction were applied. The ^{18}F-flutemetamol measurement was rebinned into 6 frames of 5 min. Images were reconstructed using Ordered Subsets Expectation Maximization (4 iterations x 16 subsets). The individual images of the 6 frames were realigned and summed. Subsequently, the PET summed image was spatially normalized to Montreal Neurological Institute (MNI) space using a fully automated PET-only method that made use of an adaptive template to account for the different uptake patterns in negative and positive ^{18}F-flutemetamol images [298]. On spatially normalized images (voxel size 2 x 2 x 2 mm^3) standard uptake value ratios (SUVR) were calculated with cerebellar grey matter as reference region. Mean SUVR value was calculated in a composite cortical region (SUVR$_{comp}$) consisting of 5 bilateral areas: frontal, parietal, anterior cingulate, precuneus-posterior cingulate and lateral temporal [229]. The composite cortical region and the cerebellar grey matter reference region were defined as a

Demographics and CSF biomarkers concentrations [mean (SD, range)]	
Gender (male/female)	22/16
Age (years)	73 (4.7, 65 - 80)
Education (years)	13.4 (3.1, 8 - 20)
APOE $\varepsilon 4$ (n)	19 (50%)
BDNF *met* (n)	20 (53%)
MMSE (/30)	28.9 (1.0, 27 - 30)
AVLT TL (/75)	46.2 (8.4, 31 - 69)
AVLT DR (/15)	9.8 (2.5, 5 - 14)
AVLT %DR	83.7 (11.7, 55 - 108)
BNT (/60)	54.2 (4.2, 41 - 60)
AVF (# words)	24.0 (5.5, 14 - 40)
LVF (# words)	36.0 (10.8, 17 - 64)
RPM (/60)	36.1 (9.8, 15 - 53)
TMT B/A	2.4 (0.5, 1.5 - 3.8)
Aβ38 (pg/mL)	2401 (654, 1057 - 3505)
Aβ40 (pg/mL)	8933 (2456, 3640 - 13273)
Aβ42 (pg/mL)	996 (430, 351 - 1859)
ttau (pg/mL)	360 (134, 126 - 660)
Aβ42/Aβ38	0.412 (0.119, 0.136 - 0.596)
Aβ42/Aβ40	0.110 (0.030, 0.044 - 0.148)
Aβ42/ttau	3.015 (1.246, 0.749 - 5.128)

Table 6.1: APOE = Apolipoprotein E; MMSE = Mini Mental State Examination; AVLT = Rey Auditory Verbal Learning Test; TL = total learning; DR = delayed recall; BNT = Boston Naming Test; AVF = Animal Verbal Fluency Test; LVF = Letter Verbal Fluency Test; RPM = Raven's Progressive Matrices; TMT = Trail Making Test part B divided by part A; ttau = total tau.

combination of narrow automated anatomic labeling-type regions [191] outlined on the ICBM-152 template masked with a grey matter probability mask [229]. Images were analyzed by an experienced medical imaging specialist blinded to all study information.

To estimate the SUVR_{comp} cut-off for detecting amyloid-positivity in vivo using the above described method, a receiver operating curve (ROC) analysis has been performed by Thurfjell et al. (2014) on an independent dataset of 68 SUVR_{comp} values (quantified based on the above described method) with the autopsy results as a standard-of-truth [229]. The autopsy data were classified following Vemuri's modification of the Consortium to Establish a Registry for AD criteria [299, 297]. Eight cortical regions (precuneus, midfrontal cortex, superior temporal cortex, middle temporal cortex, inferior parietal cortex, anterior cingulate gyrus, posterior cingulate gyrus, and primary visual cortex) were scored using an overall mean Bielschowsky score: 0 = 0 plaques, 1 = 1-5 plaques, 2 = 6-19 plaques, 3 $\geq$ 20 plaques. If the mean Bielschowsky score was > 1.5 in at least one region, the brain was classified as amyloid-positve, if all regions had ≤ 1.5, the brain was classified as amyloid-negative. The resulting

$SUVR_{comp}$ cut-off was 1.57 [229].

6.3.3 Lumbar puncture and CSF analysis

Lumbar punctures were carried out at the L4/5 level in the morning (10 am - 2 pm) without fasting, on average 41 days after the PET scan (range 7 to 99 days). No adverse events were reported within 24 hours after the lumbar puncture. Thirteen milliliters (mL) of CSF was sampled in 4 fractions of about 3 mL, each collected in a polypropylene tubes (Greiner Bio-one Cellstar, VWR, Leuven, Belgium, total volume 15 mL), with discarding 1 mL to avoid traumatic blood contamination. Samples were transported to the laboratory medicine department immediately after the puncture and centrifuged within 30 min after collection (2600 RPM, 10 min, 4°C). After centrifugation, supernatants were transferred in polypropylene tubes and from there aliquoted in 1.5 mL polypropylene tubes (Kartell, Noviglio, Italy, volume CSF/tube 1 mL). Samples were stored at -80°C until batch analysis. The levels of CSF Aβ1-42, Aβ1-40, Aβ1-38, and total tau (ttau) were measured in the first fraction with a new generation of single analyte enzyme-linked immunosorbent assays (EUROIMMUN, Lübeck, Germany) at ADx Ghent by two experienced laboratory technicians blinded to all study information. The Aβ assays quantify the full length of the C-terminus-specific Aβ isoforms (Aβ1-specific assay format). The tau assay is designed with a capture antibody towards the central region and one monoclonal antibody with an epitope at the amino-terminus of the protein. The assay design includes lyophylised recombinant proteins as calibrators, run-validation control samples (= calibrators added to a phosphate-buffered solution), as well as a qualification panel to evaluate the analytical performance(s) in the lab. These novel immunoassays are free from matrix interference and their intra-assay reproducibility has a coefficient of variation (CV) $\leq 5.0\%$ with an inter-assay reproducibility $\leq 8.3\%$ [300].

6.3.4 Statistical analysis

In the primary analysis we compared diagnostic accuracy of different CSF Aβ isoforms, their ratios, ttau and Aβ42/ttau to detect amyloid-positive older individuals. We used a ROC analysis with CSF analytes as variables of interest and ^{18}F-flutemetamol positivity defined based on autopsy-derived $SUVR_{comp}$ cut-off as a classifier. We also evaluated whether case classification changed when we varied the cut-off by $\pm$ 1.5%, corresponding to the test-retest variability estimated for $SUVR_{comp}$ [73]. The highest Youden index (sensitivity + specificity - 1) was used to estimate the optimal ROC cut-offs. Statistical differences between ROC curves were evaluated according to the method of DeLong et al. [301] for pairwise ROC comparisons.

Depending on the study, a high clinical specificity may be desirable even if this implies a loss of sensitivity. We therefore also evaluated sensitivities and cut-offs at a fixed prespecified specificity of 90% and 95%, respectively.

We evaluated whether this changed case classification significantly (McNemar test).

As a secondary analysis, we evaluated the continuous relationship between the different CSF analytes and ^{18}F-flutemetamol SUVR$_{comp}$ values. We tested whether a linear, polynomial (quadratic), exponential or hyperbolic relation fitted best to these data. The model assumptions were assessed by evaluating normality and homoscedasticity of residuals with q-q plots and plots of residuals versus fitted values. The best fitting model was selected based on Akaike information criterion (AIC) which is a measure of model fit. A lower AIC indicates a better fit. CSF analytes were used as dependent variables and ^{18}F-flutemetamol SUVR$_{comp}$ as an independent variable.

Statistical analyses were performed in R version 3.1.1 (http://www.r-project.org) and MedCalc version 14.8.1 (http://www.medcalc.org).

6.4 Results

Based on the autopsy-confirmed ^{18}F-flutemetamol SUVR$_{comp}$ cut-off, 7 out of 38 subjects (18%) were assigned to the amyloid-positive category (Figure 6.1A). Case assignment did not change when we varied the cut-off according to the known test-retest replicability.

Aβ42/ttau, Aβ42/Aβ40, Aβ42/Aβ38, and Aβ42 discriminated between ^{18}F-flutemetamol positive and negative subjects with high accuracy (AUC $>$ 0.908, Table 6.2, Figure 6.1B). Aβ38, Aβ40, and ttau showed a lower discriminative power with AUC $<$ 0.724 (Table 6.2). Aβ42/ttau, Aβ42/Aβ40, Aβ42/Aβ38, and Aβ42 had significantly higher AUCs than Aβ38 or Aβ40 alone (Table 6.2, $P < 0.003$). There was no significant difference between ratios Aβ42/ttau, Aβ42/Aβ40, Aβ42/Aβ38 on the one hand and Aβ42 alone, on the other hand (Table 6.2, $P > 0.32$). The AUCs of the three ratios were not statistically different from each other (Table 6.2, $P > 0.30$).

When specificity was fixed at 90%, Aβ42/ttau and Aβ42/Aβ40 had the highest sensitivity and Aβ42/Aβ38 the second highest sensitivity (Table 6.3). All three Aβ isoforms (Aβ42, Aβ40, Aβ38) used on their own detected significantly fewer amyloid PET positive cases when specificity was fixed a priori at 90% than when the cut-off was based on the Youden index (Table 6.3), indicative of a significant loss in sensitivity. This was not the case for Aβ42/ttau, Aβ42/Aβ40, Aβ42/Aβ38 ratios, and ttau (Table 6.3).

When specificity was fixed at 95%, Aβ42/ttau had the highest sensitivity (Table 6.3). All Aβ isoforms, ttau, and all ratios detected significantly less amyloid-positive cases when the specificity was fixed a priori at 95% compared to the Youden index based cut-off, with one exception namely the ratio Aβ42/ttau (Table 6.3). At a specificity of 95%, the number of amyloid PET positive cases detected based on the ratio Aβ42/ttau did not differ significantly from the number detected based on the Youden index based cut-off, although

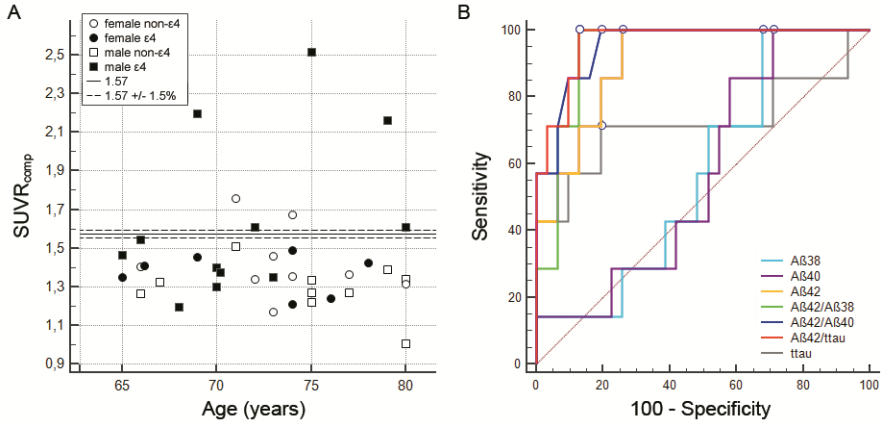

Figure 6.1: Distribution of ^{18}F-flutemetamol SUVR$_{comp}$ values and ROC curves for different CSF analytes. (A) Distribution of ^{18}F-flutemetamol SUVR$_{comp}$ values according to age, sex, and APOE genotype. Solid line = 1.57 SUVR$_{comp}$ cut-off, dashed lines = 1.57 SUVR$_{comp}$ cut-off ± 1.5% corresponding to a test-retest variability for SUVR$_{comp}$ [73] (1.594 and 1.547). (B) ROC curves for different CSF analytes, with ^{18}F-flutemetamol positivity as classifier. Dots represent optimal cut-offs for each analyte, corresponding to the highest Youden index.

Diagnostic performance of different CSF analytes with ^{18}F-flutemetamol PET as autopsy validated standard-of-truth

	AUC	SE	95% CI	Cut-off[a]	Sensitivity	Specificity
Aβ38	0.571	0.111	0.401 - 0.730	2909	100%	32.26%
Aβ40	0.571	0.112	0.401 - 0.730	10738	100%	29.03%
Aβ42*†	0.908	0.051	0.769 - 0.977	745	100%	74.19%
ttau	0.724	0.148	0.555 - 0.856	436	71.43%	80.65%
Aβ42/Aβ38*†	0.935	0.039	0.806 - 0.989	0.332	100%	87.10%
Aβ42/Aβ40*†	0.954	0.033	0.832 - 0.995	0.096	100%	80.65%
Aβ42/ttau*†	0.963	0.028	0.846 - 0.998	2.006	100%	87.10%

Table 6.2: Statistically significant differences of AUCs between analytes are indicated by * and †. *P $<$ 0.05 compared with Aβ40. †P $<$ 0.05 compared with Aβ38. No other differences of AUCs were found. [a]Cut-off corresponding to the highest Youden index. AUC = area under the ROC curve, SE = standard error, CI = confidence interval. Analyte concentrations are described as pg/mL or calculated as ratios between concentrations of two analytes.

Clinical accuracy: estimated sensitivities and cut-off values at a fixed specificity of 90% or 95%

Specificity of 90%	Sensitivity	95% CI	Cut-off	% Difference	*P*
Aβ38	14.29%	0.00 - 71.43	1446	65.79%	<0.0001
Aβ40	14.29%	0.00 - 71.43	5602	65.79%	<0.0001
Aβ42	57.14%	0.00 - 100.00	546	21.05%	0.008
ttau	57.14%	14.29 - 100.00	471	10.53%	0.125
Aβ42/Aβ38	71.43%	0.00 - 100.00	0.268	7.89%	0.250
Aβ42/Aβ40	85.71%	14.29 - 100.00	0.074	10.53%	0.125
Aβ42/ttau	85.71%	14.29 - 100.00	1.852	5.26%	0.500
Specificity of 95%	Sensitivity	95% CI	Cut-off	% Difference	*P*
Aβ38	14.29%	0.00 - 71.43	1342	68.42%	<0.0001
Aβ40	14.29%	0.00 - 71.43	5254	71.05%	<0.0001
Aβ42	42.86%	0.00 - 85.71	493	28.95%	0.001
ttau	42.86%	0.00 - 85.71	539	18.42%	0.016
Aβ42/Aβ38	28.57%	0.00 - 71.43	0.251	21.05%	0.008
Aβ42/Aβ40	57.14%	8.62 - 85.71	0.067	21.05%	0.008
Aβ42/ttau	71.43%	28.57 - 100.00	1.415	13.16%	0.063

Table 6.3: CI = confidence interval. % Difference = % of subjects who were classified differently based on the cut-offs from fixed specificities compared with the cut-offs corresponding to the highest Youden index (Table 6.2). *P* = significance for the % Difference. Analyte concentrations are described as pg/mL or calculated as ratios between concentrations of two analytes.

it was numerically lower.

Four CSF analytes, Aβ42/ttau, Aβ42/Aβ40, Aβ42/Aβ38, and Aβ42, showed a significant correlation with the ^{18}F-flutemetamol SUVR$_{comp}$ values (Figure 6.2). The linear model was rejected because it did not satisfy assumptions of the model. The hyperbolic model fitted best to the relationship between Aβ42 and ^{18}F-flutemetamol SUVR$_{comp}$. The relationships between ^{18}F-flutemetamol SUVR$_{comp}$ and Aβ42/ttau, Aβ42/Aβ40, Aβ42/Aβ38 were best described by the exponential model. However, differences between the models were small. There was no correlation between ^{18}F-flutemetamol SUVR$_{comp}$ values and Aβ38, Aβ40, and ttau (Figure 6.2), in line with a previous study [101].

6.5 Discussion

Overall, when sensitivity and specificity were combined, the ability to discriminate amyloid-positive from amyloid-negative cognitively healthy older adults was comparable between Aβ42 on its own and the ratio of Aβ42 over the isoforms examined or over total tau. However, when a high specificity of 90-95% was imposed as a criterion, the sensitivity of Aβ42 alone diminished to 43-57%. The sensitivity of the ratio over Aβ40 was acceptable at specificity of 90% (86%) but at 95% it decreased to 57%. Under these requirements, the ratio over total

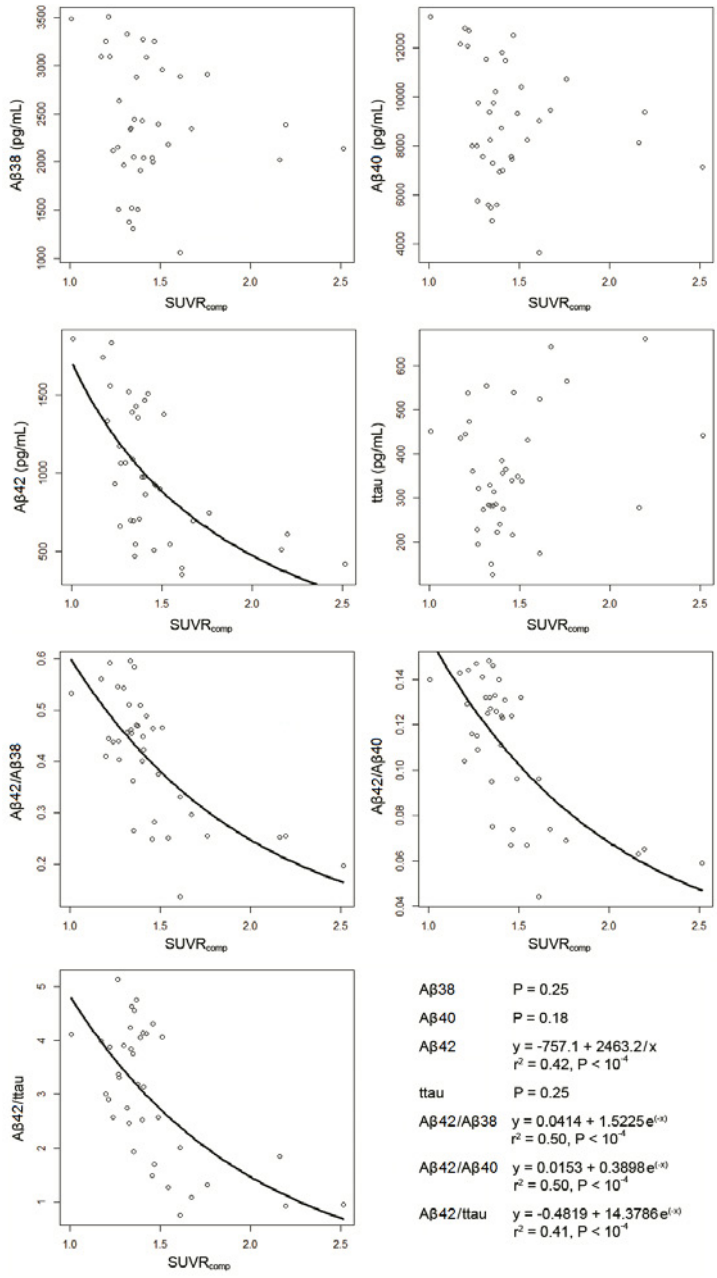

Figure 6.2: Associations between the different CSF analytes and ^{18}F-flutemetamol SUVR$_{comp}$. Black lines represent fitting of the model, shown only for the significant correlations.

tau was the only measure which retained an acceptable sensitivity (71-86%). A high specificity would for instance be desirable if the potential benefit of a study drug depends on the amyloid-positivity of cognitively normal subjects and the study drug has potentially noxious effects or a high cost. A favorable trade-off in terms of sensitivity, as was the case only for Aβ42 over total tau, would decrease the number of subjects needed to scan to reach a prespecified number of positive cases.

6.5.1 Added value of Aβ isoforms Aβ38 and Aβ40

The shorter isoforms Aβ38 and Aβ40 on their own had no diagnostic value to discriminate preclinical AD, in line with previous studies in cognitively intact healthy controls [101], and also in clinical AD patients [302]. In the context of preclinical AD, the added value of the Aβ isoforms mainly occurred when used for calculating the ratio. The ratio over Aβ40 performed better than Aβ42 alone if a high specificity was required (Table 6.3).

The impact of using Aβ isoforms on the clinical accuracy is linked in part to the context of use. In some studies comparing clinical AD with healthy controls, the ratio of Aβ42 over Aβ38 or Aβ40 improved overall diagnostic accuracy [303, 304], but in others it did not [302, 305]. For the discrimination between clinically probable AD and non-AD dementias, the discriminative value of Aβ42/Aβ40 was similar to that of the ratio over total tau and better than Aβ42 alone [306, 307]. In the MCI stage of the disease, the predictive value for progression to dementia over a 4 year interval was higher for Aβ42/Aβ40 (AUC = 0.866) than for Aβ42 alone (AUC = 0.768) [296]. In our study, Aβ42/Aβ40 still allowed acceptable sensitivity for a specificity of 90%, and more so than Aβ42 in isolation.

The reason why ratios perform better than Aβ42 in isolation may be methodological: the normalization procedure may remove a portion of the pre-analytical and analytical variability in the measurement of the protein levels that is in itself unrelated to AD. In that case, as better standards will become available for Aβ42 measurement, the benefit of using ratios will diminish. Alternatively, the ratio may perform better than Aβ42 for biological reasons. Many autosomal dominant forms of AD are associated with an increase in the ratio of Aβ42 over Aβ40 [308, 309]. Others, such as the Dutch and the Arctic APP mutation, are associated with the inverse effect [308]. If the driving force in the initial phases of sporadic AD is related to a disequilibrium between different isoforms rather than the absolute amount of Aβ42 on its own, this could theoretically explain why the ratio would be better.

6.5.2 Ratio of Aβ42 over total tau

For a fixed specificity of 95%, the highest sensitivity (71%) was obtained for Aβ42 over total tau. Total tau is generally thought to reflect neuronal loss.

Adding the separate measurement of a biomarker that increases with the intensity of the neurodegenerative process may enhance specificity because AD is a multidimensional disease [31, 310] so that adding a second dimension (neuronal loss) improves accuracy of classification.

6.5.3 Potential study limitations

Our study has some limitations. The sample size was relatively low and the number of amyloid-positive cases relatively small. For that reason, the estimates of sensitivity and specificity may not be entirely stable. Second, our standard-of-truth was ^{18}F-flutemetamol positivity based on an autopsy-validated cut-off. The autopsy study covered the different Thal stages 1-5 [142]. However, it remains possible, theoretically, that if measured in a population restricted to cognitively intact older adults, the cut-off for distinguishing moderate to high neuritic amyloid density from sparse to low density may be lower than what is found in a mixed group including patients with advanced dementia along with dementia-free individuals [142]. Third, according to the current study logic, a case who has low Aβ42 values but a normal ^{18}F-flutemetamol value would be considered a false-positive. We, however, cannot exclude that this case is in a preclinical state preceding amyloid deposition detectable by PET [101]. In the selection of subjects who have increased risk of amyloid deposition but who have not yet reached the amyloid positivity threshold, there could still be a role for Aβ isoforms beyond Aβ42, though this remains to be demonstrated. The specificity required to define preclinical AD based on biomarkers will depend on the type of clinical trial. Different therapeutic strategies may target different preclinical stages of the disease. Our findings are mainly relevant for those trials that target a phase where amyloid aggregation has already occurred.

6.5.4 Conclusion

For selection of subjects with increased PET amyloid load, if a high specificity is required, our data support the use of Aβ42 over total tau rather than using Aβ42 alone or the ratios to other Aβ isoforms.

7 General discussion

7.1 Preclinical AD in practice

In this project we define preclinical AD primarily based on amyloid PET scan in accordance with the NIA-AA criteria [55]. Overall our findings agree with the current model of preclinical AD [55, 311], however, we found several differences and novelties related to this early disease stage based on our cohort.

When we pooled together all subjects included in this project the prevalence of a positive amyloid scan was 19% (21 out of 112 subjects, Figure 7.1). This is slightly lower compared with a recent meta-analysis of prevalence of amyloid pathology in subjects with normal cognition [38]. In that meta-analysis study amyloid positivity was observed in 25% of subjects between 52 and 82 years of age. Out of all subjects in this age range, 30% were APOE $\varepsilon 4$ carriers. This meta-analysis was based on community-recruited cohorts and may be prone to selection biases which may result in a higher prevalence rate. In a population-based cross-sectional study of cognitively intact 50-89 years old adults frequency of amyloid-positive individuals was similar to that in our study [312]. Among subjects between 50-79 years of age, they reported 15% of amyloid-positive and neurodegeneration-negative cases and 5% of amyloid-positive and neurodegeneration-positive cases. That gave in total 20% of amyloid-positive subjects.

In the Mayo Clinic Study of Aging [312], in the older group between 80-89 years of age, 23.5% of subjects were amyloid-positive and neurodegeneration-negative and 32% were amyloid-positive and neurodegeneration-positive, which gave 55.5% of amyloid-positive subjects in total. Our cross-sectional study did not include subjects older than 80 years, thus we do not have data on frequency of amyloid positivity in this age range. Overall, above the age of 80 prevalence of AD and also amyloid positivity is high, but the impact of positive amyloid biomarker on cognitive decline is probably lower in the older age range

than in the younger subjects. Neuropathological studies have indicated that the association between neuritic amyloid plaque density and the occurrence of dementia is substantially lower above the age of 75 than at a younger age [29, 313].

In our cohort, between 52 and 80 years of age, 46% of subjects were APOE $\varepsilon 4$ carriers. Within the amyloid-positive group, 71% of subjects were APOE $\varepsilon 4$ carriers (15 of 21). Given that our cohort was enriched for APOE $\varepsilon 4$ carriers the percentage of amyloid-positive subjects may appear relatively low. On the other hand, 50% of APOE $\varepsilon 4$ carriers were also BDNF *val* carriers. Potentially, *val* carries could have more effective mechanisms for reducing amyloid accumulation (*Chapter 3*). Moreover, the whole cohort in our study, consisting of four genetic groups, is quite different from the general population. Our subjects were recruited from the community through advertisements in newspapers and on the internet addressed to the 50+ community. Included subjects were matched for number of factors, among them number of cases in each genetic group resulting in different genotype frequencies than in the general population, e.g. 25% of APOE $\varepsilon 4$ and BDNF *met* carriers compared with less than 10% in general population. Inversely, other community-recruited cohorts may have selection biases of their own that may have resulted in a higher prevalence of amyloid-positive cases in these studies. Therefore, we should apply with caution the expected prevalence of amyloid positivity in a specific age group based on other community-recruited studies, to our community-recruited cohort. To judge the prevalence in the general population, population-based studies, which are relatively rare, remain the gold standard. Lastly, according to a detailed interview performed during screening visit most of our subjects were educated, cognitively and/or physically active, and taking medication or following a diet for lowering cholesterol levels and blood pressure. These factors could also contribute to some differences between our and other cohorts.

Subjects with intermediate levels of amyloid deposition presented a significant concern. This concern has been raised before [37]. Instead of a clear bimodal distribution into amyloid-positive and amyloid-negative cases, a significant proportion of values in cognitively intact older individuals is around the cut-off (Figure 7.1). The intermediate cases contribute to the discordance between ^{18}F-flutemetamol and ^{11}C-PIB binary classification based on semi-quantitative assessment (*Chapter 5*). Two discordant cases were assigned to the amyloid-negative category based on ^{18}F-flutemetamol and to the amyloid-positive category based on ^{11}C-PIB. This suggests that either ^{18}F-flutemetamol is more resistant to the false positives or ^{11}C-PIB is more sensitive at an early stage of amyloidosis. A longitudinal follow up of these cases will clarify which is the correct explanation. We could not formally compare the binary classification between ^{18}F-flutemetamol and CSF Aβ levels because we did not have an independent cut-off for binary classification of CSF values at the time of writing (*Chapter 6*).

Detection of the intermediate cases may depend on procedural details, such as the method for amyloid quantification, chosen reference and target regions,

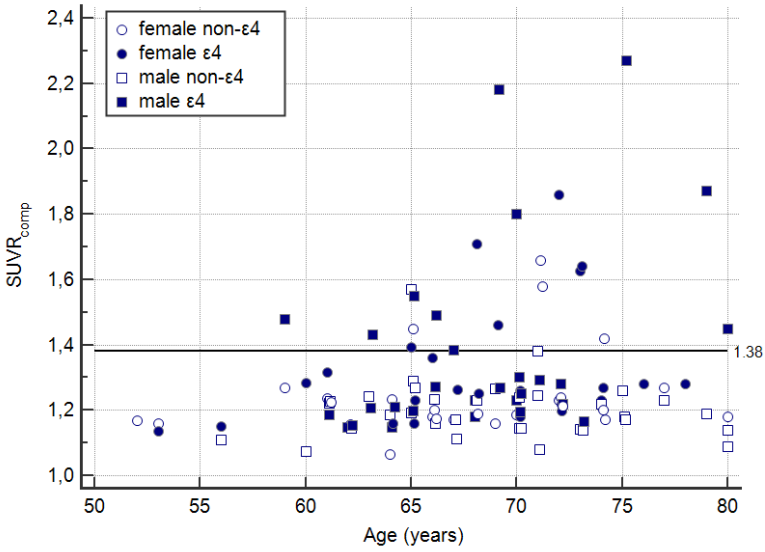

Figure 7.1: Distribution of ^{18}F-flutemetamol SUVR$_{comp}$ values according to age and APOE genotype in all included participants.

and method to define the cut-off, etc. It was suggested that by using the pons instead of cerebellar grey matter as a reference region some of the variability related to the white matter content in VOIs might be removed [314, 298] and it might be more suitable for longitudinal studies [315]. In our analysis method (*Chapter 5*), owing to the narrow MRI-based cortical VOIs which contain less white matter, the cerebellar grey matter is a preferred reference region compared with the pons.

The intermediate values may have a biological meaning. They could represent subjects on their way to increased amyloid deposition. It is important to mention here, that the design of our study was cross-sectional and one cannot directly determine from our data who will show further increase in amyloid aggregation in the future or at which age a positive subject started to accumulate amyloid prior to inclusion. Longitudinal studies showed that changes in Aβ level begin as early as middle age and in some cases they increase over time [300]. Amyloid accumulation is a progressive and dynamic process and the amyloid-positive cases represent a range of continuous values rather than a stationary amyloid-positive stage. Hence, binary classification into positive and negative subjects is somewhat artificial, albeit useful in the clinical context. In the same line, amyloid biomarkers could reflect different accumulation phases. For instance, according to a neuropathological validation study, amyloid PET with ^{18}F-flutemetamol is able to reliably discriminate between Thal amyloid phases 1-2 versus 4-5, but not 1-2 versus 3 [316]. Thus, it probably

reflects intermediate to advanced amyloid accumulation and is less sensitive to only slightly elevated amyloid deposition. On the other hand, in this study amyloid scans were assessed in a binary manner according to visual reads. If scans were assessed on a continuous scale, e.g. SUVR scale, and values were correlated to the Thal amyloid phases one potentially could detect more subtle relationships. There are some speculations that CSF measurement of Aβ42 reflects the earliest amyloid changes, and that CSF Aβ42 and amyloid PET are partially independent [102]. The soluble Aβ42 is a precursor for fibrillar amyloid plaques and is believed to be the cause of toxicity, either directly stemming from oligomeric Aβ intermediates destined for aggregation into plaques or from Aβ oligomers released from higher structure fibrils and plaques [317]. In CSF soluble Aβ is measured and is believed to reflect brain soluble Aβ fraction [104], however, there is no direct proof for that. A group from Washington University used compartmental modeling of stable isotope labeling kinetic (SILK) [318] in cognitively normal controls, and in patients with sporadic and autosomal dominant AD (ADAD) to evaluate the production and turnover rate of Aβ isoforms [319, 320]. They proved that in sporadic AD clearance rate of Aβ42 is 49% slower than in HC [319], and that in ADAD production rate of Aβ42 is 24% increased and its turnover rate relative to Aβ40 is 65% faster compared with noncarriers [320]; explaining reduced Aβ42 concentration in CSF. These experiments also shed light on different forms of soluble Aβ present in CSF (monomers, dimers, oligomers, Aβ bound to larger structures) which currently cannot be distinguished. If CSF truly represents brain soluble Aβ it seems plausible that a middle age subject with a positive CSF Aβ42 finding and a negative amyloid PET lies in the lag-phase where Aβ42 concentration is increased for longer time until it reaches a threshold to initiate Aβ42 aggregation [317]. Thus, theoretically CSF and PET could reflect different amyloid phases. Nonetheless, this needs further investigation, the best is a longitudinal study with near the same time acquisition of amyloid PET and CSF Aβ42 followed by a neuropathological validation detecting aggregated and soluble Aβ pools.

The data presented in different chapters of this thesis are part of a study to explore different aspects of amyloid deposition in the preclinical AD population. In cognitively intact older adults we aimed at (1) investigating BDNF and APOE polymorphisms' effects on amyloid load (*Chapter 3*) and an association with the patterns of functional activation (*Chapter 4*), (2) comparing performance of ^{18}F-flutemetamol PET and ^{11}C-PIB PET (*Chapter 5*) and CSF (*Chapter 6*) biomarkers for the definition of preclinical AD, and (3) defining genetic determinants of increased amyloid levels other than APOE (future work). The cognitively intact older adults have been recruited from the community for a total sample size of 180 subjects. At the time of recruitment, subjects were stratified according to a factorial design with 2 factors per 5 year age bins: BDNF (*met* allele present versus absent) and APOE (ε4 allele present versus absent). The different cells of the factorial design were matched for the number of cases, gender, age, and educational level. Note that, we had to screen a larger number of volunteers to find a sufficient number of the rare combination of BDNF *met* and APOE ε4 alleles. Since 2010 until the time of writing,

741 volunteers underwent an on-site screening visit, which included an interview about medical history, MMSE, and blood sampling for genotyping. Of these, 298 volunteers underwent a detailed neuropsychological assessment and 172 proceeded to the full study procedures: ^{18}F-flutemetamol PET, volumetric MRI, FLAIR. In addition, 64 subjects underwent an fMRI, 32 received an ^{11}C-PIB PET, and 38 received a CSF analysis for Aβ, total and phospho tau.

This doctoral research project revealed an interesting and novel finding. In preclinical AD, the BDNF gene in interaction with the APOE gene modulated amyloid deposition (*Chapter 3*). This suggests that neuroplasticity-related genes may also play a role in amyloid accumulation (see discussion in the next section).

We also found that at the preclinical AD stage increased amyloid load was associated with increased activity in the posterior temporal cortex during a language task (*Chapter 4*). Such an increased activity may have a compensatory function against toxic effects of amyloid pathology (see discussion in the next section).

To conclude, a significant proportion of the cognitively intact older adults has increased amyloid deposition, and therefore could encompass the preclinical stage of AD. It remains to be seen which subjects in our cohort will progress to the symptomatic stage and over how long time period [311]. Most recent findings indicate that subjects in preclinical stage 1-3 are at a greater risk for cognitive decline [321] and progression toward symptomatic AD [57, 58]. A longitudinal follow-up of the study participants will shed light on this issue.

7.2 Neuronal response to amyloid injury

Five years ago we started from a model in which BDNF polymorphism was expected to affect functional changes in the language and semantic system in response to amyloid deposition. Instead, we found that in interaction with APOE polymorphism, it affects amyloid accumulation (*Chapter 3*). BDNF *met* carriers intrinsically have worse neuronal plasticity and with at least one APOE ε4 allele they are additionally predisposed to a higher amyloid deposition. It has been suggested that APOE ε4 carriers with BDNF *met* cannot tolerate amyloid toxicity to the same extent as APOE ε4 carriers with BDNF *val* form [322]. In this group the neuronal survival mechanisms might be less efficient. This is concordant with the neuronal plasticity failure theory, which has been implicated as one of the potential mechanisms in AD [17, 323]. Neuroplasticity is a concept where neurons throughout life undergo adaptive changes in order to keep up with physiological needs and to cope with an injury or stress. It involves upstream changes in regulatory processes at the neuronal body level, which mediate downstream structural and functional changes of dendrites, axons, and synapses [17]. In AD, processes such as amyloid accumulation, tau tangles, loss of synapses and neurons, and cholinergic depletion, perturb normal neuronal plasticity processes at downstream dendritic and synaptic sites. This triggers

an extra upstream plasticity-related cellular activity to meet the higher needs at the downstream sites. Initially this process is compensatory but when it is active for a prolonged time it leads to maladaptive effects. This is influenced by genetic and environmental factors [17]. Let us translate this theory to the established interaction. In BDNF *val* carriers who carry an APOE $\varepsilon 4$ allele, properly functioning neuroplasticity processes would compensate for the toxic effects of Aβ, by e.g. an induction of pro-survival BDNF signalling and a chain of more complex plasticity-related reactions. In BDNF *met* carriers with APOE $\varepsilon 4$, the pro-survival BDNF signalling would be less efficient e.g. owing to the reduced BDNF secretion, and this would render neurons less resistant to the surrounding Aβ toxicity. This would also negatively affect the normal neuronal processes, such as synaptic and axonal signalling, protein transport, vesicular trafficking, and clearance of intra and extra cellular debris. Potentially this would lead to a faster amyloid accumulation among other detrimental processes.

It is important to mention that the reason we were able to detect this interaction was probably because of the genetic stratification for BDNF and APOE prior to recruitment for scanning. The combined rare forms of BDNF *met* and APOE $\varepsilon 4$ within a same subject, were present only in 10% of all candidates volunteering for the study after applying all non-genetic in/exclusion criteria. After genetic stratification this rare combination was present in 25% of cases. Therefore, we would probably miss this interaction if the study candidates would not be matched for equal number of cases in each genotype group. If one would like to replicate this findings, prior stratification might be a prerequisite for the success of the study.

The biological effect of this double risk genotype (BDNF *met*/APOE $\varepsilon 4$) seems intelligible. The mechanistic underpinnings of this interaction, however, are more difficult to explain. The interaction between BDNF and APOE will probably occur at the epistatic (gene-protein-gene) level or protein-protein level, rather than direct gene-gene interaction. A recent study showed an epistatic effect of APOE on BDNF [324]. Using human primary neuronal cells, it was shown that APOE $\varepsilon 4$ increased nuclear translocation of histon deacetylases 4 and 6 which reduced BDNF expression, whereas APOE $\varepsilon 3$ increased histon acetylation and increased BDNF expression [324]. This mechanism explained reduced BDNF expression, but did not take into account different gene products of the *val*66*met* polymorphism. The BDNF *met* carriers may have decreased activity-dependent secretion of BDNF protein, impaired dendritic trafficking and synaptic localization, rather than impaired expression [183]. A possible link in the cross-talk between BDNF and APOE could be SORLA protein (sorting protein-related receptor containing LDLR class-A repeats), which is implicated in molecular pathways of both BDNF and APOE. SORLA is a sorting receptor for the amyloid precursor protein and it regulates intracellular trafficking and processing of amyloid peptides [325]. BDNF protein activates transcription of SORLA [325]. Cellular uptake of amyloid provided by SORLA is dependent on APOE isoforms [326]. Currently very little is known about possible pathways through which BDNF and APOE proteins could cross [327, 324],

and even less is known about crossing of their genotype specific effects.

At the functional level, our current and previous findings suggest that the activity in the posterior temporal language and semantic areas may follow a characteristic temporal and spatial pattern in response to the amyloid injury [133, 132]. At the beginning of the disease, the increased activity within left posterior MTG, subserving higher demands for semantic control, may have a compensatory role which maintains a normal cognitive performance despite the present amyloidosis (*Chapter 4*). Next, consistent with the neuronal plasticity failure theory, due to a breakdown of a prolonged increased neuronal activity, a gradual degeneration of neuronal function may begin in areas more directly involved in word processing as left posterior STS, and this may lead to the first cognitive symptoms [133]. When a significant proportion of neurons is damaged in the target left-sided areas, which are not able to sustain the function any further, the homotopical right-sided regions may be recruited such as right posterior STS [132]. The increased activity in left posterior MTG in response to higher amyloid load was independent of BDNF *val*66*met* genotype. This may seem surprising since BDNF *met* carriers would be expected to have somewhat lower compensatory capacity against amyloid toxicity, according to the neuroplasticity theory. However, in light of our findings from *Chapter 4*, BDNF in interaction with APOE may be involved at a different level of the pathophysiological AD process. It may mediate amyloid aggregation rather than modulate post-hoc response to amyloid toxicity. On the other hand, BDNF *val*66*met* is known to affect episodic memory [181, 182, 183, 184, 185, 186, 187], therefore it is as well possible that we did not pick up the effect of BDNF because we focused on the language function. At a genetic level, current evidence for genetic involvement of BDNF in AD is not clear (e.g. [328, 329, 330]) but there is increasing evidence suggesting a role of BNDF in AD pathogenesis, e.g. based on studies of BDNF serum levels [222, 331, 332] or animal studies [215, 216].

A similar pattern of stage-dependent fMRI activation changes can be observed in the hippocampal formation during episodic memory tasks. In preclinical AD [265, 266, 135] and early MCI [263, 264, 134], activity during memory encoding in hippocampus is increased compared with controls. In the more advanced disease stages, late MCI [258, 262] and probable AD [257, 258, 259, 260, 138, 261], activity is decreased compared with controls.

Elman et al. [136] investigated if such increased activation is truly compensatory or rather an aberrant overactivation. Cognitively intact older and young individuals encoded visual scenes during fMRI and afterwards they were asked if the provided description matched previously viewed scenes (gist memory) and if the number of details matched a given scene (memory richness). Older subjects received a ^{11}C-PIB PET scan. They showed that older individuals with increased amyloid deposition have increased fMRI activity during gist memory encoding in task-positive areas, and decreased deactivation in task-negative areas. Amyloid-positive older subjects with increased activation in task-positive areas could recollect more details about scenes. It was concluded that increased activity in subjects with brain amyloidosis is beneficial

and reflects neural plasticity and serves a compensatory function [136].

In a longitudinal study of MCI subjects, Huijbers et al. [134] investigated fMRI activity during face-name encoding task over 3 years. MCI subjects underwent a ^{11}C-PIB PET scan at baseline and repeat MRI at 6 later time points. They reported that amyloid-positive MCI subjects had increased hippocampal activity during memory encoding compared with amyloid-negative subjects. This activity did not significantly change over time. They suggested that elevated hippocampal activity may have a compensatory function against neurodegeneration or it contributes to amyloid deposition [134].

Taken together, we can conclude that increased activation in domain specific areas (memory or language) at the early disease stages most probably have a compensatory function. Significant associations with the behavioural measures are reassuring, however, one must note that this conclusion was derived from correlational analyses and between-group comparisons. An interventional study would be necessary to further prove this compensatory function. For such purpose, transcranial magnetic stimulation may be a useful technique, which can transiently deactivate a region of interest to test its effect on behavioural performance.

7.3 Clinical applicability

The remaining question is which amyloid measure is the most accurate to define preclinical AD. This is especially important for the clinical trials of putative new treatments for AD. The success of targeted molecular therapies may critically depend on the presence of the drug target. Accurate ascertainment of amyloid-positivity prior to inclusion may constitute one of the factors that determines the success of trials in preclinical AD (importance of high specificity), as well as the cost of screening (importance of high sensitivity). Moreover, amyloid biomarkers may be used as surrogate endpoints to assess the efficacy of disease-modifying treatments.

Despite some differences in the dynamic range, the three recently FDA and EMA approved tracers ^{18}F-flutemetamol [66], ^{18}F-florbetaben [67], and ^{18}F-florbetapir [68], and also ^{11}C-PIB [105], clearly separate AD patients from controls. Binding of the approved tracers to neuritic amyloid plaques has been thoroughly validated in the pivotal phase 3 neuropathological studies [333, 226, 142] (Table 7.1). Compared with ^{18}F-flutemetamol and ^{18}F-florbetaben, ^{18}F-florbetapir has a lower slope for correlation with ^{11}C-PIB, indicating a smaller dynamic range [31, 69]. Diagnostic performance based on neuropathology as a standard-of-truth is not available for ^{11}C-PIB. However, generally ^{11}C-PIB retention correlates well with immunohistochemical measures of amyloid plaque area [334, 141, 335]. Given its shorter half-life, use of ^{11}C-PIB will be restricted to research. According to the findings reported in *Chapter 5*, a method to evaluate the amyloid PET scan in preclinical AD is preferentially quantitative. The quantitative approach offers several advantages: it is independent of reader sub-

Diagnostic performance of FDA and EMA approved amyloid PET tracers with neuropathological findings as a standard-of-truth

	^{18}F-florbetaben [333]	^{18}F-florbetapir [226]	^{18}F-flutemetamol [142]
Sensitivity % (95% CI)	98 (94 - 100)	92 (78 - 98)	86 (72 - 95)
Specificity % (95% CI)	89 (77 - 100)	100 (80 - 100)	92 (74 - 99)
AD (No)	57	29	30
MCI (No)	0	5	0
Other dementias (No)	9	13	17
HC (No)	8	12	21
Δt PET and autopsy	$\leq$ 20 months	$\leq$ 24 months	$\leq$ 13 months
Readers (No)	3	5	5

Table 7.1: Scans were evaluated visually. Values in the table represent results for majority reads. CI = confidence intervals. No = number. Δt = time between.

jectivity when evaluating images, and an identical quantification method can be applied across stages of a longitudinal study and/or across different centres [37]. In a part of the healthy older population with intermediate uptake values, the quantitative method may outperform visual reads, which are difficult to perform in such case. A reference region used to scale amyloid image is an important methodological factor which may influence the subject classification [37]. In our entire sample of 112 subjects, $SUVR_{comp}$ with the cerebellar grey matter as reference region correlated with $SUVR_{comp}$ calculated using the pons as reference region (Figure 7.2). When the pons was used as reference region, analyses from *Chapter 3* yielded the same results as those obtained with the cerebellar cortex as reference region. In *Chapter 4* using the pons generated similar results to the main analyses but with much lower values of statistical significance. In *Chapter 5* the correlation between ^{18}F-flutemetamol and ^{11}C-PIB SUVRs was weaker when the pons was used. In our cohort of cognitively intact older controls, the pons as reference region does not preform better than the cerebellar cortex, despite some suggestions from other studies [314, 298]. In agreement with the neuropathological staging, which shows that the cerebellar cortex is not affected by amyloid plaques until late AD stage [7], amyloid images of adults between 55 and 80 years of age can be scaled to a ligand uptake in the cerebellar grey matter.

For the CSF-based definition of preclinical AD, if a high specificity is required, the use of Aβ42 over total tau or over Aβ40 is preferred, rather than using Aβ42 alone (*Chapter 5*). This is in line with two recent studies showing a better discrimination between AD and HC based on Aβ42/Aβ40 ratio compared with Aβ42 alone [304, 303]. The added value of Aβ42/total tau ratio is well established in clinical populations [336]. These ratios are also useful for a differential diagnosis (see *Section 6.5.1*). A performance of the CSF measurement is clinicopathologically validated, although only for the Aβ42 isoform. Low Aβ42 levels are associated with fibrillar brain Aβ deposits postmortem [83] and in cortical biopsies [84]. The sensitivity and specificity are in the range of amyloid PET tracers, 92% and 86% respectively [83]. A limitation is

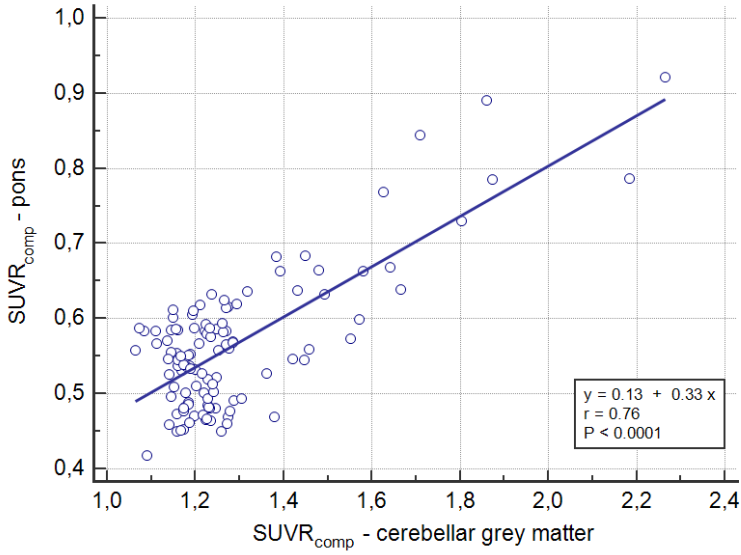

Figure 7.2: Linear regression between ^{18}F-flutemetamol SUVR$_{comp}$ values with cerebellar grey matter (X axis) and pons (Y axis) used as reference regions; based on all included participants (n = 112).

the time interval between CSF collection and autopsy, which is much longer than in the neuropathological studies of amyloid tracers.

The difference in utility between imaging and CSF biomarkers lies in the metrics of the tests, i.e. between-centre and within-centre replicability, the prevalence of intermediate values, and the between-reader variability in diagnostic interpretation of the values for amyloid imaging and CSF, respectively. From the viewpoint of implementation in a clinical environment, CSF biomarkers still have to go through the standardization steps that other diagnostic laboratory tests, e.g. for measuring protein levels in blood, have gone through [337, 338]. The values measured for the same sample vary between centres and the interpretation of a given CSF profile may also be centre- and examiner-dependent. The factors that contribute to the between-centre and within-centre variability of CSF measurements need to be better understood and improved. The neuropathological validation studies of CSF performance should be replicated in a prospective manner. In this sense, the strengths of amyloid imaging compared to CSF at the time of writing seem to lie in its performance in terms of replicability between and within centres, between-reader replicability and standardization [31].

Summary

In this thesis we focused on brain amyloid deposition in a cognitively intact older population: we described its dependence on the genetic polymorphisms and its functional consequences on language and semantic processing. Moreover, we compared the performance of different amyloid biomarkers.

All participants included in this project were community recruited cognitively intact older adults (52-74 years old *Chapter 3 and 4* or 65-80 years old *Chapter 5 and 6*) who underwent genetic stratification for APOE and BDNF, conventional neuropsychological testing, volumetric MRI, ^{18}F-flutemetamol PET, and additionally for experiments in *Chapter 3 and 4* associative-semantic fMRI and neurolinguistic assessment, or for experiments in *Chapter 5 and 6* a second PET with ^{11}C-PIB and lumbar puncture to collect cerebrospinal fluid.

In the first part of this work (*Chapter 3*), we examined whether the BDNF codon 66 polymorphism affects β amyloid deposition and the relationship between β amyloid burden and cognitive scores, and how this relates to the effect of APOE. Our study revealed two key novel findings. First, APOE ε4 carriers exhibited a higher β amyloid load in the presence of one or two BDNF *met* alleles compared to BDNF *met* non-carriers. This interaction was localized to precuneus, orbitofrontal cortex, gyrus rectus, and lateral prefrontal cortex. Second, an inverse relationship between Aβ load and episodic memory exists in BDNF *met*/APOE ε4 carriers but not in any of the other subgroups. This experiment highlights a potential role of the BDNF polymorphism in the preclinical phase of β amyloid deposition and also suggests that the BDNF codon 66 polymorphism may influence resilience against β amyloid-related effects on cognition.

In the second part of this project (*Chapter 4*), we examined whether amyloid load affects the network for language and associative-semantic processing. We found that a higher activity during associative-semantic processing in the posterior left middle temporal gyrus, correlated positively with increased amyloid load. This finding was based on a whole-brain search without prior restriction of the search volume. According to a stepwise linear regression analysis, offline naming reaction times correlated positively with amyloid levels. In a secondary

analysis based on a binary approach, the amyloid-positive group exhibited a higher activity compared to the amyloid-negative group during associative-semantic processing in the same region: the posterior left middle temporal gyrus. We concluded that the left posterior temporal activity increase may reflect higher demands for semantic control in the presence of a higher amyloid burden at the preclinical AD stage.

In the third part of this project (*Chapter 5*), we compared two amyloid imaging markers within subjects: ^{18}F-flutemetamol and ^{11}C-PIB. We found that the concordance between binary classification based on ^{18}F-flutemetamol versus ^{11}C-PIB according to semiquantitative assessment (SUVR) was 94%. Concordance of blinded binary visual reads between tracers was 84%. The correlation between ^{18}F-flutemetamol and ^{11}C-PIB SUVR values with cerebellar grey matter as reference region, was 0.84, with a slope of 0.98. Correlations in neocortical regions were significantly lower with pons as reference region. Partial volume correction improved the correlation in two out of 9 investigated regions: striatum and medial temporal cortex. This study provided evidence that for the definition of preclinical AD based on ^{18}F-flutemetamol, concordance with ^{11}C-PIB was highest using semiquantitative assessment with cerebellar grey matter as reference region.

In the last part of this work (*Chapter 6*), we compared the diagnostic accuracy of different cerebrospinal fluid Aβ isoforms, their ratios, total tau, and Aβ42/ttau for detecting amyloid-positive individuals. For this purpose we performed ROC analysis on cerebrospinal fluid analytes with ^{18}F-flutemetamol amyloid PET as classifier. Seven out of 38 subjects (18%) were assigned to the amyloid-positive category based on the PET cut-off. Aβ42/ttau, Aβ42/Aβ40, Aβ42/Aβ38, and Aβ42 had the highest accuracy to identify amyloid-positive subjects (AUC $\geq$ 0.908). Aβ40 and Aβ38 had significantly lower discriminative power (AUC = 0.571). When specificity was fixed at 90% and 95% Aβ42/ttau had the highest sensitivity, 85.71% and 71.43%, respectively. This experiment showed that for the CSF-based definition of preclinical AD, if a high specificity is required, our data support the use of Aβ42 over total tau rather than using Aβ42 in isolation.

Samenvatting

In deze thesis lag de focus op het meten van amyloidneerslag in een populatie van cognitief intacte, oudere vrijwilligers. We konden een verband beschrijven met genetische polymorfismen en de functionele gevolgen hiervan op het vlak van taal en semantische verwerking. Daarenboven hebben we de performantie van verschillende amyloid biomerkers vergeleken en beschreven.

Alle cognitief intacte, oudere vrijwilligers, werden gerecruteerd voor dit project uit de algemene bevolking (52-74 jaar oud *Chapter 3 en 4* of 65-80 jaar oud *Chapter 5 en 6*) Deze cohorten werden vervolgens genetisch gestratificieerd voor APOE en BDNF polymorfismen en ondergingen conventionele neuropsychologische testen, een volumetrische MRI en ^{18}F-flutemetamol PET. Een deel van deze vrijwilligers heeft deelgenomen aan experimenten (*Chapter 3 en 4*) met een associatieve-semantische fMRI en neurolinguistische taken, of aan experimenten (*Chapter 5 en 6*) met een tweede (^{11}C-PIB) PET scan en tenslotte een lumbale punctie voor hersenvochtanalyse.

In het eerste deel van dit werk (*Chapter 3*), onderzochten we of het BDNF codon 66 polymorphisme de β amyloidneerslag kan beïnvloeden en hoe β amyloidpathologie de cognitieve scores kan beïnvloeden, met betrekking tot effecten van het APOE gen. Onze studie kon twee belangrijke bevindingen rapporteren. Ten eerste vertoonden APOE ε4 dragers een hogere graad van β amyloidneerslag wanneer zij ook drager waren van een of twee BDNF *met* allelen vergeleken t.o.v. BDNF *met* non-carriers. Deze interactie is gelocaliseerd in de precuneus, de orbitofrontale cortex, gyrus rectus, en de lateral prefrontale cortex. Ten tweede, hebben we aangetoond dat er een inverse relatie bestaat tussen Aβ pathologie en performantie op testen die het episodisch geheugen onderzochten in de BDNF *met*/APOE ε4 dragers. Dit verband kon niet worden aangetoond in de andere subgroepen. Dit experiment wijst op een mogelijke rol van het BDNF polymorphisme in de preklinische fase van β amyloidneerslag en suggereert ook dat het BDNF codon 66 polymorfisme de veerkracht/weerstand van het brein tegen β amyloid-gerelateerde effecten op cognitie kan beïnvloeden.

In het tweede deel van dit project(*Chapter 4*), hebben we onderzocht of amyloid pathologie het taalnetwerk en het netwerk voor associatieve-semantische

verwerking beïnvloedt. We konden aantonen dat een hogere activatie gedurende associatieve-semantische verwerking in de linker posterieure midden temporale gyrus, correleerde met een hogere graad van amyloidneerslag in dit gebied. Deze bevinding was gebaseerd op een analyse van het gehele brein zonder beperking van het zoekvolume. Volgens een stapsgewijze, lineaire regressie analyse, correleerden de offline reactietijden voor het benoemen van objecten met een hogere graad van amyloidneerslag. In een secundaire analyse, gebaseerd op een binaire classificatie, bleek dat de amyloid-positieve groep een hogere activiteit vertoonde vergeleken met de amyloid-negatieve groep gedurende associatieve-semantische verwerking in dezelfde regio: de linker posterieure midden temporale gyrus. We kunnen dus besluiten dat de verhoogde activiteit in de linker posterieure temporale gebied mag een hogere semantische controle vereist, wanneer er amyloidpathologie aanwezig is in het preklinische stadium van AD.

In het derde deel van dit project (*Chapter 5*), vergeleken we twee amyloid beeldvormingsmerkers in dezelfde subjecten: ^{18}F-flutemetamol PET en ^{11}C-PIB PET. We vonden een concordantie van 94% tussen de binaire classificatie van ^{18}F-flutemetamol PET versus ^{11}C-PIB PET gebaseerd op een semiquantitatieve berekening (SUVR). De concordantie van de geblindeerde visuele lezingen van de twee type PET scans was daarentegen 84%. De correlatie tussen ^{18}F-flutemetamol en ^{11}C-PIB SUVR waarden, met de cerebellaire grijze stof als referentie regio, was 0.84, met een richtingscoefficient van 0.98. Correlaties in neocorticale regio's waren significant lager wanneer we de pons als referentie regio gebruikten. Partieel volume correctie verbeterde de correlatie in twee van de 9 onderzochte regio's: het striatum en de mediale temporale cortex. Deze studie bevestigde dat voor de definiëring van preklinische AD ^{18}F-flutemetamol gebruikt kan worden en dat de concordantie met ^{11}C-PIB het hoogste was voor de semiquantitatieve berekening van tracer opname met cerebellaire grijze stof als referentie regio.

In het laatste deel van dit werk (*Chapter 6*), vergeleken we de diagnostische accuraatheid van merkers in het hersenvocht: verschillende Aβ isovormen, de ratios, totale tau, en Aβ42/ttau om amyloid-positieve subjecten te kunnen onderscheiden van amyloide-negatieve subjecten. We maakten hiervoor gebruik van ROC analyse op de hersenvochtmerkers met ^{18}F-flutemetamol amyloid PET als 'classifier'. Zeven van de 38 subjecten (18%) werden ingedeeld in de amyloid-positieve categorie gebaseerd op de PET grenswaarde. Aβ42/ttau, Aβ42/Aβ40, Aβ42/Aβ38, en Aβ42 waren het meest accuraat in het identificeren van amyloid-positieve subjecten (AUC $\geq$ 0.908). Aβ40 en Aβ38 hadden minder discriminerende waarde (AUC = 0.571). Wanneer de specificiteit beperkt werd tot 90% en 95%, dan had Aβ42/ttau de hoogste sensitiviteit (85.71% and 71.43%, respectievelijk). Dit experiment toont aan dat voor de hersenvocht-gebaseerde definitie van preklinische AD, een hoge specificiteit vereist is en dat het gebruik van Aβ42 in combinatie met total tau een betere diagnostische waarde heeft dan Aβ42 op zich.

Bibliography

[1] Brookmeyer R, Johnson E, Ziegler-Graham K, Arrighi HM. Forecasting the global burden of Alzheimer's disease. 2007 Alzheimers Dement;3(3):186–191.

[2] Hebert LE, Beckett LA, Scherr PA, Evans DA. Annual incidence of Alzheimer disease in the United States projected to the years 2000 through 2050. 2001 Alzheimer Dis Assoc Disord;15(4):169–173.

[3] Brookmeyer R, Gray S, Kawas C. Projections of Alzheimer's disease in the United States and the public health impact of delaying disease onset. 1998 Am J Public Health;88(9):1337–1342.

[4] Hyman BT, Phelps CH, Beach TG, Bigio EH, Cairns NJ, Carrillo MC, et al. National Institute on Aging-Alzheimer's Association guidelines for the neuropathologic assessment of Alzheimer's disease. 2012 Alzheimers Dement;8(1):1–13.

[5] Masliah E, Terry RD, Mallory M, Alford M, Hansen LA. Diffuse plaques do not accentuate synapse loss in Alzheimer's disease. 1990 Am J Pathol;137(6):1293–1297.

[6] Morris JC, Storandt M, McKeel D Jr, Rubin EH, Price JL, Grant EA, et al. Cerebral amyloid deposition and diffuse plaques in "normal" aging: Evidence for presymptomatic and very mild Alzheimer's disease. 1996 Neurology;46(3):707–719.

[7] Thal DR, Rüb U, Orantes M, Braak H. Phases of A beta-deposition in the human brain and its relevance for the development of AD. 2002 Neurology;58(12):1791–1800.

[8] Christie RH, Bacskai BJ, Zipfel WR, Williams RM, Kajdasz ST, Webb WW, et al. Growth arrest of individual senile plaques in a model of Alzheimer's disease observed by in vivo multiphoton microscopy. 2001 J Neurosci;21(3):858–864.

[9] Hyman BT, Marzloff K, Arriagada PV. The lack of accumulation of senile plaques or amyloid burden in Alzheimer's disease suggests a dynamic balance between amyloid deposition and resolution. 1993 J Neuropathol Exp Neurol;52(6):594–600.

[10] Braak H, Braak E. Neuropathological stageing of Alzheimer-related changes. 1991 Acta Neuropathol;82(4):239–259.

[11] Tiraboschi P, Hansen LA, Thal LJ, Corey-Bloom J. The importance of neuritic plaques and tangles to the development and evolution of AD. 2004 Neurology;62(11):1984–1989.

[12] Arriagada PV, Growdon JH, Hedley-Whyte ET, Hyman BT. Neurofibrillary tangles but not senile plaques parallel duration and severity of Alzheimer's disease. 1992 Neurology;42(3 Pt 1):631–639.

[13] Bancher C, Braak H, Fischer P, Jellinger KA. Neuropathological staging of Alzheimer lesions and intellectual status in Alzheimer's and Parkinson's disease patients. 1993 Neurosci Lett;162(1-2):179–182.

[14] Giannakopoulos P, Hof PR, Bouras C. Selective vulnerability of neocortical association areas in Alzheimer's disease. 1998 Microsc Res Tech;43(1):16–23.

[15] Giannakopoulos P, Herrmann FR, Bussière T, Bouras C, Kövari E, Perl DP, et al. Tangle and neuron numbers, but not amyloid load, predict cognitive status in Alzheimer's disease. 2003 Neurology;60(9):1495–1500.

[16] Guillozet AL, Weintraub S, Mash DC, Mesulam MM. Neurofibrillary tangles, amyloid, and memory in aging and mild cognitive impairment. 2003 Arch Neurol;60(5):729–736.

[17] Mesulam MM. Neuroplasticity failure in Alzheimer's disease: bridging the gap between plaques and tangles. 1999 Neuron;24(3):521–529.

[18] Mesulam M, Shaw P, Mash D, Weintraub S. Cholinergic nucleus basalis tauopathy emerges early in the aging-MCI-AD continuum. 2004 Ann Neurol;55(6):815–828.

[19] Davis DG, Schmitt FA, Wekstein DR, Markesbery WR. Alzheimer neuropathologic alterations in aged cognitively normal subjects. 1999 J Neuropathol Exp Neurol;58(4):376–388.

[20] DeKosky ST, Scheff SW. Synapse loss in frontal cortex biopsies in Alzheimer's disease: correlation with cognitive severity. 1990 Ann Neurol;27(5):457–464.

[21] Scheff SW, Price DA, Schmitt FA, Mufson EJ. Hippocampal synaptic loss in early Alzheimer's disease and mild cognitive impairment. 2006 Neurobiol Aging;27(10):1372–1384.

[22] Terry RD, Masliah E, Salmon DP, Butters N, DeTeresa R, Hill R, et al. Physical basis of cognitive alterations in Alzheimer's disease: synapse loss is the major correlate of cognitive impairment. 1991 Ann Neurol;30(4):572–580.

[23] Gómez-Isla T, Price JL, McKeel D Jr, Morris JC, Growdon JH, Hyman BT. Profound loss of layer II entorhinal cortex neurons occurs in very mild Alzheimer's disease. 1996 J Neurosci;16(14):4491–4500.

[24] Hardy J, Selkoe DJ. The amyloid hypothesis of Alzheimer's disease: progress and problems on the road to therapeutics. 2002 Science;297(5580):353–356.

[25] Fleisher AS, Chen K, Quiroz YT, Jakimovich LJ, Gomez MG, Langois CM, et al. Florbetapir PET analysis of amyloid-β deposition in the presenilin 1 E280A autosomal dominant Alzheimer's disease kindred: a cross-sectional study. 2012 Lancet Neurol;11(12):1057–1065.

[26] Bateman RJ, Xiong C, Benzinger TLS, Fagan AM, Goate A, Fox NC, et al. Clinical and biomarker changes in dominantly inherited Alzheimer's disease. 2012 N Engl J Med;367(9):795–804.

[27] Jack CR Jr, Knopman DS, Jagust WJ, Shaw LM, Aisen PS, Weiner MW, et al. Hypothetical model of dynamic biomarkers of the Alzheimer's pathological cascade. 2010 Lancet Neurol;9(1):119–128.

[28] Jack CR Jr, Knopman DS, Jagust WJ, Petersen RC, Weiner MW, Aisen PS, et al. Tracking pathophysiological processes in Alzheimer's disease: an updated hypothetical model of dynamic biomarkers. 2013 Lancet Neurol;12(2):207–216.

[29] Savva GM, Wharton SB, Ince PG, Forster G, Matthews FE, Brayne C, et al. Age, neuropathology, and dementia. 2009 N Engl J Med;360(22):2302–2309.

[30] Herrup K. Reimagining Alzheimer's disease–an age-based hypothesis. 2010 J Neurosci;30(50):16755–16762.

[31] Vandenberghe R, Adamczuk K, Dupont P, Van Laere K, Chételat G. Amyloid PET in clinical practice: Its place in the multidimensional space of Alzheimer's disease. 2013 Neuroimage Clin;2(6):497–511.

[32] Chételat G. Alzheimer disease: Aβ-independent processes-rethinking preclinical AD. 2013 Nat Rev Neurol;9(3):123–124.

[33] Braak H, Braak E. Frequency of stages of Alzheimer-related lesions in different age categories. 1997 Neurobiol Aging;18(4):351–357.

[34] Crystal H, Dickson D, Fuld P, Masur D, Scott R, Mehler M, et al. Clinico-pathologic studies in dementia: nondemented subjects with pathologically confirmed Alzheimer's disease. 1988 Neurology;38(11):1682–1687.

[35] Katzman R, Terry R, DeTeresa R, Brown T, Davies P, Fuld P, et al. Clinical, pathological, and neurochemical changes in dementia: a subgroup with preserved mental status and numerous neocortical plaques. 1988 Ann Neurol;23(2):138–144.

[36] Price JL, Morris JC. Tangles and plaques in nondemented aging and "preclinical" Alzheimer's disease. 1999 Ann Neurol;45(3):358–368.

[37] Chételat G, La Joie R, Villain N, Perrotin A, de La Sayette V, Eustache F, et al. Amyloid imaging in cognitively normal individuals, at-risk populations and preclinical Alzheimer's disease. 2013 Neuroimage Clin;2:356–365.

[38] Jansen WJ, Ossenkoppele R, Knol DL, Tijms BM, Scheltens P, Verhey FRJ, et al. Prevalence of cerebral amyloid pathology in persons without dementia: a meta-analysis. 2015 JAMA;313(19):1924–1938.

[39] Jack CR Jr, Knopman DS, Weigand SD, Wiste HJ, Vemuri P, Lowe V, et al. An operational approach to National Institute on Aging-Alzheimer's Association criteria for preclinical Alzheimer disease. 2012 Ann Neurol;71(6):765–775.

[40] Landau SM, Mintun MA, Joshi AD, Koeppe RA, Petersen RC, Aisen PS, et al. Amyloid deposition, hypometabolism, and longitudinal cognitive decline. 2012 Ann Neurol;72(4):578–586.

[41] Mathis CA, Mason NS, Lopresti BJ, Klunk WE. Development of Positron Emission Tomography β-Amyloid Plaque Imaging Agents. 2012 Semin Nucl Med;42(6):423–432.

[42] Snitz BE, Weissfeld LA, Lopez OL, Kuller LH, Saxton J, Singhabahu DM, et al. Cognitive trajectories associated with β-amyloid deposition in the oldest-old without dementia. 2013 Neurology;80(15):1378–1384.

[43] Villemagne VL, Pike KE, Chételat G, Ellis KA, Mulligan RS, Bourgeat P, et al. Longitudinal assessment of Aβ and cognition in aging and Alzheimer disease. 2011 Ann Neurol;69(1):181–192.

[44] Chételat G, Villemagne VL, Villain N, Jones G, Ellis KA, Ames D, et al. Accelerated cortical atrophy in cognitively normal elderly with high β-amyloid deposition. 2012 Neurology;78(7):477–484.

[45] Sjögren M, Vanderstichele H, Agren H, Zachrisson O, Edsbagge M, WikkelsøC, et al. Tau and Abeta42 in cerebrospinal fluid from healthy adults 21-93 years of age: establishment of reference values. 2001 Clin Chem;47(10):1776–1781.

[46] Shaw LM, Vanderstichele H, Knapik-Czajka M, Clark CM, Aisen PS, Petersen RC, et al. Cerebrospinal fluid biomarker signature in Alzheimer's disease neuroimaging initiative subjects. 2009 Ann Neurol;65(4):403–413.

[47] Antonell A, Fortea J, Rami L, Bosch B, Balasa M, Sánchez-Valle R, et al. Different profiles of Alzheimer's disease cerebrospinal fluid biomarkers in controls and subjects with subjective memory complaints. 2011 J Neural Transm;118(2):259–262.

[48] Lautner R, Palmqvist S, Mattsson N, Andreasson U, Wallin A, Pålsson E, et al. Apolipoprotein E genotype and the diagnostic accuracy of cerebrospinal fluid biomarkers for Alzheimer disease. 2014 JAMA Psychiatry;71(10):1183–1191.

[49] Mattsson N, Insel PS, Donohue M, Jagust W, Sperling R, Aisen P, et al. Predicting Reduction of Cerebrospinal Fluid β-Amyloid 42 in Cognitively Healthy Controls. 2015 JAMA Neurol;72(5):554–560.

[50] Fagan AM, Xiong C, Jasielec MS, Bateman RJ, Goate AM, Benzinger TLS, et al. Longitudinal change in CSF biomarkers in autosomal-dominant Alzheimer's disease. 2014 Sci Transl Med;6(226):226ra30.

[51] Schott JM, Bartlett JW, Fox NC, Barnes J, ADNI. Increased brain atrophy rates in cognitively normal older adults with low cerebrospinal fluid Aβ1-42. 2010 Ann Neurol;68(6):825–834.

[52] Stomrud E, Hansson O, Zetterberg H, Blennow K, Minthon L, Londos E. Correlation of longitudinal cerebrospinal fluid biomarkers with cognitive decline in healthy older adults. 2010 Arch Neurol;67(2):217–223.

[53] Rolstad S, Berg AI, Bjerke M, Blennow K, Johansson B, Zetterberg H, et al. Amyloid-β42 is associated with cognitive impairment in healthy elderly and subjective cognitive impairment. 2011 J Alzheimers Dis;26(1):135–142.

[54] Gustafson DR, Skoog I, Rosengren L, Zetterberg H, Blennow K. Cerebrospinal fluid beta-amyloid 1-42 concentration may predict cognitive decline in older women. 2007 J Neurol Neurosurg Psychiatry;78(5):461–464.

[55] Sperling RA, Aisen PS, Beckett LA, Bennett DA, Craft S, Fagan AM, et al. Toward defining the preclinical stages of Alzheimer's disease: recommendations from the National Institute on Aging-Alzheimer's Association workgroups on diagnostic guidelines for Alzheimer's disease. 2011 Alzheimers Dement;7(3):280–292.

[56] Dubois B, Feldman HH, Jacova C, Cummings JL, Dekosky ST, Barberger-Gateau P, et al. Revising the definition of Alzheimer's disease: a new lexicon. 2010 Lancet Neurol;9(11):1118–1127.

[57] Knopman DS, Jack C Jr, Wiste HJ, Weigand SD, Vemuri P, Lowe V, et al. Short-term clinical outcomes for stages of NIA-AA preclinical Alzheimer disease. 2012 Neurology;78(20):1576–1582.

[58] Vos SJ, Xiong C, Visser PJ, Jasielec MS, Hassenstab J, Grant EA, et al. Preclinical Alzheimer's disease and its outcome: a longitudinal cohort study. 2013 Lancet Neurol;12(10):957–965.

[59] Knopman DS, Jack CR Jr, Wiste HJ, Weigand SD, Vemuri P, Lowe VJ, et al. Selective worsening of brain injury biomarker abnormalities in cognitively normal elderly persons with β-amyloidosis. 2013 JAMA Neurol;70(8):1030–1038.

[60] McKhann GM, Knopman DS, Chertkow H, Hyman BT, Jack CR Jr, Kawas CH, et al. The diagnosis of dementia due to Alzheimer's disease: recommendations from the National Institute on Aging-Alzheimer's Association workgroups on diagnostic guidelines for Alzheimer's disease. 2011 Alzheimers Dement;7(3):263–269.

[61] Albert MS, DeKosky ST, Dickson D, Dubois B, Feldman HH, Fox NC, et al. The diagnosis of mild cognitive impairment due to Alzheimer's disease: recommendations from the National Institute on Aging-Alzheimer's Association workgroups on diagnostic guidelines for Alzheimer's disease. 2011 Alzheimers Dement;7(3):270–279.

[62] Dubois B, Feldman HH, Jacova C, Dekosky ST, Barberger-Gateau P, Cummings J, et al. Research criteria for the diagnosis of Alzheimer's disease: revising the NINCDS-ADRDA criteria. 2007 Lancet Neurol;6(8):734–746.

[63] Dubois B, Feldman HH, Jacova C, Hampel H, Molinuevo JL, Blennow K, et al. Advancing research diagnostic criteria for Alzheimer's disease: the IWG-2 criteria. 2014 Lancet Neurol;13(6):614–629.

[64] Ni R, Gillberg PG, Bergfors A, Marutle A, Nordberg A. Amyloid tracers detect multiple binding sites in Alzheimer's disease brain tissue. 2013 Brain;136(Pt 7):2217–2227.

[65] Koole M, Lewis DM, Buckley C, Nelissen N, Vandenbulcke M, Brooks DJ, et al. Whole-body biodistribution and radiation dosimetry of 18F-GE067: a radioligand for in vivo brain amyloid imaging. 2009 J Nucl Med;50(5):818–822.

[66] Nelissen N, Van Laere K, Thurfjell L, Owenius R, Vandenbulcke M, Koole M, et al. Phase 1 study of the Pittsburgh compound B derivative 18F-flutemetamol in healthy volunteers and patients with probable Alzheimer disease. 2009 J Nucl Med;50(8):1251–1259.

[67] Rowe CC, Ackerman U, Browne W, Mulligan R, Pike KL, O'Keefe G, et al. Imaging of amyloid beta in Alzheimer's disease with 18F-BAY94-9172, a novel PET tracer: proof of mechanism. 2008 Lancet Neurol;7(2):129–135.

[68] Wong DF, Rosenberg PB, Zhou Y, Kumar A, Raymont V, Ravert HT, et al. In vivo imaging of amyloid deposition in Alzheimer disease using the radioligand 18F-AV-45 (florbetapir F18). 2010 J Nucl Med;51(6):913–920.

[69] Vandenberghe R, Adamczuk K, Van Laere K. The interest of amyloid PET imaging in the diagnosis of Alzheimer's disease. 2013 Curr Opin Neurol;26(6):646–655.

[70] Wolk DA, Zhang Z, Boudhar S, Clark CM, Pontecorvo MJ, Arnold SE. Amyloid imaging in Alzheimer's disease: comparison of florbetapir and Pittsburgh compound-B positron emission tomography. 2012 J Neurol Neurosurg Psychiatry;83(9):923–926.

[71] Landau SM, Breault C, Joshi AD, Pontecorvo M, Mathis CA, Jagust WJ, et al. Amyloid-β imaging with Pittsburgh compound B and florbetapir: comparing radiotracers and quantification methods. 2013 J Nucl Med;54(1):70–77.

[72] Rowe CC, Pejoska S, Mulligan RS, Jones G, Chan JG, Svensson S, et al. Head-to-head comparison of 11C-PiB and 18F-AZD4694 (NAV4694) for β-amyloid imaging in aging and dementia. 2013 J Nucl Med;54(6):880–886.

[73] Vandenberghe R, Van Laere K, Ivanoiu A, Salmon E, Bastin C, Triau E, et al. 18F-flutemetamol amyloid imaging in Alzheimer disease and mild cognitive impairment: a phase 2 trial. 2010 Ann Neurol;68(3):319–329.

[74] Joshi AD, Pontecorvo MJ, Clark CM, Carpenter AP, Jennings DL, Sadowsky CH, et al. Performance characteristics of amyloid PET with florbetapir F18 in patients with Alzheimer's disease and cognitively normal subjects. 2012 J Nucl Med;53(3):378–384.

[75] Villemagne VL, Ong K, Mulligan RS, Holl G, Pejoska S, Jones G, et al. Amyloid imaging with (18)F-florbetaben in Alzheimer disease and other dementias. 2011 J Nucl Med;52(8):1210–1217.

[76] Cselényi Z, Jönhagen ME, Forsberg A, Halldin C, Julin P, Schou M, et al. Clinical validation of 18F-AZD4694, an amyloid-β-specific PET radioligand. 2012 J Nucl Med;53(3):415–424.

[77] Rinne JO, Wong DF, Wolk DA, Leinonen V, Arnold SE, Buckley C, et al. [(18)F]Flutemetamol PET imaging and cortical biopsy histopathology for fibrillar amyloid β detection in living subjects with normal pressure hydrocephalus: pooled analysis of four studies. 2012 Acta Neuropathol;124(6):833–845.

[78] Ng S, Villemagne VL, Berlangieri S, Lee ST, Cherk M, Gong SJ, et al. Visual assessment versus quantitative assessment of 11C-PIB PET and 18F-FDG PET for detection of Alzheimer's disease. 2007 J Nucl Med;48(4):547–552.

[79] Doraiswamy PM, Sperling RA, Coleman RE, Johnson KA, Reiman EM, Davis MD, et al. Amyloid-β assessed by florbetapir F 18 PET and 18-month cognitive decline: a multicenter study. 2012 Neurology;79(16):1636–1644.

[80] Barthel H, Gertz HJ, Dresel S, Peters O, Bartenstein P, Buerger K, et al. Cerebral amyloid-PET with florbetaben (18F) in patients with Alzheimer's disease and healthy controls: a multicentre phase 2 diagnostic study. 2011 Lancet Neurol;10(5):424–435.

[81] Tiepolt S, Barthel H, Butzke D, Hesse S, Patt M, Gertz HJ, et al. Influence of scan duration on the accuracy of β-amyloid PET with florbetaben in patients with Alzheimer's disease and healthy volunteers. 2013 Eur J Nucl Med Mol Imaging;40(2):238–244.

[82] Villemagne VL, Mulligan RS, Pejoska S, Ong K, Jones G, O'Keefe G, et al. Comparison of 11C-PiB and 18F-florbetaben for Aβ imaging in ageing and Alzheimer's disease. 2012 Eur J Nucl Med Mol Imaging;39(6):983–989.

[83] Tapiola T, Alafuzoff I, Herukka SK, Parkkinen L, Hartikainen P, Soininen H, et al. Cerebrospinal fluid β-amyloid 42 and tau proteins as biomarkers of Alzheimer-type pathologic changes in the brain. 2009 Arch Neurol;66(3):382–389.

[84] Seppälä TT, Nerg O, Koivisto AM, Rummukainen J, Puli L, Zetterberg H, et al. CSF biomarkers for Alzheimer disease correlate with cortical brain biopsy findings. 2012 Neurology;78(20):1568–1575.

[85] Engelborghs S, De Vreese K, Van de Casteele T, Vanderstichele H, Van Everbroeck B, Cras P, et al. Diagnostic performance of a CSF-biomarker panel in autopsy-confirmed dementia. 2008 Neurobiol Aging;29(8):1143–1159.

[86] Toledo JB, Brettschneider J, Grossman M, Arnold SE, Hu WT, Xie SX, et al. CSF biomarkers cutoffs: the importance of coincident neuropathological diseases. 2012 Acta Neuropathol;124(1):23–35.

[87] Struyfs H, Molinuevo JL, Martin JJ, De Deyn PP, Engelborghs S. Validation of the AD-CSF-index in autopsy-confirmed Alzheimer's disease patients and healthy controls. 2014 J Alzheimers Dis;41(3):903–909.

[88] De Meyer G, Shapiro F, Vanderstichele H, Vanmechelen E, Engelborghs S, De Deyn PP, et al. Diagnosis-independent Alzheimer disease biomarker signature in cognitively normal elderly people. 2010 Arch Neurol;67(8):949–956.

[89] Buchhave P, Minthon L, Zetterberg H, Wallin AK, Blennow K, Hansson O. Cerebrospinal fluid levels of β-amyloid 1-42, but not of tau, are fully changed already 5 to 10 years before the onset of Alzheimer dementia. 2012 Arch Gen Psychiatry;69(1):98–106.

[90] Visser PJ, Verhey F, Knol DL, Scheltens P, Wahlund LO, Freund-Levi Y, et al. Prevalence and prognostic value of CSF markers of Alzheimer's disease pathology in patients with subjective cognitive impairment or mild cognitive impairment in the DESCRIPA study: a prospective cohort study. 2009 Lancet Neurol;8(7):619–627.

[91] Andreasson U, Vanmechelen E, Shaw LM, Zetterberg H, Vanderstichele H. Analytical aspects of molecular Alzheimer's disease biomarkers. 2012 Biomark Med;6(4):377–389.

[92] Bjerke M, Portelius E, Minthon L, Wallin A, Anckarsäter H, Anckarsäter R, et al. Confounding factors influencing amyloid Beta concentration in cerebrospinal fluid. 2010 Int J Alzheimers Dis; doi:10.4061/2010/986310.

[93] Mattsson N, Andreasson U, Persson S, Carrillo MC, Collins S, Chalbot S, et al. CSF biomarker variability in the Alzheimer's Association quality control program. 2013 Alzheimers Dement;9(3):251–261.

[94] Fagan AM, Mintun MA, Mach RH, Lee SY, Dence CS, Shah AR, et al. Inverse relation between in vivo amyloid imaging load and cerebrospinal fluid Abeta42 in humans. 2006 Ann Neurol;59(3):512–519.

[95] Forsberg A, Engler H, Almkvist O, Blomquist G, Hagman G, Wall A, et al. PET imaging of amyloid deposition in patients with mild cognitive impairment. 2008 Neurobiol Aging;29(10):1456–1465.

[96] Jagust WJ, Landau SM, Shaw LM, Trojanowski JQ, Koeppe RA, Reiman EM, et al. Relationships between biomarkers in aging and dementia. 2009 Neurology;73(15):1193–1199.

[97] Tolboom N, van der Flier WM, Yaqub M, Boellaard R, Verwey NA, Blankenstein MA, et al. Relationship of cerebrospinal fluid markers to 11C-PiB and 18F-FDDNP binding. 2009 J Nucl Med;50(9):1464–1470.

[98] Landau SM, Lu M, Joshi AD, Pontecorvo M, Mintun MA, Trojanowski JQ, et al. Comparing positron emission tomography imaging and cerebrospinal fluid measurements of β-amyloid. 2013 Ann Neurol;74(6):826–836.

[99] Mattsson N, Insel PS, Landau S, Jagust W, Donohue M, Shaw LM, et al. Diagnostic accuracy of CSF Ab42 and florbetapir PET for Alzheimer's disease. 2014 Ann Clin Transl Neurol;1(8):534–543.

[100] Palmqvist S, Zetterberg H, Blennow K, Vestberg S, Andreasson U, Brooks DJ, et al. Accuracy of brain amyloid detection in clinical practice using cerebrospinal fluid β-amyloid 42: a cross-validation study against amyloid positron emission tomography. 2014 JAMA Neurol;71(10):1282–1289.

[101] Fagan AM, Mintun MA, Shah AR, Aldea P, Roe CM, Mach RH, et al. Cerebrospinal fluid tau and ptau(181) increase with cortical amyloid deposition in cognitively normal individuals: implications for future clinical trials of Alzheimer's disease. 2009 EMBO Mol Med;1(8-9):371–380.

[102] Mattsson N, Insel PS, Donohue M, Landau S, Jagust WJ, Shaw LM, et al. Independent information from cerebrospinal fluid amyloid-β and florbetapir imaging in Alzheimer's disease. 2015 Brain;138(Pt 3):772–783.

[103] Toledo JB, Bjerke M, Da X, Landau SM, Foster NL, Jagust W, et al. Nonlinear Association Between Cerebrospinal Fluid and Florbetapir F-18 β-Amyloid Measures Across the Spectrum of Alzheimer Disease. 2015 JAMA Neurol;72(5):571–581.

[104] Wang R, Sweeney D, Gandy SE, Sisodia SS. The profile of soluble amyloid beta protein in cultured cell media. Detection and quantification of amyloid beta protein and variants by immunoprecipitation-mass spectrometry. 1996 J Biol Chem;271(50):31894–31902.

[105] Klunk WE, Engler H, Nordberg A, Wang Y, Blomqvist G, Holt DP, et al. Imaging brain amyloid in Alzheimer's disease with Pittsburgh Compound-B. 2004 Ann Neurol;55(3):306–319.

[106] Corder EH, Saunders AM, Risch NJ, Strittmatter WJ, Schmechel DE, Gaskell P Jr, et al. Protective effect of apolipoprotein E type 2 allele for late onset Alzheimer disease. 1994 Nat Genet;7(2):180–184.

[107] Corder EH, Saunders AM, Strittmatter WJ, Schmechel DE, Gaskell PC, Small GW, et al. Gene dose of apolipoprotein E type 4 allele and the risk of Alzheimer's disease in late onset families. 1993 Science;261(5123):921–923.

[108] Saunders AM, Strittmatter WJ, Schmechel D, George-Hyslop PH, Pericak-Vance MA, Joo SH, et al. Association of apolipoprotein E allele epsilon 4 with late-onset familial and sporadic Alzheimer's disease. 1993 Neurology;43(8):1467–1472.

[109] Farrer LA, Cupples LA, Haines JL, Hyman B, Kukull WA, Mayeux R, et al. Effects of age, sex, and ethnicity on the association between apolipoprotein E genotype and Alzheimer disease. A meta-analysis. APOE and Alzheimer Disease Meta Analysis Consortium. 1997 JAMA;278(16):1349–1356.

[110] Seshadri S, Drachman DA, Lippa CF. Apolipoprotein E epsilon 4 allele and the lifetime risk of Alzheimer's disease. What physicians know, and what they should know. 1995 Arch Neurol;52(11):1074–1079.

[111] Altmann A, Tian L, Henderson VW, Greicius MD, ADNI. Sex modifies the APOE-related risk of developing Alzheimer disease. 2014 Ann Neurol;75(4):563–573.

[112] Drzezga A, Grimmer T, Henriksen G, Mühlau M, Perneczky R, Miederer I, et al. Effect of APOE genotype on amyloid plaque load and gray matter volume in Alzheimer disease. 2009 Neurology;72(17):1487–1494.

[113] Reiman EM, Chen K, Liu X, Bandy D, Yu M, Lee W, et al. Fibrillar amyloid-beta burden in cognitively normal people at 3 levels of genetic risk for Alzheimer's disease. 2009 Proc Natl Acad Sci U S A;106(16):6820–6825.

[114] Fleisher AS, Chen K, Liu X, Ayutyanont N, Roontiva A, Thiyyagura P, et al. Apolipoprotein E $\varepsilon 4$ and age effects on florbetapir positron emission tomography in healthy aging and Alzheimer disease. 2013 Neurobiol Aging;34(1):1–12.

[115] Galasko D, Chang L, Motter R, Clark CM, Kaye J, Knopman D, et al. High cerebrospinal fluid tau and low amyloid beta42 levels in the clinical diagnosis of Alzheimer disease and relation to apolipoprotein E genotype. 1998 Arch Neurol;55(7):937–945.

[116] Sunderland T, Mirza N, Putnam KT, Linker G, Bhupali D, Durham R, et al. Cerebrospinal fluid beta-amyloid1-42 and tau in control subjects at risk for Alzheimer's disease: the effect of APOE epsilon4 allele. 2004 Biol Psychiatry;56(9):670–676.

[117] Vemuri P, Wiste HJ, Weigand SD, Knopman DS, Shaw LM, Trojanowski JQ, et al. Effect of apolipoprotein E on biomarkers of amyloid load and neuronal pathology in Alzheimer disease. 2010 Ann Neurol;67(3):308–316.

[118] Polvikoski T, Sulkava R, Haltia M, Kainulainen K, Vuorio A, Verkkoniemi A, et al. Apolipoprotein E, dementia, and cortical deposition of beta-amyloid protein. 1995 N Engl J Med;333(19):1242–1247.

[119] Ossenkoppele R, van der Flier WM, Zwan MD, Adriaanse SF, Boellaard R, Windhorst AD, et al. Differential effect of APOE genotype on amyloid load and glucose metabolism in AD dementia. 2013 Neurology;80(4):359–365.

[120] Castellano JM, Kim J, Stewart FR, Jiang H, DeMattos RB, Patterson BW, et al. Human apoE isoforms differentially regulate brain amyloid-β peptide clearance. 2011 Sci Transl Med;3(89):89ra57.

[121] Verghese PB, Castellano JM, Garai K, Wang Y, Jiang H, Shah A, et al. ApoE influences amyloid-β (Aβ) clearance despite minimal apoE/Aβ association in physiological conditions. 2013 Proc Natl Acad Sci U S A;110(19):E1807–E1816.

[122] Fratiglioni L, Ahlbom A, Viitanen M, Winblad B. Risk factors for late-onset Alzheimer's disease: a population-based, case-control study. 1993 Ann Neurol;33(3):258–266.

[123] Green RC, Cupples LA, Go R, Benke KS, Edeki T, Griffith PA, et al. Risk of dementia among white and African American relatives of patients with Alzheimer disease. 2002 JAMA;287(3):329–336.

[124] Mosconi L, Rinne JO, Tsui WH, Berti V, Li Y, Wang H, et al. Increased fibrillar amyloid-beta burden in normal individuals with a family history of late-onset Alzheimer's. 2010 Proc Natl Acad Sci U S A;107(13):5949–5954.

[125] Xiong C, Roe CM, Buckles V, Fagan A, Holtzman D, Balota D, et al. Role of family history for Alzheimer biomarker abnormalities in the adult children study. 2011 Arch Neurol;68(10):1313–1319.

[126] Chibnik LB, Shulman JM, Leurgans SE, Schneider JA, Wilson RS, Tran D, et al. CR1 is associated with amyloid plaque burden and age-related cognitive decline. 2011 Ann Neurol;69(3):560–569.

[127] Shulman JM, Chen K, Keenan BT, Chibnik LB, Fleisher A, Thiyyagura P, et al. Genetic susceptibility for Alzheimer disease neuritic plaque pathology. 2013 JAMA Neurol;70(9):1150–1157.

[128] Hohman TJ, Koran ME, Thornton-Wells T, ADNI. Epistatic genetic effects among Alzheimer's candidate genes. 2013 PLoS One;8(11):e80839.

[129] Thambisetty M, An Y, Nalls M, Sojkova J, Swaminathan S, Zhou Y, et al. Effect of Complement CR1 on brain amyloid burden during aging and its modification by APOE genotype. 2013 Biol Psychiatry;73(5):422–428.

[130] Swaminathan S, Shen L, Risacher SL, Yoder KK, West JD, Kim S, et al. Amyloid pathway-based candidate gene analysis of [(11)C]PiB-PET in the Alzheimer's Disease Neuroimaging Initiative (ADNI) cohort. 2012 Brain Imaging Behav;6(1):1–15.

[131] Bettens K, Sleegers K, Van Broeckhoven C. Genetic insights in Alzheimer's disease. 2013 Lancet Neurol;12(1):92–104.

[132] Nelissen N, Vandenbulcke M, Fannes K, Verbruggen A, Peeters R, Dupont P, et al. Abeta amyloid deposition in the language system and how the brain responds. 2007 Brain;130(Pt 8):2055–2069.

[133] Vandenbulcke M, Peeters R, Dupont P, Van Hecke P, Vandenberghe R. Word reading and posterior temporal dysfunction in amnestic mild cognitive impairment. 2007 Cereb Cortex;17(3):542–551.

[134] Huijbers W, Mormino EC, Schultz AP, Wigman S, Ward AM, Larvie M, et al. Amyloid-β deposition in mild cognitive impairment is associated with increased hippocampal activity, atrophy and clinical progression. 2015 Brain;138(Pt 4):1023–1035.

[135] Mormino EC, Brandel MG, Madison CM, Marks S, Baker SL, Jagust WJ. Aβ deposition in aging is associated with increases in brain activation during successful memory encoding. 2012 Cereb Cortex;22(8):1813–1823.

[136] Elman JA, Oh H, Madison CM, Baker SL, Vogel JW, Marks SM, et al. Neural compensation in older people with brain amyloid-β deposition. 2014 Nat Neurosci;17(10):1316–1318.

[137] Sperling RA, Laviolette PS, O'Keefe K, O'Brien J, Rentz DM, Pihlajamaki M, et al. Amyloid deposition is associated with impaired default network function in older persons without dementia. 2009 Neuron;63(2):178–188.

[138] Celone KA, Calhoun VD, Dickerson BC, Atri A, Chua EF, Miller SL, et al. Alterations in memory networks in mild cognitive impairment and Alzheimer's disease: an independent component analysis. 2006 J Neurosci;26(40):10222–10231.

[139] Bacskai BJ, Frosch MP, Freeman SH, Raymond SB, Augustinack JC, Johnson KA, et al. Molecular imaging with Pittsburgh Compound B confirmed at autopsy: a case report. 2007 Arch Neurol;64(3):431–434.

[140] Ikonomovic MD, Klunk WE, Abrahamson EE, Mathis CA, Price JC, Tsopelas ND, et al. Post-mortem correlates of in vivo PiB-PET amyloid imaging in a typical case of Alzheimer's disease. 2008 Brain;131(Pt 6):1630–1645.

[141] Driscoll I, Troncoso JC, Rudow G, Sojkova J, Pletnikova O, Zhou Y, et al. Correspondence between in vivo (11)C-PiB-PET amyloid imaging and postmortem, region-matched assessment of plaques. 2012 Acta Neuropathol;124(6):823–831.

[142] Curtis C, Gamez JE, Singh U, Sadowsky CH, Villena T, Sabbagh MN, et al. Phase 3 trial of flutemetamol labeled with radioactive fluorine 18 imaging and neuritic plaque density. 2015 JAMA Neurol;72(3):287–294.

[143] Suetens P. Fundamentals of medical imaging. Chapters: Nuclear medicine imaging, X-ray computed tomography. Cambridge university press; 2009.

[144] Nelissen N, Warwick J, Dupont P. Positron Emission Tomography–Current Clinical and Research Aspects. Chapter: Kinetic Modelling in Human Brain Imaging. Hsieh CH, editor. InTech; 2012.

[145] Friston KJ, Holmes AP, Worsley KJ, Poline JP, Frith CD, Frackowiak RSJ. Statistical Parametric Maps in Functional Imaging: A General Linear Approach. 1995 Human Brain Mapping;2:189–210.

[146] Müller-Gärtner HW, Links JM, Prince JL, Bryan RN, McVeigh E, Leal JP, et al. Measurement of radiotracer concentration in brain gray matter using positron emission tomography: MRI-based correction for partial volume effects. 1992 J Cereb Blood Flow Metab;12(4):571–583.

[147] Friston KJ, Holmes A, Poline JB, Price CJ, Frith CD. Detecting activations in PET and fMRI: levels of inference and power. 1996 Neuroimage;4(3 Pt 1):223–235.

[148] Poline JB, Worsley KJ, Evans AC, Friston KJ. Combining spatial extent and peak intensity to test for activations in functional imaging. 1997 Neuroimage;5(2):83–96.

[149] Huettel SA, Song AW, McCarthy G. Functional magnetic resonance imaging. Sinauer Associates Sunderland; 2009.

[150] Howard D, Patterson KE. The Pyramids and Palm Trees Test: A test of semantic access from words and pictures. Thames Valley Test Company; 1992.

[151] Folstein MF, Folstein SE, McHugh PR. Mini-mental state. A practical method for grading the cognitive state of patients for the clinician. 1975 J Psychiatr Res;12(3):189–198.

[152] Morris JC, Ernesto C, Schafer K, Coats M, Leon S, Sano M, et al. Clinical dementia rating training and reliability in multicenter studies: the Alzheimer's Disease Cooperative Study experience. 1997 Neurology;48(6):1508–1510.

[153] Ivnik R, Malec J, Tangalos E, Petersen R, Kokmen E, Kurland L. The Auditory Verbal Learning test (AVLT): Norms for ages 55 years and older. 1990 Psychol Assess;2:304–312.

[154] Kaplan E, Goodglass H, Weintraub S. The Boston Naming Test. Philadelphia: Lea and Febiger; 1983.

[155] Mariën P, Mampaey E, Vervaet A, Saerens J, De Deyn PP. Normative data for the Boston naming test in native Dutch-speaking Belgian elderly. 1998 Brain Lang;65(3):447–467.

[156] Goodglass H, Kaplan E. The assessment of aphasia and related disorders. Philadelphia: Lea and Febiger; 1983.

[157] Raven JC, Court JH, Raven JE. Coloured progressive matrices. Oxford: Oxford Psychologists Press; 1995.

[158] Armitage SG. An analysis of certain psychological tests used in the evaluation of brain injury. 1946 Psych Mono;60:1–48.

[159] Laiacona M, Capitani E. A case of prevailing deficit of nonliving categories or a case of prevailing sparing of living categories? 2001 Cogn Neuropsychol;18(1):39–70.

[160] Bastiaanse R, Bosje M, Visch-Brink E. Psycholinguïstische testbatterij voor de taalverwerking van Afasiepatiënten (PALPA). 1995 Hove: Lawrence Erlbaum Associates;.

[161] Grossman M, Koenig P, Glosser G, DeVita C, Moore P, Rhee J, et al. Neural basis for semantic memory difficulty in Alzheimer's disease: an fMRI study. 2003a Brain;126(Pt 2):292–311.

[162] Grossman M, Koenig P, DeVita C, Glosser G, Moore P, Gee J, et al. Neural basis for verb processing in Alzheimer's disease: an fMRI study. 2003b Neuropsychology;17(4):658–674.

[163] Seidenberg M, Guidotti L, Nielson KA, Woodard JL, Durgerian S, Antuono P, et al. Semantic memory activation in individuals at risk for developing Alzheimer disease. 2009 Neurology;73(8):612–620.

[164] Aizenstein HJ, Nebes RD, Saxton JA, Price JC, Mathis CA, Tsopelas ND, et al. Frequent amyloid deposition without significant cognitive impairment among the elderly. 2008 Arch Neurol;65(11):1509–1517.

[165] Mintun MA, Larossa GN, Sheline YI, Dence CS, Lee SY, Mach RH, et al. [11C]PIB in a nondemented population: potential antecedent marker of Alzheimer disease. 2006 Neurology;67(3):446–452.

[166] Morris JC, Roe CM, Xiong C, Fagan AM, Goate AM, Holtzman DM, et al. APOE predicts amyloid-beta but not tau Alzheimer pathology in cognitively normal aging. 2010 Ann Neurol;67(1):122–131.

[167] Pike KE, Savage G, Villemagne VL, Ng S, Moss SA, Maruff P, et al. Beta-amyloid imaging and memory in non-demented individuals: evidence for preclinical Alzheimer's disease. 2007 Brain;130(Pt 11):2837–2844.

[168] Rowe CC, Ng S, Ackermann U, Gong SJ, Pike K, Savage G, et al. Imaging beta-amyloid burden in aging and dementia. 2007 Neurology;68(20):1718–1725.

[169] Rowe CC, Ellis KA, Rimajova M, Bourgeat P, Pike KE, Jones G, et al. Amyloid imaging results from the Australian Imaging, Biomarkers and Lifestyle (AIBL) study of aging. 2010 Neurobiol Aging;31(8):1275–1283.

[170] Rebeck GW, Reiter JS, Strickland DK, Hyman BT. Apolipoprotein E in sporadic Alzheimer's disease: allelic variation and receptor interactions. 1993 Neuron;11(4):575–580.

[171] Arendt T. Disturbance of neuronal plasticity is a critical pathogenetic event in Alzheimer's disease. 2001 Int J Dev Neurosci;19(3):231–245.

[172] Ashford JW, Jarvik L. Alzheimer's disease: does neuron plasticity predispose to axonal neurofibrillary degeneration? 1985 N Engl J Med;313(6):388–389.

[173] Mesulam MM. A plasticity-based theory of the pathogenesis of Alzheimer's disease. 2000 Ann N Y Acad Sci;924:42–52.

[174] Teter B. ApoE-dependent plasticity in Alzheimer's disease. 2004 J Mol Neurosci;23(3):167–179.

[175] Gorski JA, Zeiler SR, Tamowski S, Jones KR. Brain-derived neurotrophic factor is required for the maintenance of cortical dendrites. 2003 J Neurosci;23(17):6856–6865.

[176] Webster MJ, Herman MM, Kleinman JE, Shannon Weickert C. BDNF and trkB mRNA expression in the hippocampus and temporal cortex during the human lifespan. 2006 Gene Expr Patterns;6(8):941–951.

[177] Erickson KI, Voss MW, Prakash RS, Basak C, Szabo A, Chaddock L, et al. Exercise training increases size of hippocampus and improves memory. 2011 Proc Natl Acad Sci U S A;108(7):3017–3022.

[178] Li Y, Luikart BW, Birnbaum S, Chen J, Kwon CH, Kernie SG, et al. TrkB regulates hippocampal neurogenesis and governs sensitivity to antidepressive treatment. 2008 Neuron;59(3):399–412.

[179] Okuno H, Tokuyama W, Li YX, Hashimoto T, Miyashita Y. Quantitative evaluation of neurotrophin and trk mRNA expression in visual and limbic areas along the occipito-temporo-hippocampal pathway in adult macaque monkeys. 1999 J Comp Neurol;408(3):378–398.

[180] Osada T, Adachi Y, Kimura HM, Miyashita Y. Towards understanding of the cortical network underlying associative memory. 2008 Philos Trans R Soc Lond B Biol Sci;363(1500):2187–2199.

[181] Chen ZY, Patel PD, Sant G, Meng CX, Teng KK, Hempstead BL, et al. Variant brain-derived neurotrophic factor (BDNF) (Met66) alters the intracellular trafficking and activity-dependent secretion of wild-type BDNF in neurosecretory cells and cortical neurons. 2004 J Neurosci;24(18):4401–4411.

[182] Dennis NA, Cabeza R, Need AC, Waters-Metenier S, Goldstein DB, LaBar KS. Brain-derived neurotrophic factor val66met polymorphism and hippocampal activation during episodic encoding and retrieval tasks. 2011 Hippocampus;21(9):980–989.

[183] Egan MF, Kojima M, Callicott JH, Goldberg TE, Kolachana BS, Bertolino A, et al. The BDNF val66met polymorphism affects activity-dependent secretion of BDNF and human memory and hippocampal function. 2003 Cell;112(2):257–269.

[184] Hariri AR, Goldberg TE, Mattay VS, Kolachana BS, Callicott JH, Egan MF, et al. Brain-derived neurotrophic factor val66met polymorphism affects human memory-related hippocampal activity and predicts memory performance. 2003 J Neurosci;23(17):6690–6694.

[185] McAllister TW, Tyler AL, Flashman LA, Rhodes CH, McDonald BC, Saykin AJ, et al. Polymorphisms in the brain-derived neurotrophic factor gene influence memory and processing speed one month after brain injury. 2012 J Neurotrauma;29(6):1111–1118.

[186] Miyajima F, Ollier W, Mayes A, Jackson A, Thacker N, Rabbitt P, et al. Brain-derived neurotrophic factor polymorphism Val66Met influences cognitive abilities in the elderly. 2008 Genes Brain Behav;7(4):411–417.

[187] Voineskos AN, Lerch JP, Felsky D, Shaikh S, Rajji TK, Miranda D, et al. The brain-derived neurotrophic factor Val66Met polymorphism and prediction of neural risk for Alzheimer disease. 2011 Arch Gen Psychiatry;68(2):198–206.

[188] Pezawas L, Verchinski BA, Mattay VS, Callicott JH, Kolachana BS, Straub RE, et al. The brain-derived neurotrophic factor val66met polymorphism and variation in human cortical morphology. 2004 J Neurosci;24(45):10099–10102.

[189] Cheeran B, Talelli P, Mori F, Koch G, Suppa A, Edwards M, et al. A common polymorphism in the brain-derived neurotrophic factor gene (BDNF) modulates human cortical plasticity and the response to rTMS. 2008 J Physiol;586(Pt 23):5717–5725.

[190] Vandenberghe R, Nelissen N, Salmon E, Ivanoiu A, Hasselbalch S, Andersen A, et al. Binary classification of 18F-flutemetamol PET using machine learning: comparison with visual reads and structural MRI. 2013 Neuroimage;64:517–525.

[191] Tzourio-Mazoyer N, Landeau B, Papathanassiou D, Crivello F, Etard O, Delcroix N, et al. Automated anatomical labeling of activations in SPM using a macroscopic anatomical parcellation of the MNI MRI single-subject brain. 2002 Neuroimage;15(1):273–289.

[192] Thöni H. Testing the difference between two coefficients of correlation. 1977 Biometrical Journal;19(5):355–359.

[193] Fleisher AS, Chen K, Liu X, Roontiva A, Thiyyagura P, Ayutyanont N, et al. Using positron emission tomography and florbetapir F18 to image cortical amyloid in patients with mild cognitive impairment or dementia due to Alzheimer disease. 2011 Arch Neurol;68(11):1404–1411.

[194] Buckner RL, Sepulcre J, Talukdar T, Krienen FM, Liu H, Hedden T, et al. Cortical hubs revealed by intrinsic functional connectivity: mapping, assessment of stability, and relation to Alzheimer's disease. 2009 J Neurosci;29(6):1860–1873.

[195] Mormino EC, Smiljic A, Hayenga AO, Onami SH, Greicius MD, Rabinovici GD, et al. Relationships between beta-amyloid and functional

connectivity in different components of the default mode network in aging. 2011 Cereb Cortex;21(10):2399–2407.

[196] Mesulam MM, Van Hoesen GW, Pandya DN, Geschwind N. Limbic and sensory connections of the inferior parietal lobule (area PG) in the rhesus monkey: a study with a new method for horseradish peroxidase histochemistry. 1977 Brain Res;136(3):393–414.

[197] Seltzer B, Pandya DN. Parietal, temporal, and occipital projections to cortex of the superior temporal sulcus in the rhesus monkey: a retrograde tracer study. 1994 J Comp Neurol;343(3):445–463.

[198] Chételat G, Villemagne VL, Bourgeat P, Pike KE, Jones G, Ames D, et al. Relationship between atrophy and beta-amyloid deposition in Alzheimer disease. 2010 Ann Neurol;67(3):317–324.

[199] Chételat G, Villemagne VL, Pike KE, Ellis KA, Bourgeat P, Jones G, et al. Independent contribution of temporal beta-amyloid deposition to memory decline in the pre-dementia phase of Alzheimer's disease. 2011 Brain;134(Pt 3):798–807.

[200] Herholz K, Salmon E, Perani D, Baron JC, Holthoff V, Frölich L, et al. Discrimination between Alzheimer dementia and controls by automated analysis of multicenter FDG PET. 2002 Neuroimage;17(1):302–316.

[201] Mormino EC, Kluth JT, Madison CM, Rabinovici GD, Baker SL, Miller BL, et al. Episodic memory loss is related to hippocampal-mediated beta-amyloid deposition in elderly subjects. 2009 Brain;132(Pt 5):1310–1323.

[202] Rentz DM, Locascio JJ, Becker JA, Moran EK, Eng E, Buckner RL, et al. Cognition, reserve, and amyloid deposition in normal aging. 2010 Ann Neurol;67(3):353–364.

[203] Resnick SM, Sojkova J, Zhou Y, An Y, Ye W, Holt DP, et al. Longitudinal cognitive decline is associated with fibrillar amyloid-beta measured by [11C]PiB. 2010 Neurology;74(10):807–815.

[204] Bueller JA, Aftab M, Sen S, Gomez-Hassan D, Burmeister M, Zubieta JK. BDNF Val66Met allele is associated with reduced hippocampal volume in healthy subjects. 2006 Biol Psychiatry;59(9):812–815.

[205] Hajek T, Kopecek M, Höschl C. Reduced hippocampal volumes in healthy carriers of brain-derived neurotrophic factor Val66Met polymorphism: meta-analysis. 2012 World J Biol Psychiatry;13(3):178–187.

[206] Szeszko PR, Lipsky R, Mentschel C, Robinson D, Gunduz-Bruce H, Sevy S, et al. Brain-derived neurotrophic factor val66met polymorphism and volume of the hippocampal formation. 2005 Mol Psychiatry;10(7):631–636.

[207] Nemoto K, Ohnishi T, Mori T, Moriguchi Y, Hashimoto R, Asada T, et al. The Val66Met polymorphism of the brain-derived neurotrophic factor gene affects age-related brain morphology. 2006 Neurosci Lett;397(1-2):25–29.

[208] Yang X, Liu P, Sun J, Wang G, Zeng F, Yuan K, et al. Impact of brain-derived neurotrophic factor Val66Met polymorphism on cortical thickness and voxel-based morphometry in healthy Chinese young adults. 2012 PLoS One;7(6):e37777.

[209] Sublette ME, Baca-Garcia E, Parsey RV, Oquendo MA, Rodrigues SM, Galfalvy H, et al. Effect of BDNF val66met polymorphism on age-related amygdala volume changes in healthy subjects. 2008 Prog Neuropsychopharmacol Biol Psychiatry;32(7):1652–1655.

[210] Montag C, Weber B, Fliessbach K, Elger C, Reuter M. The BDNF Val66Met polymorphism impacts parahippocampal and amygdala volume in healthy humans: incremental support for a genetic risk factor for depression. 2009 Psychol Med;39(11):1831–1839.

[211] Chiang MC, Avedissian C, Barysheva M, Toga AW, McMahon KL, de Zubicaray GI, et al. Extending genetic linkage analysis to diffusion tensor images to map single gene effects on brain fiber architecture. 2009 Med Image Comput Comput Assist Interv;12(Pt 2):506–513.

[212] Xu C, Wang Z, Fan M, Liu B, Song M, Zhen X, et al. Effects of BDNF Val66Met polymorphism on brain metabolism in Alzheimer's disease. 2010 Neuroreport;21(12):802–807.

[213] Huang R, Huang J, Cathcart H, Smith S, Poduslo SE. Genetic variants in brain-derived neurotrophic factor associated with Alzheimer's disease. 2007 J Med Genet;44(2):e66.

[214] Cordell HJ. Detecting gene-gene interactions that underlie human diseases. 2009 Nat Rev Genet;10(6):392–404.

[215] Christensen R, Marcussen AB, Wörtwein G, Knudsen GM, Aznar S. Abeta(1-42) injection causes memory impairment, lowered cortical and serum BDNF levels, and decreased hippocampal 5-HT(2A) levels. 2008 Exp Neurol;210(1):164–171.

[216] Nagahara AH, Merrill DA, Coppola G, Tsukada S, Schroeder BE, Shaked GM, et al. Neuroprotective effects of brain-derived neurotrophic factor in rodent and primate models of Alzheimer's disease. 2009 Nat Med;15(3):331–337.

[217] Connor B, Young D, Yan Q, Faull RL, Synek B, Dragunow M. Brain-derived neurotrophic factor is reduced in Alzheimer's disease. 1997 Brain Res Mol Brain Res;49(1-2):71–81.

[218] Ferrer I, Marín C, Rey MJ, Ribalta T, Goutan E, Blanco R, et al. BDNF and full-length and truncated TrkB expression in Alzheimer disease. Implications in therapeutic strategies. 1999 J Neuropathol Exp Neurol;58(7):729–739.

[219] Hock C, Heese K, Hulette C, Rosenberg C, Otten U. Region-specific neurotrophin imbalances in Alzheimer disease: decreased levels of brain-derived neurotrophic factor and increased levels of nerve growth factor in hippocampus and cortical areas. 2000 Arch Neurol;57(6):846–851.

[220] Holsinger RM, Schnarr J, Henry P, Castelo VT, Fahnestock M. Quantitation of BDNF mRNA in human parietal cortex by competitive reverse transcription-polymerase chain reaction: decreased levels in Alzheimer's disease. 2000 Brain Res Mol Brain Res;76(2):347–354.

[221] Phillips HS, Hains JM, Armanini M, Laramee GR, Johnson SA, Winslow JW. BDNF mRNA is decreased in the hippocampus of individuals with Alzheimer's disease. 1991 Neuron;7(5):695–702.

[222] Laske C, Stransky E, Leyhe T, Eschweiler GW, Wittorf A, Richartz E, et al. Stage-dependent BDNF serum concentrations in Alzheimer's disease. 2006 J Neural Transm;113(9):1217–1224.

[223] Erickson KI, Prakash RS, Voss MW, Chaddock L, Heo S, McLaren M, et al. Brain-derived neurotrophic factor is associated with age-related decline in hippocampal volume. 2010 J Neurosci;30(15):5368–5375.

[224] Clark CM, Schneider JA, Bedell BJ, Beach TG, Bilker WB, Mintun MA, et al. Use of florbetapir-PET for imaging beta-amyloid pathology. 2011 JAMA;305(3):275–283.

[225] Herholz K, Ebmeier K. Clinical amyloid imaging in Alzheimer's disease. 2011 Lancet Neurol;10(7):667–670.

[226] Clark CM, Pontecorvo MJ, Beach TG, Bedell BJ, Coleman RE, Doraiswamy PM, et al. Cerebral PET with florbetapir compared with neuropathology at autopsy for detection of neuritic amyloid-β plaques: a prospective cohort study. 2012 Lancet Neurol;11(8):669–678.

[227] Morris JC, Roe CM, Grant EA, Head D, Storandt M, Goate AM, et al. Pittsburgh compound B imaging and prediction of progression from cognitive normality to symptomatic Alzheimer disease. 2009 Arch Neurol;66(12):1469–1475.

[228] Hatashita S, Yamasaki H, Suzuki Y, Tanaka K, Wakebe D, Hayakawa H. [18F]Flutemetamol amyloid-beta PET imaging compared with [11C]PIB across the spectrum of Alzheimer's disease. 2014 Eur J Nucl Med Mol Imaging;41(2):290–300.

[229] Thurfjell L, Lilja J, Lundqvist R, Buckley C, Smith A, Vandenberghe R, et al. Automated quantification of 18F-flutemetamol PET activity for categorizing scans as negative or positive for brain amyloid: concordance with visual image reads. 2014 J Nucl Med;55(10):1623–1628.

[230] Bayles KA, Tomoeda CK. Confrontation naming impairment in dementia. 1983 Brain Lang;19(1):98–114.

[231] Huff FJ, Corkin S, Growdon JH. Semantic impairment and anomia in Alzheimer's disease. 1986 Brain Lang;28(2):235–249.

[232] Chertkow H, Bub D. Semantic memory loss in dementia of Alzheimer's type. What do various measures measure? 1990 Brain;113:397–417.

[233] Apostolova LG, Lu P, Rogers S, Dutton RA, Hayashi KM, Toga AW, et al. 3D mapping of language networks in clinical and pre-clinical Alzheimer's disease. 2008 Brain Lang;104(1):33–41.

[234] Clark LJ, Gatz M, Zheng L, Chen YL, McCleary C, Mack WJ. Longitudinal verbal fluency in normal aging, preclinical, and prevalent Alzheimer's disease. 2009 Am J Alzheimers Dis Other Demen;24(6):461–468.

[235] Sugarman MA, Woodard JL, Nielson KA, Seidenberg M, Smith JC, Durgerian S, et al. Functional magnetic resonance imaging of semantic memory as a presymptomatic biomarker of Alzheimer's disease risk. 2012 Biochim Biophys Acta;1822(3):442–456.

[236] Troncoso JC, Martin LJ, Dal Forno G, Kawas CH. Neuropathology in controls and demented subjects from the Baltimore Longitudinal Study of Aging. 1996 Neurobiol Aging;17(3):365–371.

[237] Driscoll I, Resnick SM, Troncoso JC, An Y, O'Brien R, Zonderman AB. Impact of Alzheimer's pathology on cognitive trajectories in nondemented elderly. 2006 Ann Neurol;60(6):688–695.

[238] Hyman BT, Kromer LJ, Van Hoesen GW. Reinnervation of the hippocampal perforant pathway zone in Alzheimer's disease. 1987 Ann Neurol;21(3):259–267.

[239] Nathan BP, Bellosta S, Sanan DA, Weisgraber KH, Mahley RW, Pitas RE. Differential effects of apolipoproteins E3 and E4 on neuronal growth in vitro. 1994 Science;264(5160):850–852.

[240] Becker JT, Mintun MA, Aleva K, Wiseman MB, Nichols T, DeKosky ST. Compensatory reallocation of brain resources supporting verbal episodic memory in Alzheimer's disease. 1996 Neurology;46(3):692–700.

[241] Arendt T, Schindler C, Brückner MK, Eschrich K, Bigl V, Zedlick D, et al. Plastic neuronal remodeling is impaired in patients with Alzheimer's disease carrying apolipoprotein epsilon 4 allele. 1997 J Neurosci;17(2):516–529.

[242] Saykin AJ, Flashman LA, Frutiger SA, Johnson SC, Mamourian AC, Moritz CH, et al. Neuroanatomic substrates of semantic memory impairment in Alzheimer's disease: patterns of functional MRI activation. 1999 J Int Neuropsychol Soc;5(5):377–392.

[243] Grady CL, Furey ML, Pietrini P, Horwitz B, Rapoport SI. Altered brain functional connectivity and impaired short-term memory in Alzheimer's disease. 2001 Brain;124(Pt 4):739–756.

[244] Adamczuk K, De Weer AS, Nelissen N, Chen K, Sleegers K, Bettens K, et al. Polymorphism of Brain Derived Neurotrophic Factor influences β amyloid load in cognitively intact Apolipoprotein E $\varepsilon 4$ carriers. 2013 Neuroimage Clin;2:512–520.

[245] Snodgrass JG, Vanderwart M. A standardized set of 260 pictures: norms for name agreement, image agreement, familiarity, and visual complexity. 1980 J Exp Psychol Hum Learn;6(2):174–215.

[246] Pallier C. Computing discriminability and bias with the R software. 2002 URL http://wwwpallierorg/ressources/aprime/aprime.pdf.

[247] Verhaeghen P, Vandenbroucke A, Dierckx V. Growing slower and less accurate: adult age differences in time-accuracy functions for recall and recognition from episodic memory. 1998 Exp Aging Res;24(1):3–19.

[248] Vandenberghe R, Price C, Wise R, Josephs O, Frackowiak RS. Functional anatomy of a common semantic system for words and pictures. 1996 Nature;383(6597):254–256.

[249] Vandenbulcke M, Peeters R, Van Hecke P, Vandenberghe R. Anterior temporal laterality in primary progressive aphasia shifts to the right. 2005 Ann Neurol;58(3):362–370.

[250] Vandenbulcke M, Peeters R, Fannes K, Vandenberghe R. Knowledge of visual attributes in the right hemisphere. 2006 Nat Neurosci;9(7):964–970.

[251] Nelissen N, Dupont P, Vandenbulcke M, Tousseyn T, Peeters R, Vandenberghe R. Right hemisphere recruitment during language processing in frontotemporal lobar degeneration and Alzheimer's disease. 2011 J Mol Neurosci;45(3):637–647.

[252] Vandenberghe R, Wang Y, Nelissen N, Vandenbulcke M, Dhollander T, Sunaert S, et al. The associative-semantic network for words and pictures: effective connectivity and graph analysis. 2013 Brain Lang;127(2):264–272.

[253] Casanova R, Srikanth R, Baer A, Laurienti PJ, Burdette JH, Hayasaka S, et al. Biological parametric mapping: A statistical toolbox for multimodality brain image analysis. 2007 Neuroimage;34(1):137–143.

[254] Ricci PT, Zelkowicz BJ, Nebes RD, Meltzer CC, Mintun MA, Becker JT. Functional neuroanatomy of semantic memory: recognition of semantic associations. 1999 Neuroimage;9(1):88–96.

[255] Cabeza R. Hemispheric asymmetry reduction in older adults: the HAROLD model. 2002 Psychol Aging;17(1):85–100.

[256] Cabeza R, Nyberg L, Park DC. Cognitive Neuroscience of Aging. Oxford University Press; 2005.

[257] Small SA, Perera GM, DeLaPaz R, Mayeux R, Stern Y. Differential regional dysfunction of the hippocampal formation among elderly with memory decline and Alzheimer's disease. 1999 Ann Neurol;45(4):466–472.

[258] Machulda MM, Ward HA, Borowski B, Gunter JL, Cha RH, O'Brien PC, et al. Comparison of memory fMRI response among normal, MCI, and Alzheimer's patients. 2003 Neurology;61(4):500–506.

[259] Sperling RA, Bates JF, Chua EF, Cocchiarella AJ, Rentz DM, Rosen BR, et al. fMRI studies of associative encoding in young and elderly controls and mild Alzheimer's disease. 2003 J Neurol Neurosurg Psychiatry;74(1):44–50.

[260] Golby A, Silverberg G, Race E, Gabrieli S, O'Shea J, Knierim K, et al. Memory encoding in Alzheimer's disease: an fMRI study of explicit and implicit memory. 2005 Brain;128(Pt 4):773–787.

[261] Sperling R. Functional MRI studies of associative encoding in normal aging, mild cognitive impairment, and Alzheimer's disease. 2007 Ann N Y Acad Sci;1097:146–155.

[262] Johnson SC, Schmitz TW, Moritz CH, Meyerand ME, Rowley HA, Alexander AL, et al. Activation of brain regions vulnerable to Alzheimer's disease: the effect of mild cognitive impairment. 2006 Neurobiol Aging;27(11):1604–1612.

[263] Dickerson BC, Salat DH, Greve DN, Chua EF, Rand-Giovannetti E, Rentz DM, et al. Increased hippocampal activation in mild cognitive impairment compared to normal aging and AD. 2005 Neurology;65(3):404–411.

[264] Johnson SC, Schmitz TW, Trivedi MA, Ries ML, Torgerson BM, Carlsson CM, et al. The influence of Alzheimer disease family history and apolipoprotein E epsilon4 on mesial temporal lobe activation. 2006 J Neurosci;26(22):6069–6076.

[265] Mondadori CRA, Buchmann A, Mustovic H, Schmidt CF, Boesiger P, Nitsch RM, et al. Enhanced brain activity may precede the diagnosis of Alzheimer's disease by 30 years. 2006 Brain;129(Pt 11):2908–2922.

[266] Reiman EM, Quiroz YT, Fleisher AS, Chen K, Velez-Pardo C, Jimenez-Del-Rio M, et al. Brain imaging and fluid biomarker analysis in young adults at genetic risk for autosomal dominant Alzheimer's disease in the presenilin 1 E280A kindred: a case-control study. 2012 Lancet Neurol;11(12):1048–1056.

[267] Fleisher AS, Houston WS, Eyler LT, Frye S, Jenkins C, Thal LJ, et al. Identification of Alzheimer disease risk by functional magnetic resonance imaging. 2005 Arch Neurol;62(12):1881–1888.

[268] Grady CL, McIntosh AR, Beig S, Keightley ML, Burian H, Black SE. Evidence from functional neuroimaging of a compensatory prefrontal network in Alzheimer's disease. 2003 J Neurosci;23(3):986–993.

[269] Binder JR, Frost JA, Hammeke TA, Bellgowan PS, Springer JA, Kaufman JN, et al. Human temporal lobe activation by speech and nonspeech sounds. 2000 Cereb Cortex;10(5):512–528.

[270] Price CJ, Mechelli A. Reading and reading disturbance. 2005 Curr Opin Neurobiol;15(2):231–238.

[271] Buckner RL, Snyder AZ, Shannon BJ, LaRossa G, Sachs R, Fotenos AF, et al. Molecular, structural, and functional characterization of Alzheimer's disease: evidence for a relationship between default activity, amyloid, and memory. 2005 J Neurosci;25(34):7709–7717.

[272] Whitney C, Kirk M, O'Sullivan J, Lambon Ralph MA, Jefferies E. The neural organization of semantic control: TMS evidence for a distributed network in left inferior frontal and posterior middle temporal gyrus. 2011 Cereb Cortex;21(5):1066–1075.

[273] Whitney C, Kirk M, O'Sullivan J, Lambon Ralph MA, Jefferies E. Executive semantic processing is underpinned by a large-scale neural network: revealing the contribution of left prefrontal, posterior temporal, and parietal cortex to controlled retrieval and selection using TMS. 2012 J Cogn Neurosci;24(1):133–147.

[274] Lehtovirta M, Soininen H, Helisalmi S, Mannermaa A, Helkala EL, Hartikainen P, et al. Clinical and neuropsychological characteristics in familial and sporadic Alzheimer's disease: relation to apolipoprotein E polymorphism. 1996 Neurology;46(2):413–419.

[275] Rasmusson DX, Dal Forno G, Brandt J, Warren AC, Troncoso J, Lyketsos C. Apo-E genotype and verbal deficits in Alzheimer's disease. 1996 J Neuropsychiatry Clin Neurosci;8(3):335–337.

[276] Mendez MF. Early-onset Alzheimer's disease: nonamnestic subtypes and type 2 AD. 2012 Arch Med Res;43(8):677–685.

[277] Mez J, Cosentino S, Brickman AM, Huey ED, Mayeux R. Different demographic, genetic, and longitudinal traits in language versus memory Alzheimer's subgroups. 2013 J Alzheimers Dis;37(1):137–146.

[278] Woodard JL, Seidenberg M, Nielson KA, Antuono P, Guidotti L, Durgerian S, et al. Semantic memory activation in amnestic mild cognitive impairment. 2009 Brain;132(Pt 8):2068–2078.

[279] Freundlieb N, Philipp S, Schneider SA, Brüggemann N, Klein C, Gerloff C, et al. No association of the BDNF val66met polymorphism with implicit associative vocabulary and motor learning. 2012 PLoS One;7(11):e48327.

[280] Simmons TR, Flax JF, Azaro MA, Hayter JE, Justice LM, Petrill SA, et al. Increasing genotype-phenotype model determinism: application to bivariate reading/language traits and epistatic interactions in language-impaired families. 2010 Hum Hered;70(4):232–244.

[281] Li N, Bartlett CW. Defining the genetic architecture of human developmental language impairment. 2012 Life Sci;90(13-14):469–475.

[282] Kebir O, Mouaffak F, Chayet M, Leroy S, Tordjman S, Amado I, et al. Semantic but not phonological verbal fluency associated with BDNF Val66Met polymorphism in schizophrenia. 2009 Am J Med Genet B Neuropsychiatr Genet;150B(3):441–442.

[283] Jagust WJ. Amyloid imaging: coming to a PET scanner near you. 2010 Ann Neurol;68(3):277–278.

[284] Adamczuk K, De Weer AS, Nelissen N, Dupont P, Sunaert S, Bettens K, et al. Functional Changes in the Language Network in Response to Increased Amyloid β Deposition in Cognitively Intact Older Adults. 2014 Cereb Cortex; doi:10.1093/cercor/bhu286.

[285] Ahmad R, Goffin K, Van den Stock J, De Winter FL, Cleeren E, Bormans G, et al. In vivo type 1 cannabinoid receptor availability in Alzheimer's disease. 2014 Eur Neuropsychopharmacol;24(2):242–250.

[286] Bland JM, Altman DG. Statistical methods for assessing agreement between two methods of clinical measurement. 1986 Lancet;1(8476):307–310.

[287] Villemagne VL, Burnham S, Bourgeat P, Brown B, Ellis KA, Salvado O, et al. Amyloid β deposition, neurodegeneration, and cognitive decline in sporadic Alzheimer's disease: a prospective cohort study. 2013 Lancet Neurol;12(4):357–367.

[288] Klunk WE, Koeppe RA, Price JC, Benzinger TL, Devous MD Sr, Jagust WJ, et al. The Centiloid Project: standardizing quantitative amyloid plaque estimation by PET. 2015 Alzheimers Dement;11(1):1–15.e1–4.

[289] Wiltfang J, Esselmann H, Bibl M, Hüll M, Hampel H, Kessler H, et al. Amyloid beta peptide ratio 42/40 but not A beta 42 correlates with phospho-Tau in patients with low- and high-CSF A beta 40 load. 2007 J Neurochem;101(4):1053–1059.

[290] Roher AE, Cribbs DH, Kim RC, Maarouf CL, Whiteside CM, Kokjohn TA, et al. Bapineuzumab alters aβ composition: implications for the amyloid cascade hypothesis and anti-amyloid immunotherapy. 2013 PLoS One;8(3):e59735.

[291] Roher AE, Maarouf CL, Kokjohn TA, Whiteside CM, Kalback WM, Serrano G, et al. Neuropathological and biochemical assessments of an Alzheimer's disease patient treated with the γ-secretase inhibitor semagacestat. 2014 Am J Neurodegener Dis;3(3):115–133.

[292] Jeppsson A, Zetterberg H, Blennow K, Wikkelsø C. Idiopathic normal-pressure hydrocephalus: pathophysiology and diagnosis by CSF biomarkers. 2013 Neurology;80(15):1385–1392.

[293] Verbeek MM, Kremer BPH, Rikkert MO, Van Domburg PHMF, Skehan ME, Greenberg SM. Cerebrospinal fluid amyloid beta(40) is decreased in cerebral amyloid angiopathy. 2009 Ann Neurol;66(2):245–249.

[294] Bibl M, Gallus M, Welge V, Esselmann H, Wolf S, Rüther E, et al. Cerebrospinal fluid amyloid-β 2-42 is decreased in Alzheimer's, but not in frontotemporal dementia. 2012 J Neural Transm;119(7):805–813.

[295] Mulugeta E, Londos E, Ballard C, Alves G, Zetterberg H, Blennow K, et al. CSF amyloid β38 as a novel diagnostic marker for dementia with Lewy bodies. 2011 J Neurol Neurosurg Psychiatry;82(2):160–164.

[296] Hansson O, Zetterberg H, Buchhave P, Andreasson U, Londos E, Minthon L, et al. Prediction of Alzheimer's disease using the CSF Abeta42/Abeta40 ratio in patients with mild cognitive impairment. 2007 Dement Geriatr Cogn Disord;23(5):316–320.

[297] Vemuri P, Whitwell JL, Kantarci K, Josephs KA, Parisi JE, Shiung MS, et al. Antemortem MRI based STructural Abnormality iNDex (STAND)-scores correlate with postmortem Braak neurofibrillary tangle stage. 2008 Neuroimage;42(2):559–567.

[298] Lundqvist R, Lilja J, Thomas BA, Lötjönen J, Villemagne VL, Rowe CC, et al. Implementation and validation of an adaptive template registration method for 18F-flutemetamol imaging data. 2013 J Nucl Med;54(8):1472–1478.

[299] Mirra SS, Heyman A, McKeel D, Sumi SM, Crain BJ, Brownlee LM, et al. The Consortium to Establish a Registry for Alzheimer's Disease (CERAD). Part II. Standardization of the neuropathologic assessment of Alzheimer's disease. 1991 Neurology;41(4):479–486.

[300] Sutphen CL, Jasielec MS, Shah AR, Macy EM, Xiong C, Vlassenko AG, et al. Longitudinal Cerebrospinal Fluid Biomarker Changes in Preclinical Alzheimer Disease During Middle Age. 2015 JAMA Neurol; doi:10.1001/jamaneurol.2015.1285.

[301] DeLong ER, DeLong DM, Clarke-Pearson DL. Comparing the areas under two or more correlated receiver operating characteristic curves: a nonparametric approach. 1988 Biometrics;44(3):837–845.

[302] Schoonenboom NS, Mulder C, Van Kamp GJ, Mehta SP, Scheltens P, Blankenstein MA, et al. Amyloid beta 38, 40, and 42 species in cerebrospinal fluid: more of the same? 2005 Ann Neurol;58(1):139–142.

[303] Slaets S, Le Bastard N, Martin JJ, Sleegers K, Van Broeckhoven C, De Deyn PP, et al. Cerebrospinal fluid Aβ1-40 improves differential dementia diagnosis in patients with intermediate P-tau181P levels. 2013 J Alzheimers Dis;36(4):759–767.

[304] Lewczuk P, Lelental N, Spitzer P, Maler JM, Kornhuber J. Amyloid-β 42/40 cerebrospinal fluid concentration ratio in the diagnostics of Alzheimer's disease: validation of two novel assays. 2015 J Alzheimers Dis;43(1):183–191.

[305] Mehta PD, Pirttila T. Increased cerebrospinal fluid A beta38/A beta42 ratio in Alzheimer disease. 2005 Neurodegener Dis;2(5):242–245.

[306] Welge V, Fiege O, Lewczuk P, Mollenhauer B, Esselmann H, Klafki HW, et al. Combined CSF tau, p-tau181 and amyloid-beta 38/40/42 for diagnosing Alzheimer's disease. 2009 J Neural Transm;116(2):203–212.

[307] Spies PE, Slats D, Sjögren JMC, Kremer BPH, Verhey FRJ, Rikkert MGMO, et al. The cerebrospinal fluid amyloid beta42/40 ratio in the differentiation of Alzheimer's disease from non-Alzheimer's dementia. 2010 Curr Alzheimer Res;7(5):470–476.

[308] Theuns J, Marjaux E, Vandenbulcke M, Van Laere K, Kumar-Singh S, Bormans G, et al. Alzheimer dementia caused by a novel mutation located in the APP C-terminal intracytosolic fragment. 2006 Hum Mutat;27(9):888–896.

[309] Zhou L, Brouwers N, Benilova I, Vandersteen A, Mercken M, Van Laere K, et al. Amyloid precursor protein mutation E682K at the alternative β-secretase cleavage β'-site increases Aβ generation. 2011 EMBO Mol Med;3(5):291–302.

[310] Vandenberghe R. The relationship between amyloid deposition, neurodegeneration, and cognitive decline in dementia. 2014 Curr Neurol Neurosci Rep;14(11):498.

[311] Sperling R, Mormino E, Johnson K. The evolution of preclinical Alzheimer's disease: implications for prevention trials. 2014 Neuron;84(3):608–622.

[312] Jack CR Jr, Wiste HJ, Weigand SD, Rocca WA, Knopman DS, Mielke MM, et al. Age-specific population frequencies of cerebral β-amyloidosis and neurodegeneration among people with normal cognitive function aged 50-89 years: a cross-sectional study. 2014 Lancet Neurol;13(10):997–1005.

[313] Middleton LE, Grinberg LT, Miller B, Kawas C, Yaffe K. Neuropathologic features associated with Alzheimer disease diagnosis: age matters. 2011 Neurology;77(19):1737–1744.

[314] Landau SM, Thomas BA, Thurfjell L, Schmidt M, Margolin R, Mintun M, et al. Amyloid PET imaging in Alzheimer's disease: a comparison of three radiotracers. 2014 Eur J Nucl Med Mol Imaging;41(7):1398–1407.

[315] Villain N, Chételat G, Grassiot B, Bourgeat P, Jones G, Ellis KA, et al. Regional dynamics of amyloid-β deposition in healthy elderly, mild cognitive impairment and Alzheimer's disease: a voxelwise PiB-PET longitudinal study. 2012 Brain;135(Pt 7):2126–2139.

[316] Thal DR, Beach TG, Zanette M, Heurling K, Chakrabarty A, Ismail A, et al. [(18)F]flutemetamol amyloid positron emission tomography in preclinical and symptomatic Alzheimer's disease: Specific detection of advanced phases of amyloid-β pathology. 2015 Alzheimers Dement;11(8):975–985.

[317] Thal DR, Walter J, Saido TC, Fändrich M. Neuropathology and biochemistry of Aβ and its aggregates in Alzheimer's disease. 2015 Acta Neuropathol;129(2):167–182.

[318] Bateman RJ, Munsell LY, Morris JC, Swarm R, Yarasheski KE, Holtzman DM. Human amyloid-beta synthesis and clearance rates as measured in cerebrospinal fluid in vivo. 2006 Nat Med;12(7):856–861.

[319] Mawuenyega KG, Sigurdson W, Ovod V, Munsell L, Kasten T, Morris JC, et al. Decreased clearance of CNS beta-amyloid in Alzheimer's disease. 2010 Science;330(6012):1774.

[320] Potter R, Patterson BW, Elbert DL, Ovod V, Kasten T, Sigurdson W, et al. Increased in vivo amyloid-β42 production, exchange, and loss in presenilin mutation carriers. 2013 Sci Transl Med;5(189):189ra77.

[321] Mormino EC, Betensky RA, Hedden T, Schultz AP, Amariglio RE, Rentz DM, et al. Synergistic effect of β-amyloid and neurodegeneration on cognitive decline in clinically normal individuals. 2014 JAMA Neurol;71(11):1379–1385.

[322] Lim YY, Villemagne VL, Laws SM, Pietrzak RH, Snyder PJ, Ames D, et al. APOE and BDNF polymorphisms moderate amyloid β-related cognitive decline in preclinical Alzheimer's disease. 2014 Mol Psychiatry; doi:10.1038/mp.2014.

[323] Mesulam MM. Principles of Behavioral and Cognitive Neurology. Chapter: Plasticity Failure - A Hypothesis for Unifying the Pathogenesis of Plaques and Tangles. Mesulam MM, editor. Oxford University Press; 2000.

[324] Sen A, Nelson TJ, Alkon DL. ApoE4 and Aβ Oligomers Reduce BDNF Expression via HDAC Nuclear Translocation. 2015 J Neurosci;35(19):7538–7551.

[325] Rohe M, Synowitz M, Glass R, Paul SM, Nykjaer A, Willnow TE. Brain-derived neurotrophic factor reduces amyloidogenic processing through control of SORLA gene expression. 2009 J Neurosci;29(49):15472–15478.

[326] Yajima R, Tokutake T, Koyama A, Kasuga K, Tezuka T, Nishizawa M, et al. ApoE-isoform-dependent cellular uptake of amyloid-β is mediated by lipoprotein receptor LR11/SorLA. 2015 Biochem Biophys Res Commun;456(1):482–488.

[327] Liu DS, Pan XD, Zhang J, Shen H, Collins NC, Cole AM, et al. APOE4 enhances age-dependent decline in cognitive function by down-regulating an NMDA receptor pathway in EFAD-Tg mice. 2015 Mol Neurodegener;10(1):7.

[328] Honea RA, Cruchaga C, Perea RD, Saykin AJ, Burns JM, Weinberger DR, et al. Characterizing the role of brain derived neurotrophic factor genetic variation in Alzheimer's disease neurodegeneration. 2013 PLoS One;8(9):e76001.

[329] Lin Y, Cheng S, Xie Z, Zhang D. Association of rs6265 and rs2030324 polymorphisms in brain-derived neurotrophic factor gene with Alzheimer's disease: a meta-analysis. 2014 PLoS One;9(4):e94961.

[330] Ji H, Dai D, Wang Y, Jiang D, Zhou X, Lin P, et al. Association of BDNF and BCHE with Alzheimer's disease: Meta-analysis based on 56 genetic case-control studies of 12,563 cases and 12,622 controls. 2015 Exp Ther Med;9(5):1831–1840.

[331] Laske C, Stellos K, Hoffmann N, Stransky E, Straten G, Eschweiler GW, et al. Higher BDNF serum levels predict slower cognitive decline in Alzheimer's disease patients. 2011 Int J Neuropsychopharmacol;14(3):399–404.

[332] Hwang KS, Lazaris AS, Eastman JA, Teng E, Thompson PM, Gylys KH, et al. Plasma BDNF levels associate with Pittsburgh compound B binding in the brain. 2015 Alzheimers Dement (Amst);1(2):187–193.

[333] Sabri O, Sabbagh MN, Seibyl J, Barthel H, Akatsu H, Ouchi Y, et al. Florbetaben PET imaging to detect amyloid beta plaques in Alzheimer disease: Phase 3 study. 2015 Alzheimers Dement;11(8):964–974.

[334] Sojkova J, Driscoll I, Iacono D, Zhou Y, Codispoti KE, Kraut MA, et al. In vivo fibrillar beta-amyloid detected using [11C]PiB positron emission tomography and neuropathologic assessment in older adults. 2011 Arch Neurol;68(2):232–240.

[335] Hatsuta H, Takao M, Ishii K, Ishiwata K, Saito Y, Kanemaru K, et al. Amyloid β Accumulation Assessed with 11C-Pittsburgh Compound B PET and Postmortem Neuropathology. 2015 Curr Alzheimer Res;12(3):278–286.

[336] Maddalena A, Papassotiropoulos A, Müller-Tillmanns B, Jung HH, Hegi T, Nitsch RM, et al. Biochemical diagnosis of Alzheimer disease by measuring the cerebrospinal fluid ratio of phosphorylated tau protein to beta-amyloid peptide42. 2003 Arch Neurol;60(9):1202–1206.

[337] Bartlett JW, Frost C, Mattsson N, Skillbäck T, Blennow K, Zetterberg H, et al. Determining cut-points for Alzheimer's disease biomarkers: statistical issues, methods and challenges. 2012 Biomark Med;6(4):391–400.

[338] Mattsson N, Andreasson U, Carrillo MC, Persson S, Shaw LM, Zegers I, et al. Proficiency testing programs for Alzheimer's disease cerebrospinal fluid biomarkers. 2012 Biomark Med;6(4):401–407.

Acknowledgements

"Whatever you do, or dream you can, begin it.
Boldness has genius and power and magic in it."
Johann Wolfgang von Goethe

So, here we are, at the end of this PhD. Work on it was challenging, exciting, stressful and joyful all at once and it was probably one of the best periods of my life. It took a lot of my energy to reach the end of this project, and also a lot of energy from other people to whom I am very grateful. Before I even begin, I would like to thank the volunteers who participated in this study. You were the foundation of this project and without you none of these results would have been found.

First of all, I would like to thank my promoter, Prof. Rik Vandenberghe. Dear Rik, it was an honour, a pleasure, and a challenge working with you. When someone chooses to begin a PhD, two things are most important: the topic of the PhD project (which you must love and be dedicated to) and a promoter (whom you must trust and respect). There are different student-promoter relations. In my view, our combination was perfect. You were always demanding - this brought out the best in me. Always aiming high and pushing for the best results - this gave me adrenaline to stay focused and be efficient. I admire your dedication and motivation for medicine and science. You are a great example how to be an excellent clinician, a critical researcher, a lecturer, and a father, at the same time. I could not imagine a better promoter. Thank you for this PhD journey and the opportunities. I learned a lot from you.

I would like to thank the members of the jury for the participation in the thesis defence and for their time. Prof. William Klunk, Prof. Eric Salmon, Prof. Jos Tournoy, and Prof. Wim Van Paesschen, thank you for your constructive comments on the draft of this thesis manuscript. Prof. Bénédicte Dubois, thank you for chairing the public defence, and Prof. Peter Hoet, thank you for leading the evaluation process of the manuscript.

One person I am especially grateful, Dr. Natalie Nelissen. Natalie, in the last few years you have become a colleague and a close friend. Your critical

scientific insight was invaluable to me. You were always willing to discuss complex analytical matters and my often unusual ideas. Thank you also for all the non-scientific chats, which often turned a bad day into a cheerful one. I think the "weird fish" is what I will remember forever :) You showed me that all you need in science is a sharp mind, motivation, a good sense of humour, and a bit of sarcasm.

Time in the Laboratory for Cognitive Neurology would not be the same without Prof. Patrick Dupont. Patrick, you are the physico-mathematico-philosophico-social core of the lab. Thank you for the "short" meetings, explanations, constructive criticism, and philosophical discussions.

This project would not have been the same either without the best visual readers: Prof. Koen Van Laere, Prof. Mathieu Vandenbulcke, and Prof. Karolien Goffin. Koen, thank you for your critical and rapid comments to the papers and abstracts, and discussions on PET methodological issues, and thanks for always finding a moment for a meeting. Mathieu, thank you for the input to the papers and for explaining me issues in the Memory Clinic from a psychiatric perspective, and also for the opportunity to explore the ECT results. Karolien, thank you for your time and smooth collaboration.

The experts in the laboratory medicine and especially in CSF analysis Prof. Koen Poesen and Dr. Hugo Vanderstichele, thank you and your teams for CSF analysis and the insights on procedural details.

The effort to genotype all candidates included in the study would not have been possible without the laboratory of Prof. An Goris. An, thank you for letting me work in your lab and for the help with data interpretation. Ine, Kelly, and Klara, thank you for the explanation and guidance.

Thanks to the fantastic team of the Neurology and Memory Clinic. Carine Schildermans, you were essential in the screening procedure. In your very busy schedule you always found time to help with the blood sampling and planning. Dorien Timmers and Eva Dries, thank you for all the great job with neuropsychological testing: your unbiased opinion was crucial to the project. I am also most grateful to the Neurology assistants who performed lumbar punctures with high precision.

A big thank you to the people from GE: Danielle De Greef, Paulette Lartategui, Paola Ranson for the smooth product logistics, Johan Lilja and Dr. Lennart Thurfjell for the image analysis and feedback, Dr. Gill Farrar for organizing the collaboration.

Almost 200 PET scans would not have been possible without the Nuclear Medicine team. Kwinten Porters, with your perfect time-managing, scans were always on time even in the busiest days. Mieke Steukers, you managed to put even the most anxious volunteers at ease. Jef Van Loock, you have great examples to follow and I am sure you will soon be as perfect as they are. To my fellow PhD students and postdoc Rawaha, Gil, Sofie, Jenny, and my neighbour Andrej: thanks for the interesting discussions often going well with a cup of

coffee, and thanks to Prof. Michel Koole for the inspiring talks, even at strange hours.

I am grateful to the staff of Radiology, Dr. Ron Peeters for finding solutions for sometimes stubborn fMRI scans and being at the spot in an instant, and to Prof. Stefan Sunaert for your kind feedback on fMRI and DTI.

The strategic power - Olivia Nackaerts, Francine Reniers, Stefanie Geysels, and Bea Weynants: you were always willing to guide me through the sea of administrative procedures, thank you for this.

Thanks to the current and former members of the Laboratory for Cognitive Neurology for the supportive talks and discussions: An-Sofie, we started together, your courage and effectiveness will stay in my mind, Gabriella, you bring the positive spirit to the lab, Jolien, thank you for the great help with the project, I am sure it was a good introduction to your own, Yu, we've made it, Eshwar, Veerle, Maarten, success with your PhD projects, Tatjana, Celine, Rose, good luck in your future careers.

People "next" to the lab, François-Laurent, Laura S, Louise, our chats and emails always made me smile, FL thanks for your black humour, Laura for your optimism, and Louise for "you're a star".

I am also thankful to my best friends, who I met long time ago or just here in Leuven. Thanks to you I see the world from different perspectives. Gosia, znamy się 22 lata. Jesteś dla mnie bardzo ważną osobą, którą podziwiam za determinację i wszechstronność i od której ciągle się uczę. Zawsze mogę polegać na Twoich radach i wsparciu. To szczęście mieć taką przyjaciółkę jak Ty. Maja, my z kolei znamy się od liceum, ale po pierwszych naszych rozmowach miałam wrażenie, że znamy się całe życie. Nie zapomnę naszych długich powrotów do domu i dyskusji przy jabłku i bananie z budki pod KULem. Dziękuję za to, że pokazujesz mi świat z innej - lingwistycznej strony. Natalie Caspari, we met just here in Leuven in our first year of PhD and we departed from the common TMS island. Throughout those years you have become a loyal friend, ready for help at any moment. I admire your dedication to the things you love: science and sports. I hope I can be as great a friend to you as you are to me. Ola i Aleks, wy jesteście siłą napędową życia w Leuven poza pracą. Dzięki wam odkryłam ile odcieni może mieć jedzenie. Dziękuję, za nezliczone wieczory spędzone razem i rozmowy, które zawsze wprowadziły coś nowego w moje życie.

W tym miejscu chciałabym podziękować mojej rodzinie. Mamo, Ty jesteś początkiem wszystkiego. Nauczyłaś mnie żyć, uczyć się, kochać. Nauczyłaś mnie ciekawości do świata i poczucia, że mogę osiągnąć wszystko. Dziękuję Ci za Twój czas i wysiłek w wychowaniu. Dziękuję Ci, że zapaliłaś we mnie chęć do tego doktoratu i wspierałaś mnie w nim każdego dnia. Jesteś najlepszą Mamą na świecie! Ciociu Elu i Wujku Krzysiu, jesteście od samego początku bardzo ważną częścią mojego życia. Mieliście bardzo duży wpływ na moje wychowanie i postrzeganie świata. Dziękuję wam za opiekę i miłość, i za to, że wspieraliscie mnie w tym doktoracie.

Tomasz, my dear fiancé... I was wondering in which language to write. I have chosen English, so that these important words reach a broader public. Thank you for being next to me in all these moments, good ones and bad ones. You always support my decisions, even the ones that are difficult for you. You are like a rock, which always stands steadfast next to me. You remind me that besides science there is also a static world, where the centre of gravity lies in everyday pleasures, problems, and dreams. I want to explore this world with you. You are my love!

Curriculum vitae

Personal data

Name:	Katarzyna (Kate) Adamczuk
Date of birth:	22nd November 1986
Nationality:	Polish
Address:	Daszyńskiego 17/18, 20-250 Lublin, Poland
Phone:	+32 488 28 27 06
Email:	keights@gmail.com

Education

2002 - 2005: 1st Secondary School name of Stanisław Staszic in Lublin
Al. Racławickie 26, 20-043 Lublin, Poland

2005 - 2010: Master of Biotechnology
Graduated *very good*
University of Life Sciences, Lublin, Poland
Master thesis in collaboration with Ghent University:
The role of US3-mediated activation of p21-activated kinases in viral spread
Promoter: Prof. Dr. Herman Favoreel
Co-promoter: Prof. Dr. Łukasz Adaszek

2007 - 2010:	Master of Biochemistry and Biotechnolgy: International Exchange Graduated *summa cum laude* Ghent University, Ghent, Belgium Master thesis: *The role of US3-mediated activation of p21-activated kinases in viral spread* Promoter: Prof. Dr. Herman Favoreel Co-promoter: Prof. Dr. Łukasz Adaszek
2007 - 2008:	Research project at the LEGEST Laboratory Ghent University, Ghent, Belgium Title: *Hormone receptor-based molecular mechanisms to combat inflammation* Supervisor: Prof. Dr. Karolien DeBosscher
2009 August - September:	Research project at the Laboratory of Pharmaceutical Biotechnology Ghent University, Ghent, Belgium Title: *Optimization of DNA extraction protocols for forensic reference samples. Investigation of the presence of cell-free DNA in human body fluids* Supervisors: Prof. Dr. Dieter Deforce and Dr. Mado Vandewoestyne
2010 - now:	PhD student at the Laboratory for Cognitive Neurology KU Leuven, Leuven, Belgium PhD project: *Amyloid load in the brain of cognitively intact older adults* Promoter: Prof. Dr. Rik Vandenberghe
2010 - now:	Doctoral training in Cognitive and Molecular Neurosciences Doctoral School Biomedical Sciences, Faculty of Medicine KU Leuven, Leuven, Belgium
2012 - now:	PhD fellow of the Research Foundation Flanders (FWO)

Awards and honours

2012 Travel Award, Alzheimer's Association International Conference. Vancouver, Canada, July 14-19, 2012.

2013 Travel Award, Human Amyloid Imaging Conference. Miami, Florida, USA, January 16-18, 2013.

2013 Junior Faculty Award, International Conference on Alzheimer's and Parkinson's Diseases. Florence, Italy, March 6-10, 2013.

2014 Travel Award, Alzheimer's Association International Conference. Copenhagen, Denmark, July 13-17, 2014.

2015 A delegate for the Young Leaders Discussion to Address Dementia organized by the UK Government's Science and Innovation Network in partnership with the World Dementia Council and the Global Action Against Dementia. London, UK, February 27, 2015.

2015 Chair of the session: Cerebrospinal fluid and imaging biomarkers of Alzheimer's disease. International Conference on Alzheimer's and Parkinson's Diseases. Nice, France, March 18-22, 2015.

Publications

Publications in peer-reviewed journals

Vandenbulcke M, Bouckaert F, De Winter FL, Koole M, **Adamczuk K**, Vandenberghe R, Emsell L, Van Laere K. Asymmetric amyloid deposition in the brain following unilateral electroconvulsive therapy. Under review.

Adamczuk K, Schaeverbeke J, Vanderstichele HMJ, Nelissen N, Van Laere K, Dupont P, Hilven K, Poesen K, Vandenberghe K. Comparison of cerebrospinal fluid Aβ isoforms for detection of preclinical Alzheimer's disease. Under revision.

Adamczuk K, Schaeverbeke J, Nelissen N, Neyens V, Vandenbulcke M, Goffin K, Lilja J, Hilven K, Dupont P, Van Laere K, Vandenberghe R. Amyloid imaging in cognitively normal older adults: Comparison between ^{18}F-flutemetamol and ^{11}C-Pittsburgh Compound B. Eur J Nucl Med Mol Imaging. 2015; doi:10.1007/s00259-015-3156-9.

Liuzzi AG, Bruffaerts R, Dupont P, **Adamczuk K**, Peeters R, De Deyne S, Storms G, Vandenberghe R. Left perirhinal cortex codes for similarity in meaning between written words. Neuropsychologia. 2015; Mar 18. pii: S0028-3932(15)00121-9.

Wang Y, Nelissen N, **Adamczuk K**, De Weer AS, Vandenbulcke M, Sunaert S, Vandenberghe R, Dupont P. Reproducibility and Robustness of Graph Mea-

sures of the Associative-Semantic Network. PLoS One. 2014; 9:e115215.

Adamczuk K, De Weer AS, Nelissen N, Dupont P, Sunaert S, Bettens K, Sleegers K, Van Broeckhoven C, Van Laere K, Vandenberghe R. Functional changes in the language network in response to increased amyloid beta deposition in cognitively intact older adults. Cereb Cortex. 2014; doi:10.1093/cercor/bhu286.

Adamczuk K, De Weer AS, Nelissen N, Chen K, Sleegers K, Bettens K, Van Broeckhoven C, Vandenbulcke M, Thiyyagura P, Dupont P, Van Laere K, Reiman EM, Vandenberghe R. Polymorphism of brain derived neurotrophic factor influences β amyloid load in cognitively intact apolipoprotein E $\varepsilon 4$ carriers. Neuroimage Clin. 2013; 2:512-520.

Vandenberghe R, **Adamczuk K**, Dupont P, Van Laere K, Chètelat G. Amyloid PET in clinical practice: Its place in the multidimensional space of Alzheimer's disease. Neuroimage Clin. 2013; 2:497-511.

Vandenberghe R, **Adamczuk K**, Van Laere K. The interest of amyloid PET imaging in the diagnosis of Alzheimer's disease. Curr Opin Neurol. 2013; 26:646-655.

Barao S, Zhou L, **Adamczuk K**, Vanhoutvin T, Van Leuven F, Demedts D, Vijverman AC, Bossuyt X, Vandenberghe R, De Strooper B. BACE1 levels correlate with phospho-tau levels in human cerebrospinal fluid. Curr Alzheimer Res. 2013; 10:671-678.

Van Doren L, Schrooten M, **Adamczuk K**, Dupont P, Vandenberghe R. Chronometry of word and picture identification: common and modality-specific effects. Neuroimage. 2012; 59:3701-3712.

Conference abstracts

Adamczuk K, Schaeverbeke J, Bruffaerts R, Nelissen N, Neyens V, Dupont P, Goffin K, Vandenbulcke M, Van Laere K, Tournoy J, Poesen K, Vandenberghe R. Comparison of three amyloid biomarkers for preclinical Alzheimer's disease. Oral presentation, International Conference on Alzheimer's and Parkinson's Diseases, Nice, France, March 18-22, 2015.

Adamczuk K, Schaeverbeke J, Bruffaerts R, Nelissen N, Neyens V, Dupont P, Goffin K, Vandenbulcke M, Van Laere K, Tournoy J, Poesen K, Vandenberghe R. Amyloid biomarkers in cognitively normal older adults: comparison of [18]F-flutemetamol to [11]C-PIB and CSF Aβ42. Poster, Human Amyloid Imaging, Miami, USA, January 14-16, 2015.

Adamczuk K, Schaeverbeke J, Bruffaerts R, Nelissen N, Neyens V, Dupont P, Goffin K, Vandenbulcke M, Van Laere K, Poesen K, Vandenberghe R. Definition of preclinical Alzheimer's disease with three amyloid biomarkers. Oral presentation, Leuven research Institute for Neuroscience & Disease Seminar, Mechelen, Belgium, December 5, 2014.

Adamczuk K, De Weer AS, Nelissen N, Dupont P, Sunaert S, Van Laere K, Vandenberghe R. Functional changes in the language network in response to increased amyloid β deposition in cognitively intact older adults. Oral presentation, World Federation of Neurology Research Group on Aphasia, Dementia and Cognitive Disorders, Hong Kong, China, November 27-30, 2014.

Adamczuk K, Schaeverbeke J, Bruffaerts R, Nelissen N, Neyens V, Dupont P, Goffin K, Vandenbulcke M, Van Laere K, Poesen K, Vandenberghe R. Amyloid PET imaging in cognitively normal older adults: Comparison of ^{18}F-flutemetamol to ^{11}C-PIB and CSF measurements of Aβ42. Poster, World Federation of Neurology Research Group on Aphasia, Dementia and Cognitive Disorders, Hong Kong, China, November 27-30, 2014.

Adamczuk K, De Weer AS, Nelissen N, Dupont P, Van Laere K, Vandenberghe R. Functional response of the language system to increased amyloid load in cognitively intact older adults. Oral presentation, Society for Neuroscience Annual Meeting, Washington DC, USA, November 15-19, 2014.

Schaeverbeke J, **Adamczuk K**, Bruffaerts R, Nelissen N, Neyens V, Dupont P, Van Laere K, Poesen K, Vandenberghe R. Comparison of ^{18}F-flutemetamol uptake and CSF measurements in cognitively intact older individuals. Oral presentation, Alzheimer's Association International Conference, Copenhagen, Denmark, July 12-17, 2014.

Adamczuk K, Schaeverbeke J, Nelissen N, Neyens V, Dupont P, Goffin K, Vandenbulcke M, Van Laere K, Vandenberghe R. Comparison between semi-quantitative measures and reader concordance of amyloid load based on ^{18}F-Flutemetamol versus ^{11}C-PIB in cognitively intact older adults. Oral presentation, Alzheimer's Association International Conference, Copenhagen, Denmark, July 12-17, 2014.

Adamczuk K, De Weer AS, Nelissen N, Dupont P, Van Laere K, Vandenberghe R. Functional changes in the language network in cognitively intact older adults in relation to cerebral amyloid load. Poster, Alzheimer's Association International Conference, Copenhagen, Denmark, July 12-17, 2014.

Seynaeve L, **Adamczuk K**, Kovacs S, Vandenberghe R, Sunaert S, Dupont P, Van Paesschen W. Comparison of language fMRI during two paradigms of language in temporal lobe epilepsy. Poster, Organization for Human Brain Mapping, Hamburg, Germany, June 8-12, 2014.

Liuzzi AG, Bruffaerts R, **Adamczuk K**, Peeters R, Dupont P, Vandenberghe R. How sensory input-modality influences the responses during property verification. Poster, Organization for Human Brain Mapping, Hamburg, Germany, June 8-12, 2014.

Wang Y, **Adamczuk K**, De Weer AS, Sunaert S, Vandenberghe R, Dupont P. Combined voxel- and region-based analysis of associative-semantic network. Poster, Organization for Human Brain Mapping, Hamburg, Germany, June 8-12, 2014.

Adamczuk K, De Weer AS, Nelissen N, Dupont P, Van Laere K, Vanden-

berghe R. Early functional changes in the language network in response to increased amyloid beta deposition in healthy older adults. Poster, Human Amyloid Imaging, Miami, USA, January 15-17, 2014.

Adamczuk K, De Weer AS, Nelissen N, Chen K, Sleegers K, Van Broeckhoven C, Vandenbulcke M, Van Laere K, Reiman EM, Vandenberghe R. Effect of Brain Derived Neurotrophic Factor val66met polymorphism on amyloid load in Apolipoprotein E $\varepsilon 4$ carriers. Oral presentation, International Conference on Alzheimer's and Parkinson's Diseases, Florence, Italy, March 6-10, 2013.

Vandenberghe R, **Adamczuk K**, De Weer AS, Nelissen N, Sleegers K, Bettens K, Van Broeckhoven C, Vandenbulcke M, Van Laere K. Relationship of cerebral amyloid load to episodic memory performance in cognitively intact older individuals: effect of Brain Derived Neurotrophic Factor (BDNF) val66met polymorphism. Poster, Human Amyloid Imaging Conference, Miami, USA, January 16-18, 2013.

Adamczuk K, De Weer AS, Chen K, Nelissen N, Sleegers K, Van Broeckhoven C, Vandenbulcke M, Van Laere K, Reiman EM, Vandenberghe R. Effect of Brain Derived Neurotrophic Factor (BDNF) val66met polymorphism on amyloid load in cognitively intact older adult APOE $\varepsilon 4$ carriers. Poster, Human Amyloid Imaging Conference, Miami, USA, January 16-18, 2013.

Adamczuk K, De Weer AS, Nelissen N, Sleegers K, Van Broeckhoven C, Vandenbulcke M, Van Laere K, Vandenberghe R. Brain Derived Neurotrophic Factor and subclinical amyloid deposition in cognitively intact older individuals. Poster, Belgian Brain Council, Liège, Belgium, October 27, 2012.

Adamczuk K, De Weer AS, Nelissen N, Sleegers K, Bettens K, Van Broeckhoven C, Vandenbulcke M, Van Laere K, Vandenberghe R. Cerebral amyloid load in cognitively intact elderly individuals: Effect of Brain Derived Neurotrophic Factor val66met polymorphism. Poster, Society for Neuroscience Annual Meeting, New Orleans, USA, October 13-17, 2012.

Vandenberghe R, De Weer AS, **Adamczuk K**, Vandenbulcke M, Nelissen N, Farrar G, Thurfjell L, Van Laere K. Comparison of three diagnostic methods for determining amyloid positivity in cognitively intact elderly controls. Poster, Alzheimer's Association International Conference, Vancouver, Canada, July 14-19, 2012.

Adamczuk K, De Weer AS, Sleegers K, Nelissen N, Farrar G, Thurfjell L, Van Broeckhoven C, Van Laere K, Vandenberghe R. Gene-gene interaction and subclinical amyloid levels in cognitively intact elderly individuals. Oral presentation, Alzheimer's Association International Conference, Vancouver, Canada, July 14-19, 2012.